Supplement of Earth Syst. Sci. Data, 16, 2605–2624, 2024
https://doi.org/10.5194/essd-16-2605-2024-supplement

Open Access Earth System Science Data

Supplement of

The ABoVE L-band and P-band airborne synthetic aperture radar surveys

Charles E. Miller et al.

Correspondence to: Charles E. Miller (charles.e.miller@jpl.nasa.gov)

Summary

NASA's Arctic Boreal Vulnerability Experiment (ABoVE) conducted airborne synthetic aperture radar (SAR) surveys of over 120,000 km^2 in Alaska and northwestern Canada during 2017, 2018, 2019, and 2022 (**Figure S1**). Here, we present an annotated guide to the L-band and P-band airborne SAR data acquired during the ABoVE airborne campaigns [Miller et al. 2019]. We provide a detailed description of the ~80 SAR flight lines and how each fits into the ABoVE experimental design. Extensive maps, tables, and hyperlinks give direct access to every flight plan as well as individual flight lines. This entry is a guide to enable interested readers to fully explore the ABoVE L- and P-band SAR data.

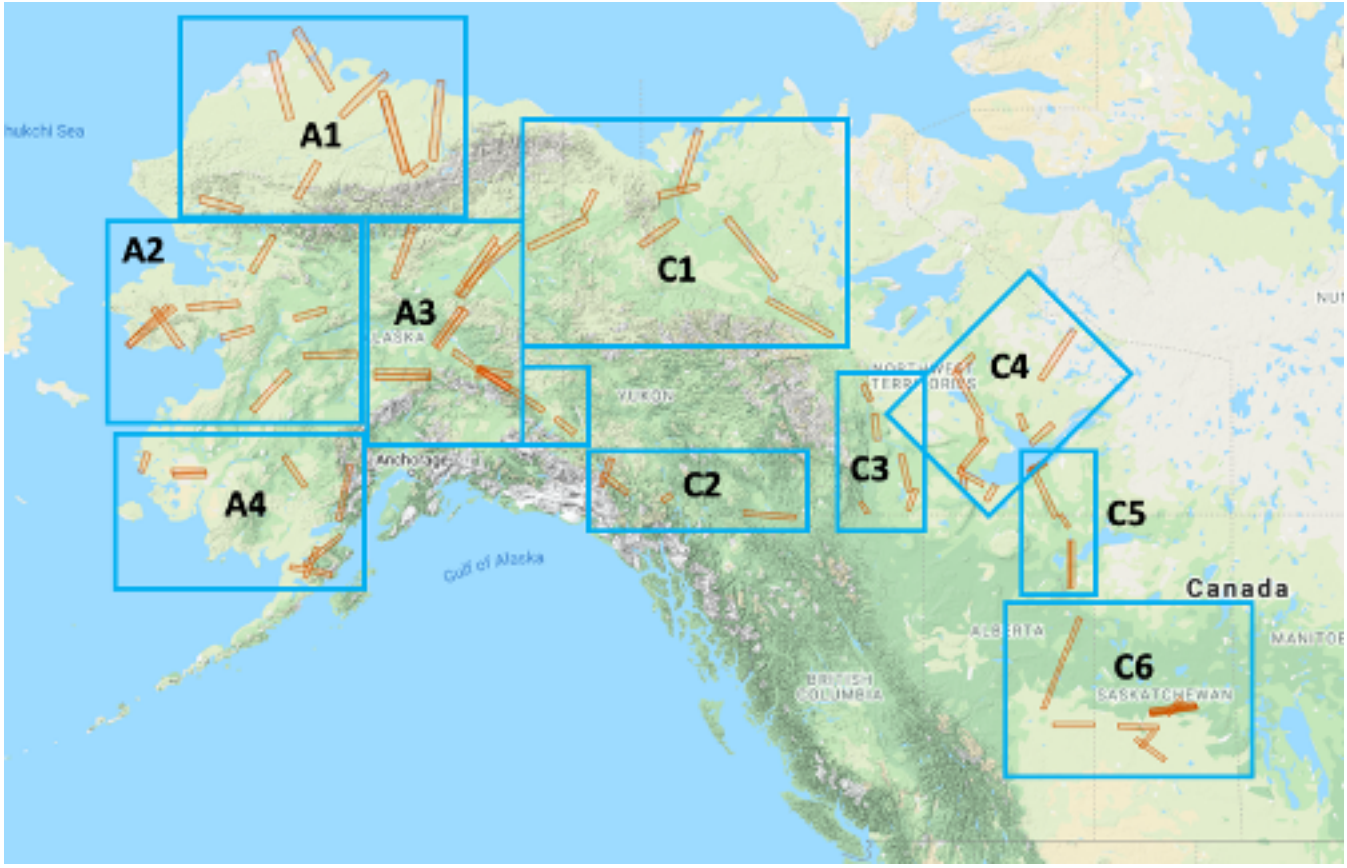

Figure S1. Flight lines for L-band and P-band PolInSAR measurements capture critical bioclimatic, permafrost, and geographic gradients as well as key field sites and long-term measurement records across the 4 Mkm^2 ABoVE domain. The flight lines are collected into 10 composites which roughly correspond to the Alaskan (A1-A4) and Canadian (C1-C6) regions sampled on individual flight days. © Google Maps

Data Availability

Miller, Charles E., Peter C. Griffith, Elizabeth Hoy, Naiara S. Pinto, Yunling Lou, Scott Hensley, Bruce D. Chapman, Jennifer Baltzer, Kazem Bakian-Dogaheh, W. Robert Bolton, Laura Bourgeau-Chavez, Richard H. Chen, Byung-Hun Choe, Leah Clayton, Thomas A. Douglas, Nancy French, Jean E. Holloway, Gang Hong, Lingcao Huang, Go Iwahana, Liza Jenkins, John S. Kimball, Tatiana Loboda, Michelle Mack, Philip Marsh, Roger J. Michaelides, Mahta Moghaddam, Andrew Parsekian, Kevin Schaefer, Paul R. Siqueira, Debjani Singh, Alireza Tabatabaeenejad, Merritt Turetsky, Ridha Touzi, Elizabeth Wig, Cathy J. Wilson, Paul Wilson, Stan D. Wullschleger, Yonghong Yi, Howard A. Zebker[22], Yu Zhang, Yuhuan Zhao, Scott J. Goetz. 2022. Summary of the ABoVE L-band and P-band Airborne SAR Surveys. ORNL DAAC, Oak Ridge, Tennessee, USA. https://doi.org/10.3334/ORNLDAAC/2150

Table of Contents

1. Dataset Overview

The L-band and P-band SARs are foundational measurements in the ABoVE airborne campaign strategy [Miller et al. 2019]. The ~80 flight lines described here form the framework for the remainder of ABoVE airborne remote sensing acquisitions. The baseline L-band campaigns were flown in June (DOY 164-173, **Table S1**) and September (DOY 251-263, **Table S2**) of 2017 to characterize the land surface during periods of minimum and maximum active layer thickness, respectively. Subsequent L-band campaigns in 2018 (DOY 231-241, **Table S3**), 2019 (DOY 247-260, **Table S4**), and 2022 (DOY 226-237, **Table S5**) provide a time series synched to maximum annual active layer thickness. P-band campaigns were conducted in May-June (DOY 142-157, **Table S6**) and August (DOY 219-227, **Table S7**) of 2017. There was a 2-day P-band mini-campaign in October 2017 to extend the legacy time series of early cold season acquisitions over the Seward Peninsula, NW Alaska and North Slope Alaska (DOY 280-283, **Table S8**).

ABoVE SAR flight lines (**Figure S1**) leverage legacy L- and P-band SAR transects acquired during the pre-ABoVE period; remotely-sensed permafrost active layer thickness time series derived from satellite interferometric SAR observations (ReSALT) [Schaefer et al. 2015]; SAR data from PALSAR, PALSAR-2, RadarSat, RadarSat-2, and Sentinel-1; historic or planned airborne LiDAR acquisitions; and data from existing field sites [Hoy et al. 2018]. Legacy airborne SAR flight lines include the L-band grid acquired over the Boreal Ecosystem Research and Monitoring Sites (BERMS) area near Prince Albert, SK during SMAP CanEx 2010 [Magagi et al. 2012], the P-band lines over the BERMS area

acquired from 2012-2015 during the Airborne Microwave Observatory of Subcanopy and Subsurface (AirMOSS) Earth Ventures Sub-orbital (EV-S1) investigation [Allen et al. 2010; Moghaddam et al. 2016], and a collection of 10 L- and P-band flight lines acquired over the Seward Peninsula, Northwestern Interior, and North Slope of Alaska during 2014 and 2015 [Chen et al. 2019a, 2019b]. The BERMS area observations link ABoVE to the Boreal Ecosystem–Atmosphere Study (BOREAS) studies of the 1990s [Sellers et al. 1995; 1997].

1.1 L-band and P-band Campaign Summaries

The baseline L-band campaigns were flown in June (DOY 164-173, **Table S1**) and September (DOY 251-263, **Table S2**) of 2017 to characterize the land surface during periods of minimum and maximum active layer thickness, respectively. Subsequent L-band campaigns in 2018 (DOY 231-241, **Table S3**), 2019 (DOY 247-260, **Table S4**), and 2022 (DOY 226-235, **Table S5**) provide a time series synched to maximum annual active layer thickness. P-band campaigns were conducted in May-June (DOY 142-157, **Table S6**) and August (DOY 219-227, **Table S7**) of 2017. There was a 2-day P-band mini-campaign in October 2017 to extend the legacy time series of early cold season acquisitions over the Seward Peninsula, NW Alaska and North Slope Alaska (DOY 280-283, **Table S8**).

Table S1. ABoVE L-band PolInSAR Campaign #1: June 2017

Flight Plan	Sortie Date	Regions Sampled (hyperlink to flight line map)
17062	2017-06-13	PAD-Transboundary Watershed
17063	2017-06-14	Great Slave Lake Region
17064	2017-06-15	Yellowknife – Fairbanks Transit
17065	2017-06-16	Southwest Alaska
17066	2017-06-17	Southwest Alaska & YK Delta
17067	2017-06-19	Seward Peninsula & NW Alaska
17068	2017-06-20	Mackenzie Valley & Upper Yukon Territory
17069	2017-06-21	North Slope Alaska & Yukon Flats
17070	2017-06-22	Mackenzie Valley Reflight

Table S2. ABoVE L-Band PolInSAR Campaign #2: September 2017

Flight Plan	Sortie Date	Regions Sampled (hyperlink to flight line map)
17093	2017-09-08	BERMS - PAD-Transboundary Watershed
17094	2017-09-09	Great Slave Lake Region & Upper Mackenzie Valley
17095	2017-09-10	Yellowknife – Fairbanks Transit
17096	2017-09-12	Mackenzie Valley & Upper Yukon Territory

17097	2017-09-15	Seward Peninsula & NW Alaska
17098	2017-09-16	North Slope Alaska & Yukon Flats
17099	2017-09-17	Southwest Alaska & YK Delta
17100	2017-09-19	Interior Alaska
17101	2017-09-20	Delta Junction AK TomoSAR

Table S3. ABoVE L-Band PolInSAR Campaign #3: August 2018

Flight Plan	Sortie Date	Regions Sampled (hyperlink to flight line map)
18046	2018-08-19	BERMS TomoSAR
18047	2018-08-21	PAD & Great Slave Lake 1
18048	2018-08-22	Great Slave Lake Region & Scotty Creek
18049	2018-08-24	Yellowknife – Fairbanks Transit
18050	2018-08-26	North Slope Alaska
18051	2018-08-27	Interior Alaska
18052	2018-08-28	Southwest Alaska & YK Delta
18053	2018-08-29	Mackenzie Valley & Upper Yukon Territory

Table S4. ABoVE L-Band PolInSAR Campaign #4: September 2019

Flight Plan	Sortie Date	Regions Sampled (hyperlink to flight line map)
19059	2019-09-04	PAD & Great Slave Lake 1
19060	2019-09-05	Great Slave Lake Region & Scotty Creek
19061	2019-09-11	Yellowknife – Fairbanks Transit
19062	2019-09-12	Seward Peninsula & NW Alaska
19063	2019-09-13	North Slope Alaska
19064	2019-09-14	Interior Alaska
19065	2019-09-16	Mackenzie Valley & Upper Yukon Territory
19066	2019-09-17	Southwest Alaska & YK Delta

Table S5. ABoVE L-Band PolInSAR Campaign #5: August 2022

Flight Plan	Sortie Date	Regions Sampled
22031	2022-08-14	BERMS TomoSAR
22032	2022-08-15	PAD & Great Slave Lake 1

22033	2022-08-16	Great Slave Lake Region & Scotty Creek
22034	2022-08-18	Yellowknife – Fairbanks Transit
22035	2022-08-19	Seward Peninsula & NW Alaska
22036	2022-08-20	North Slope Alaska
22037	2022-08-22	Mackenzie Valley & Upper Yukon Territory
22038	2022-08-23	Southwest Alaska & YK Delta
22039	2022-08-24	Interior Alaska
22040	2022-08-25	British Columbia

Table S6. ABoVE P-band PolInSAR Campaign #1: May-June 2017

Flight Plan	Sortie Date	Regions Sampled (hyperlink to flight line map)
17051	2017-05-22	PAD-Transboundary Watershed
17052	2017-05-23	Great Slave Lake Region & Upper Mackenzie Valley
17053	2017-05-25	Yellowknife – Fairbanks Transit
17054	2017-05-26	Interior & Southwest Alaska
17055	2017-05-27	YK Delta & NW Alaska
17056	2017-05-29	Seward Peninsula, NW Alaska & Yukon Flats
17057	2017-06-05	Mackenzie Valley & Upper Yukon Territory
17058	2017-06-06	North Slope Alaska

Table S7. ABoVE P-Band PolInSAR Campaign #2: August 2017

Flight Plan	Sortie Date	Regions Sampled (hyperlink to flight line map)
17075	2017-08-07	BERMS & Southern Boreal Forest
17076	2017-08-08	PAD-Transboundary Watershed & Great Slave Lake 1
17077	2017-08-09	Great Slave Lake Region & Upper Mackenzie Valley
17078	2017-08-11	Daring & Yellowknife – Fairbanks Transit
17079	2017-08-13	North Slope Alaska
17080	2017-08-14	Southwest Alaska & YK Delta
17081	2017-08-15	Delta Junction, AK tomoSAR
17082	2017-08-17	Seward Peninsula, NW Alaska, & Yukon Flats
17083	2017-08-18	Mackenzie Valley & Upper Yukon Territory

Table S8. ABoVE P-Band PolInSAR Campaign #3: October 2017

Flight Plan	Sortie Date	Regions Sampled (hyperlink to flight line map)
17109	2017-10-07	North Slope Alaska
17110	2017-10-10	Seward Peninsula

2 Alaskan Flight Lines

The Alaskan SAR flight lines are broken into four main regional collections: A1) North Slope Alaska, A2) Seward Peninsula and Northwest Alaska, A3) Eastern Interior, and A4) Southwest Alaska and the Yukon-Kuskokwim Delta (**Figure S1**). Legacy L- and P-band flight lines from the AirMOSS EV-S1 investigation [Allen et al. 2010; Moghaddam et al. 2016] in the Seward Peninsula, NW Alaska, and the North Slope were adapted for ABoVE use. The P-band acquisitions are designed to overlap with the near field portions of the L-band lines. Line IDs for the L-band and P-band flight lines differ slightly because they acquire data with slightly different off-nadir viewing geometries [Miller et al. 2019]. Acquisition of P-band flight lines in the central Interior was not possible due to a military radar keep-out zone centered near Clear, AK (**Figure S2**).

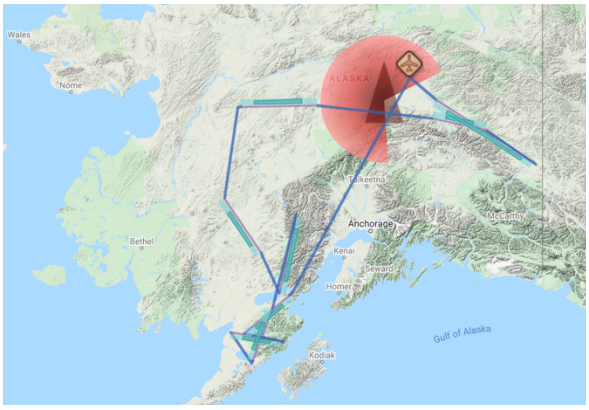

Figure S2. The military radar at Clear, AK creates a large P-band operations keep-out zone in the central Interior (red areas). The aircraft symbol marks our Fairbanks International Airport (PAFA) base of operations. Data acquisitions (blue bars) are from Flight Plan 17054. © Google Maps

2.1 Region A1: North Slope Alaska

Figure S3 shows the flight lines for Region A1: North Slope Alaska. Details for individual L-band SAR flight lines are given in **Table S9**. The P-band flight line details are given in **Table S21**. The North Slope region features several important legacy flight lines established by AirMOSS (**Table S34, Table S35**). Of particular note are the lines covering Utqiaġvik (Barrow, 15018) and the Dalton Highway from Deadhorse on the Arctic Coastal Plain to the Brooks Range foothills (18519). Both of these lines leverage long-term ground-based measurements and provide critical calibration and validation data for higher level data products.

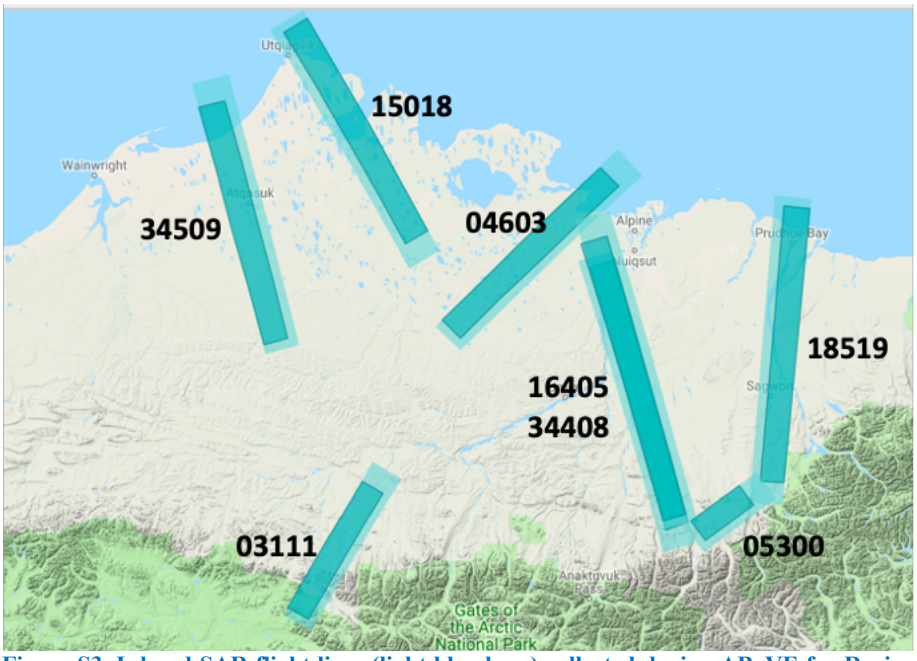

Figure S3. L-band SAR flight lines (light blue bars) collected during ABoVE for Region A1: North Slope Alaska. Flight line IDs are listed next to each line. These lines provide regional sampling for many areas where ground-based measurements have characterized local landscapes such as Atqasuk (Line 34509), Utqiaġvik (Line 15018), Deadhorse and the Dalton Highway (Line 18519), and Toolik Lake (Line 05300). © Google Maps

Line 03111: Ivotuk. The Ivotuk flight line overlaps the legacy line 03109 (**Table S35**) and is anchored by the Ivotuk flux tower (US-IVO) [Zona et al. 2016; Davidson et al. 2017], a CALM 1 km grid (Ivotuk, site U26), and three GTN-P permafrost boreholes near Ivotuk. The flight line extends ~135 km from the southern edge of the Brooks Range foothills in the south to the Colville River in the north. Vegetation cover is mostly upland tundra with increasing soil saturation closer to the river.

Line 34509: Atqasu. The Atqasuk flight line overlaps the legacy line 34506 (**Table S35**) and is anchored by the Atqasuk flux tower (US-ATQ) [Zona et al. 2016], CALM 1 km grid at Atqasuk (site U3), and a UNAVCO GPS base station at Atqasuk. The flight line extends ~160 km from the southern edge of the Arctic Coastal Plain across the Meade River to the Arctic Ocean coast. It overflies numerous lakes with known CH4 seeps [Walter Anthony et al. 2016]. Vegetation cover consists of mostly graminoid and tussock tundra with many dried lake beds distributed across the landscape.

Line 15018: Barrow. The Barrow (Utqiaġvik) flight line overlaps the legacy line 15008 (**Table S35**). It is anchored by the extensive science infrastructure in and around the Barrow Peninsula including: DOE NGEE-Arctic experimental sites; Barrow area flux towers (US-BRW, US-BES, US-BEO, US-NGB)

[Oechel 2000; Dengel 2020]; the NEON Utqiaġvik D18 tundra relocatable terrestrial site (BARR) and Airborne Observation Platform (AOP) box; the NOAA-CMDL Barrow Atmospheric Baseline Observatory (BRW); DOE Atmospheric Research and Monitoring North Slope Alaska (NSA) site; Barrow area CALM sites U1 and U2; a cluster of a dozen GTN-P boreholes on the Barrow Peninsula and one at Kuyanak (TSP.814); the Barrow Domain remotely sensed active layer thickness (ReSALT) time series [Schaefer et al. 2015; Liu et al. 2015a]; ground penetrating radar transects for active layer thickness and volumetric water content [Jafarov et al. 2017]; In situ soil moisture and thaw depth measurements [Wilson 2018]; and numerous long-term experimental plots. The flight line extends southeast ~165 km from Point Barrow over the Elson Lagoon and terminates south of Teshekpuk Lake. It samples a multitude of lakes, dry lakebeds, small rivers and tundra polygons.

Line 04063: Inigok. The Inigok flight line is anchored by the CALM sites at Inigok (U21) and Fish Creek (U22) as well as GTN-P boreholes at North Inigok (NING, TSP.813), West Fish Creek 1 (FCK, TSP.825), Atigaru (ATI, TSP.827), and South Harrison (SOH, TSP.828). The flight line extends northeast ~150 km from the southern edge of the Arctic Coastal Plain to the Arctic Ocean coast halfway between Teshekpuk Lake and the Colville Delta.

Lines 34408 and 16405: AnaktE and AnaktW. The Anaktuvuk flight lines map the 2007 Anaktuvuk River fire scar [Jones et al. 2009; Mack et al. 2011], running ~200 km from near Toolik Lake in the south to the Colville River in the north (**Figure S4**). The fire scar is bounded by the Anaktuvuk and Kuparuk Rivers on the east and west, respectively, and ranges from 15 to 20 km in width. More than 50% of the area burned severely [Jones et al. 2009] and it is thought to be the largest Arctic tundra fire in the last 5,000 years [Hu et al. 2010]. Anchor points include three flux towers in the southern end of the scar [Rocha et al. 2011a,b], and numerous ABoVE field plots [Chen et al. 2016]. The spacing of the L-band flight lines is based on the narrower P-band swath and allows complete mapping of the complete fire scar by both L-band and P-band SARs. These lines are used to study changes in soil moisture, surface roughness, ALT, etc. in disturbed vs undisturbed areas. Interferometric SAR will be used to map surface elevation changes and track the evolution of permafrost degradation within the scar compared to LiDAR surface elevation data [Jones et al. 2015] and PALSAR time series [Liu et al. 2014; Iwahana et al. 2016].

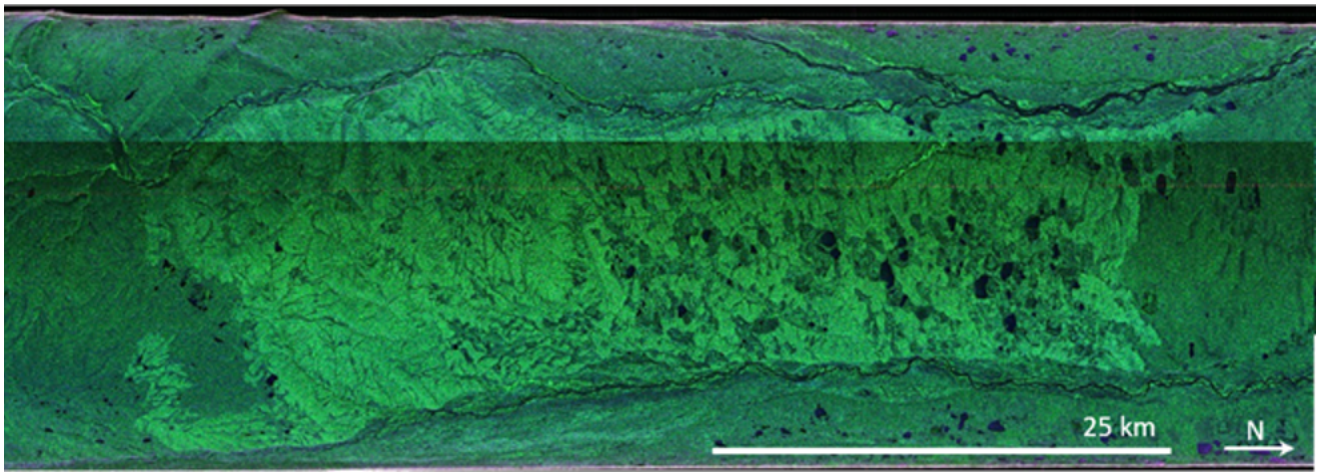

Figure S4. P-band PolSAR composite image showing complete mapping of the 2007 Anaktuvuk River fire scar (light green area in the center of the image) on 13 August 2017. Intrinsic resolution of the P-band PolSAR imagery is approximately 12 meters and reveals shaper features along the fire scar boundaries as well as indications of increased surface roughness and permafrost degradation within the fire scar compared to the adjacent undisturbed areas (darker green). Lakes, ponds, and rivers appear as black areas in this image.

Line 18519: Dhorse. The Deadhorse flight line overlaps the legacy line 18516 (**Table S35**). It extends ~190 km from Prudhoe Bay south over the energy exploration infrastructure in Deadhorse and then south along the Dalton Highway. It is anchored by seven CALM sites, including the 1 km grids at West Dock (U5), Betty Pingo (U7A), and Happy Valley (U9B); the ReSALT thermokarst time series and GPR transects along the Pipeline approximately 15 km south of Deadhorse [Liu et al. 2015]; and myriad field sites that have been established adjacent to the highway over the years. In particular, ABoVE researchers monitored high resolution soil moisture and soil dielectric constant vertical profiles along the highway to validate L- and P-band retrievals of active layer properties [Chen et al. 2016; 2018; 2019 a,b; Bakian-Dogaheh et al. 2020] and enable modeling [Yi et al. 2018]. Schaefer and coworkers also acquired numerous ground penetrating radar (GPR) transects to validate the ReSALT and airborne SAR active layer thickness retrieval algorithms [Chen et al. 2016].

Line 05300: Toolik. The Toolik flight line extends ~80 km along the Dalton Highway from Pump Station #3 over Imnavait Creek to Toolik Lake. It is anchored by the extensive scientific infrastructure surrounding the Arctic Long Term Ecological Research (LTER) site at Toolik Lake; the NEON D18 tundra sites Toolik (TOOL, core terrestrial), Oksrukuyik Creek (OKSR, core aquatic), and Toolik Lake (TOOK, relocatable aquatic) as well as the northern portion of the Toolik AOP flight box; CALM active layer thickness measurements at Imnaviat Creek WET (U11B) and MAT (U11C), Toolik MAT (U12B), and Toolik LTER (U13) as well as the Toolik 1 km grid (U12A); ground penetrating radar (GPR) [Gusmeroli et al. 2015; Chen et al. 2016]; in situ soil measurements including soil dielectric properties, temperature, and moisture profiles, ALT, and measurements of soil organic matter, bulk density, porosity, texture, and coarse root biomass [Bakian-Dogaheh et al. 2020]; in situ active layer thickness measurements [Chen et al. 2020]; high-resolution shrub biomass maps [Greaves et al. 2018]; and three

Imnavait Creek flux towers [Euskirchen et al. 2012]. Road access and proximity to many long-term data records made this a high priority area for many ABoVE field activities.

Table S9. Region A1 (North Slope Alaska) L-band Line Summary Data

Line ID	Short Name	Flight Plan	Date	Comments
03111	Ivotuk	22036 19063 17097 17067	2022-08-20 2019-09-13 2017-09-15 2017-06-19	Ivotuk flux tower, CALM site, GTN-P boreholes
34509	Atqasu	22036 19063 18050 17098 17069	2022-08-20 2019-09-13 2018-08-26 2017-09-16 2017-06-21	Atqasuk flux tower; CALM site
15018	Barrow	22036 19063 18050 17098 17069	2022-08-20 2019-09-13 2018-08-26 2017-09-16 2017-06-21	Legacy line; NGEE-Artic, NEON, BEO flux towers, CALM sites
04603	Inigok	22036 19063 18050 17098 17069	2022-08-20 2019-09-13 2018-08-26 2017-09-16 2017-06-21	North Slope CALM sites, boreholes
34408	AnaktE	22036 19063 18050 17098 17069	2022-08-20 2019-09-13 2018-08-26 2017-09-16 2017-06-21	Anaktuvuk River fire scar, eastern transect
16405	AnaktW	22036 19063 18050 17098 17069	2022-08-20 2019-09-13 2018-08-26 2017-09-16 2017-06-21	Anaktuvuk River fire scar, western transect
18519	Dhorse	22036 19063 18050 17098 17069	2022-08-20 2019-09-13 2018-08-26 2017-09-16 2017-06-21	North-South transect running from the Arctic Ocean coast through Deadhorse and south along the Dalton Highway; covers numerous calibration sites

05300	Toolik	22036	2022-08-20	Toolik Lake Research area, NEON box
		19063	2019-09-13	
		18050	2018-08-26	
		17098	2017-09-16	
		17069	2017-06-21	

2.2 Region A2: Seward Peninsula and the Northwest Interior

Figure S5 shows the transects for Region A2: Seward Peninsula and the Northwest Interior. Details for individual L-band SAR flight lines are given in **Table S10**; the P-band acquisition details are given **Table S22**. The Seward Peninsula region features flight lines over the NGEE-Arctic Council, Kougarok, and Teller watersheds where intensive ground-based measurements provide critical validation data for the SAR products as well as other geophysical characterizations that can be used to help contextualize the SAR data [Wilson et al. 2018]. The other northwestern Alaska flight lines extend the time series from legacy acquisitions [**Table S34, Table S35**; Chen et al. 2016] and surveys of fire disturbance in the Noatak River Valley [Higuera et al. 2011].

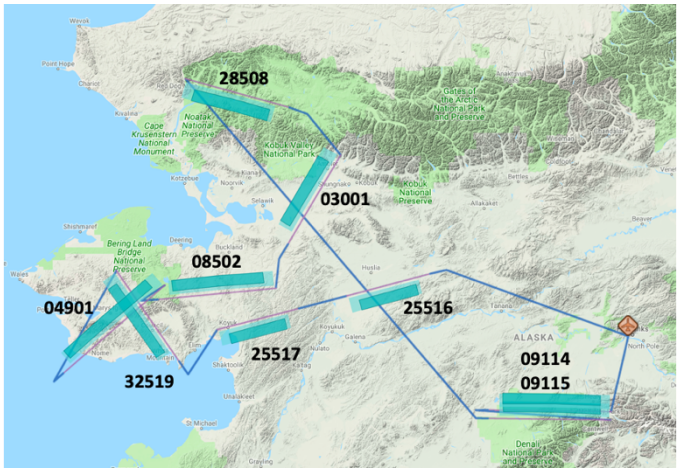

Figure S5. L-band SAR flight lines (light blue bars) collected during ABoVE for Region A2: Seward Peninsula and Northwest Interior. Flight line IDs are listed next to each line. Flight lines 09114 and 09115 are part of the Eastern Interior (Region A3) collection but were acquired during this sortie due to extra available flight time. © Google Maps

Line 25516: Huslia. The Huslia flight line overlaps the legacy line 25509 (**Table S35**). Located south of Huslia, AK in the Koyukuk NWR, it extends ~100 km parallel to the Yukon River. It samples low mountains, taiga, and boreal wetlands.

Line 25517: Koyuk. The Koyuk flight line overlaps the legacy line 25510 (**Table S35**). It starts about 60 km west of Koyukuk, AK and extends ~125 km over the coastal mountains to Koyuk, AK on Norton Bay. It is anchored by the GTN-P borehole at Koyuk (TSP.768).

Line 32519: Council. The Council flight line overlaps the legacy line 32511 (**Table S35**). It extends ~160 km from Golovin, AK on the Norton Sound over Council and past Kougarok, AK into the heart of the Seward Peninsula, overlapping with the Teller lines (04806 and 04901) near Kougarok, AK. It is anchored by the DOE NGEE-Arctic Council watershed; CALM sites at Council (U27) and Kougarok (U28); GTN-P boreholes at White Mountain (TSP.771) and Last Bridge (TSP.1188); and the Council flux tower (US-NGC) [Dengel et al. 2020]. Detailed digital elevation maps, soil moisture, active layer

thickness, and surface classification data from the NGEE-Arctic team provide same day validation for the ABoVE airborne SAR measurements and joint analysis of these data constitute a major component of the ABoVE – NGEE-Arctic scientific partnership [Wilson et al. 2018].

Lines 04806 and 04901: Teller. The Teller flight lines start in the Norton Sound just north of Sledge Island and extend inland ~190 km northeast past Kougarok towards Upper Hanum Creek, overlapping with the Council flight line (32519) near Kougarok. Flight line 04901 is anchored by the DOE NGEE-Arctic Teller and Kougarok watersheds; GTN-P boreholes at Pilgrim Hot Springs (TSP.1803), Kuzitin River (TSP.1189), and Last Bridge (TSP.1188). Flight line 04806 overflies the Teller watershed and the Kougarok (U28) CALM site. This line also captures fire scars in the Kougarok area [Liljedahl et al. 2007; Iwahana et al. 2016; Tsuyuzaki et al. 2018]. Similar to the Council flight line (32519), these lines are key contributors to the ABoVE – NGEE-Arctic scientific partnership [Wilson et al. 2018].

NOTE: In 2017 there was a mismatch between the P-band and the L-band lines covering the Teller and Kougarok sites due to geographic projection errors on the Seward Peninsula present in the online flight planning system. As a consequence, L-band line 04806 created for the 2017 campaign captured Teller to some extent but missed Kougarok entirely, and it did not align with P-band line 04900. To correct this error, we created L-band line 04901 which was properly aligned with P-band line 04900. L-band line 04901 was acquired in 2018 and 2019. We lost year-to-year change detections compared to L-band 04806 but gained alignment with P-band 04900 and achieved better coverage of the NGEE-Arctic intensive field sites.

Line 08502: Kougar. The Kougarok flight line overlaps the legacy line 08534 (**Table S35**). It extends ~145 km from the center of the Seward Peninsula to the edge of the western Interior. It overflies a mix of mountainous terrain and low-lying Bering Taiga.

Line 03001: Ambler. The Ambler flight line overlaps the legacy line 03108 (**Table S35**). It starts about 50 km southeast of Selawik, and extends ~145 km northeast past Ambler and into the southern Brooks Range. It is anchored by GTN-P boreholes at Kugurak Cabin Tundra (TSP.1802) and Ambler (TSP.780). This line samples areas of continuous permafrost.

Line 28508: Noatak. The Noatak flight line travels ~100 km parallel to the southern edge of the Brooks Range along the upper Noatak River from Kelly Bar Airport to Mount Angayukaqsraq. This flight line monitors post-fire recovery recorded at ~80 ground plots [Loboda et al. 2017] and classified for fractional cover of fuel types [He et al. 2019a,b]. It was not collected in 2019.

Table S10. Region A2: Seward Peninsula and Northwestern Interior L-band Line Summary Data

Line ID	Short Name	Flight	Date	Comments
25516	Huslia	22035 19062 18054 17097 17067	2022-08-19 2019-09-12 2018-09-01 2017-09-15 2017-06-19	Interior Alaska, Huslia village
25517	Koyuk	22035 19062 18054 17097 17067	2022-08-19 2019-09-12 2018-09-01 2017-09-15 2017-06-19	Interior Alaska, boreal forest, coastal mountains
32519	Council	22035 19062 18054 17097 17067	2022-08-19 2019-09-12 2018-09-01 2017-09-15 2017-06-19	NGEE-Arctic Council watershed and flux tower; Kougarok watershed
04806	Teller	22035 19062 17097 17067	2022-08-19 2019-09-12 2017-09-15 2017-06-19	NGEE-Arctic Teller watershed, Kougarok watershed, Kougarok area fire disturbance/recovery
04901	Teller	22035 19062 18054	2022-08-19 2019-09-12 2018-09-01	NGEE-Arctic Teller watershed, Kougarok watershed, Kougarok area fire disturbance/recovery
08502	Kougar	22035 19062 18054 17097 17067	2022-08-19 2019-09-12 2018-09-01 2017-09-15 2017-06-19	Seward Peninsula CALM sites, boreholes
03001	Ambler	22035 19062 18054 17097 17067	2022-08-19 2019-09-12 2018-09-01 2017-09-15 2017-06-19	Boreal forest-foothills gradient, boreholes
28508	Noatak	22035 18054 17097 17067	2022-08-19 2018-09-01 2017-09-15 2017-06-19	Fire disturbance/recovery

2.3 Region A3: Eastern Interior

Figure S6 shows the transects for Region A3: The Eastern Interior. Details for individual L-band SAR flight lines are given in **Table S11**; the P-band acquisition details are given in **Table S23**. ABoVE flight lines in the Eastern Interior capture the dense concentration of ground-based science infrastructure including: the NEON sites at Delta Junction, AK, the Caribou/Poker Creek Research Watershed, and Healy, AK; the NSF Boreal Forest LTER site at Bonanza Creek; and National Park Service sites in the Denali National Preserve. Additionally, the flight lines in the Yukon Flats NWR overlap legacy acquisitions of permafrost state [Minsley et al. 2012] as well as water surface elevation (WSE) observations by AirSWOT [Pitcher et al. 2019a,b]. ABoVE SAR data provide characterizations of the boreal forest and enable comparisons and fusion with the extensive airborne LiDAR data acquired throughout the Eastern Interior, particularly by NASA's LVIS [Blair et al. 2018] and G-LiHT [Alonzo et al. 2020; Chen et al. 2020] systems. A detailed analysis of the tomographic SAR (tomoSAR) flights over Delta Junction, AK (**Table S12, Table S24**) is given in Section 6 of the main text.

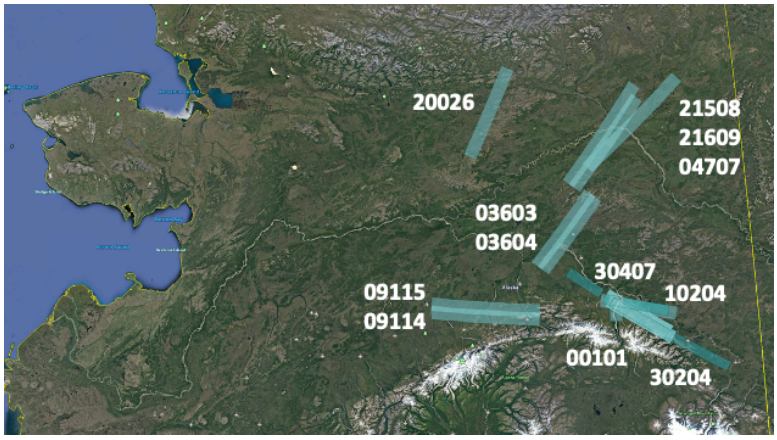

Figure S6. L-band SAR flight lines (light blue bars) collected during ABoVE for Region A3: Eastern Interior. Flight line IDs are listed next to each line. Given the proximity to the PAFA base of operations, these flight lines were typically acquired on multiple sorties during each campaign. The Delta Junction tomoSAR flight lines (Table S12) overlap with the northern end of Line 30204. © Google Earth

Line 20026: Coldfo. The Coldfoot flight line overlaps the legacy line 20015 (**Table S32**). It extends ~175 km from the southern edge of the Brooks Range near Linda Creek Airport southwest along the Dalton Highway over the villages of Coldfoot and Prospect Creek, terminating in the mountains north of the Yukon River. It is anchored by the CALM site at Old Man (U16) and GTN-P boreholes at Coldfoot (TSP.834) and Old Man (TSP.749). Vegetation is a combination of upland tundra and boreal forest covering discontinuous permafrost.

Lines 21508 YFlatW and 21609 YflatE; 04707: FtYuko. These three flight lines survey the Yukon Flats NWR and its complex permafrost wetland systems. Flight lines 21508 and 21069 sample along AEM reconnaissance lines collected by Minsley et al. [2012] to characterize areas of continuous and discontinuous permafrost. Flight line 04707 covers the Fort Yukon area where Minsley et al. acquired high density AEM survey lines. These lines also overlap with the AirSWOT airborne Ka-band survey of over 3300 km2 acquired in June 2015 [Pitcher et al. 2019a,b] and the ABoVE AirSWOT airborne Ka-band data acquired in June and Aug 2017 [Fayne et al. 2019, 2020; Kyzivat et al. 2019]. Extensive on-water validation data were acquired in 2017 and 2018.

Lines 03603 BonanW and 03604 BonanE. The Bonanza Creek lines extend ~150 km over the city of Fairbanks, Alaska within the interior boreal forest, an area of discontinuous permafrost. This area supports extensive scientific infrastructure due to its proximity to Fairbanks and its road network. The lines are anchored by the Bonanza Creek Experimental Forest and Caribou Poker Creek Watershed (both associated with the NSF Bonanza Creek Long Term Ecological Research (BNZ LTER) area); the NEON D19 taiga field site at the Caribou-Poker Creek Research Watershed (BONA); the US Army Corps of Engineers Cold Regions Research and Engineering Laboratory (CRREL) Permafrost Tunnel Research Facility [Douglas et al. 2019; 2020; 2021]; multiple boreal flux towers (see [Euskirchen and Edgar 2014-2016a,b,; Euskirchen and Edgar, 2015-2016; Kobayashi et al. 2011]); and the NOAA Global Monitoring Laboratory Earth System Research Laboratories Tall Tower in Fox, AK (CRV) [Karion et al. 2016]. Additional field measurements within the lines include multiple US Forest Service Cooperative Alaska Forest Inventory (CAFI) field sites [Malone et al. 2009]; measurements of carbon flux, winter respiration, and thaw depth [see Minions et al. 2019; and Natali et al. 2018]; numerous CALM sites; and a U.S. Climate Reference Network site (Fairbanks 11 NE). This region also contains a rich fire history with multiple burned areas. These survey lines have also been imaged by LVIS, AVIRIS, AirSWOT, CFIS and G-LiHT as part of the ABoVE airborne campaign [Miller et al. 2019].

Mitigation due to a no-fly implemented in 2022: The BonanW_03603 L-band flight line images ground sites where long-term observations are made by multiple state and federal agencies. ABoVE acquired L-band data along this flight line in 2017, 2018, and 2019, creating a time series that captures rapid change across these sites. Following the 2019 flights, a FAA no-fly zone centered on Murphy Dome was created at the request of DOD. ABoVE requested a waiver so that NASA could continue this time series of airborne observations with L-band SAR flights in August 2022. The request was not granted. Consequently, we designed two new lines to mitigate the impact of the exclusion zone and to cover the established ground sites: **BonanW_03603b** and **BonanA_05605**. BonanW_03603b is a shorter version of BonanW_03603. Data acquired in 2022 (and any subsequent years) image about 86 km of the northeast end of the original line and are suitable for InSAR or other intercomparisons with pre-2022 acquisitions of bonanW_03603. BonanA_05605 covers the ground sites that were lost from the southwest end of BonanW_03603, but at a different look angle. BonanA_05605 also provides a new look angle for some of the key sites imaged in BonanE_03604.

Lines 09115: DenalN and 09114: DenalS. The Denali lines run east-west for ~180 km from near Lake Minchumina in the west, across the Denali National Preserve, and past Healy, AK. These lines are anchored by vegetation structure and composition inventory and monitoring sites managed by the National Park Service (https://www.nps.gov/im/cakn/dena.htm); the NEON D19 taiga field site at Healy, AK (Healy); and the Eight Mile Lake flux tower (US-EML; Schuur 2008-). The SAR acquisitions support ABoVE field teams investigating winter respiration [Minions et al. 2019; and Natali et al. 2018] and permafrost dynamics [Schuur et al. 2009; Natali et al. 2014; Plaza et al. 2019].

Lines 00101: DJNEON, 30407: DeltJA, 10204: DeltJB, and 30204: DeltJC. The Delta Junction lines survey extensively studied boreal forest sites in Interior Alaska clustered near Delta Junction, AK. This is an area of discontinuous permafrost extent with low ground ice content, blanketed by a mosaic of fire

disturbances. The Delta Junction lines are anchored by the NEON D19 taiga field site at Delta Junction, AK (DEJU); airborne electro-magnetic (AEM) surveys conducted by the Alaska Division of Geological and Geophysical Surveys [Burns et al. 2008]; and numerous US Forest Service Cooperative Alaska Forest Inventory (CAFI) field site locations [Malone et al. 2009]. Additionally, both L- and P-band tomoSAR data were acquired over Delta Junction to test boreal forest structural characterization algorithms (**Table S12, Table S24**). The tomoSAR data are detailed in Section 6 of the main text.

Line 21612: HDZAOI (new in 2022). The Husky Drop Zone line covers an area of interest ~25 km southeast of Fairbanks (**Figure S7**). The Husky Drop Zone exhibits signs of active permafrost degradation and disturbance (clearing) in the area has led to top-down thaw of permafrost. Drilling in the summer of 2022 confirmed that the top of near-surface permafrost in the Husky Drop Zone clearing is ~10m below the ground surface while the top of near-surface permafrost in undisturbed forested areas nearby is 1-3 m depth. Each summer new thaw pits are exposed and polygonal ground features expand. The area has been extensively studied by the US Army Corps of Engineers Cold Regions Research and Engineering Laboratory (CRREL) for the past ten years. Activities include repeat acquisitions of airborne LiDAR, electrical resistivity tomography, ground penetrating radar, drilling, and manual thaw depth measurements [Douglas et al. 2016].

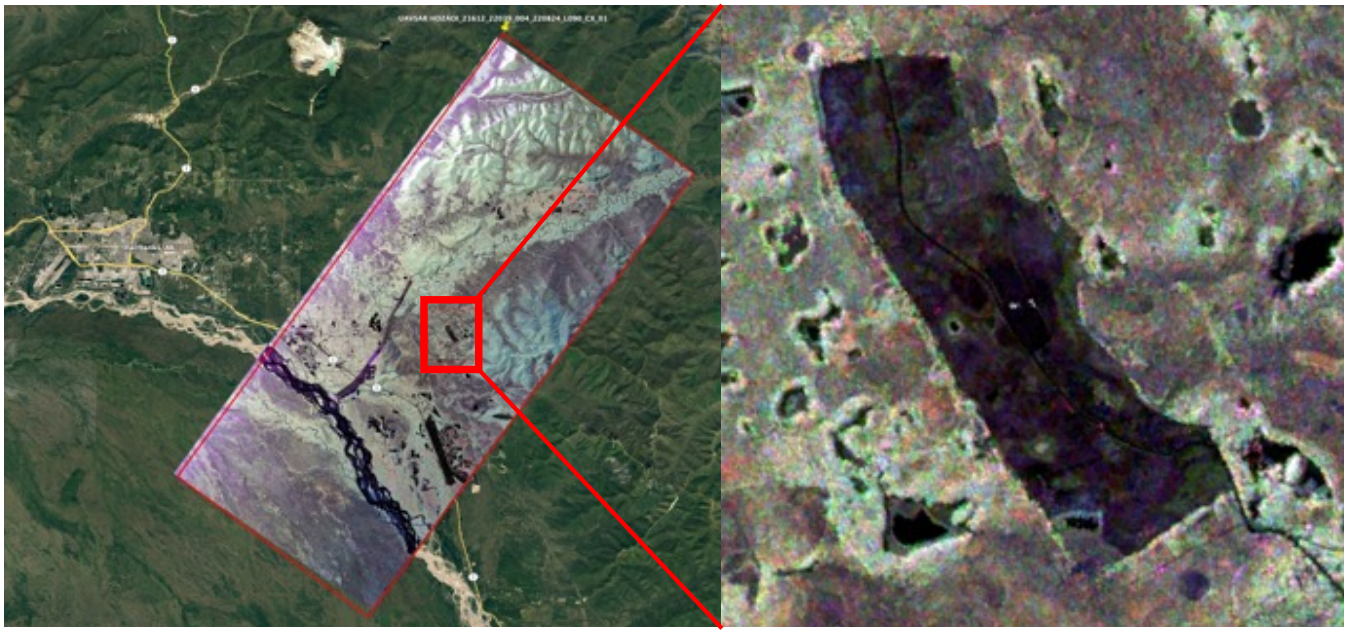

Figure S7. LEFT: Quicklook image for the L-band SAR acquisition over Husky Drop Zone (HDZAOI_21612). Fairbanks is seen on the left side of the image. RIGHT: Detail showing the distinctly different surface reflectance properties inside the HDZ due to permafrost degradation. The image is ~1000 m x 1000 m. © Google Earth.

Table S11. Region A3: Eastern Interior L-band Line Summary

Line ID	Short Name	Flight Plan	Date	Comments
20026	Coldfo	22036 19063 18050 17097 17067	2022-08-20 2019-09-13 2018-08-26 2017-09-15 2017-06-19	CALM and GTN-P sites; tundra-taiga ecotone
21508	YflatW	22037 19064 17098 17069	2022-08-22 2019-09-14 2017-09-16 2017-06-21	Overlap with AEM surveys, AirSWOT and in situ water surface elevation measurements
21609	YflatE	22037 19064 18051 17098 17069	2022-08-22 2019-09-14 2018-08-27 2017-09-16 2017-06-21	Overlap with AEM surveys, AirSWOT and in situ water surface elevation measurements
04707	FtYuko	22037 19064 18051 17098 17069	2022-08-22 2019-09-14 2018-08-27 2017-09-16 2017-06-21	Overlap with AEM surveys, AirSWOT and in situ water surface elevation measurements
03603	BonanW	22039 19065 19064 19063 19062 19061 18051 17100 17065	2022-08-24 2019-09-16 2019-09-14 2019-09-13 2019-09-13 2019-09-12 2018-08-27 2017-09-19 2017-06-16	Bonanza Creek LTER site, LiDAR over burn recovery scars
03604	BonanE	22039 19064 19063 19062 18051 17100 17065	2022-08-24 2019-09-14 2019-09-13 2019-09-13 2018-08-27 2017-09-19 2017-06-16	Bonanza Creek LTER site, LiDAR over burn recovery scars
05605	BNZalt	22039	2022-08-24	Additional Bonanza Creek area line collected in 2022 to mitigate against omissions in truncated line 03603 due to a temporary no broadcast rule

09115	DenalN	19064 18052 17100 17066	2019-09-14 2018-08-28 2017-09-19 2017-06-17	National Park Service ground sites
09114	DenalS	22039 22038 19064 18052 17100 17065	2022-08-24 2022-08-23 2019-09-14 2018-08-28 2017-09-19 2017-06-16	National Park Service ground sites
00101	DJNEON	22034 19064 18051 17095 17064	2022-08-18 2019-09-14 2018-08-27 2017-09-10 2017-06-15	NEON D19 taiga field site near Delta Junction, AK
30407	DeltJA	22034 19061 18049 17095 17064	2022-08-18 2019-09-12 2018-08-24 2017-09-10 2017-06-15	Delta Junction, AK boreal forest
10204	DeltJB	22034 19061 18049 17101 17100 17095 17064	2022-08-18 2019-09-12 2018-08-24 2017-09-20 2017-09-19 2017-09-10 2017-06-15	Delta Junction, AK boreal forest
30204	DeltJC	22034 19061 18052 17100 17066	2022-08-18 2019-09-12 2018-08-28 2017-09-19 2017-06-17	Delta Junction, AK boreal forest
21612	HDZAOI	22039	2022-08-24	Husky Drop Zone AOI – Permafrost degradation

Table S12. Delta Junction L-band TomoSAR Flight Lines

Line ID	Short Name	Flight Plan	Date	Comments
12237	DeltaA	17101	2017-09-20	TomoSAR offset 36 meters
30232	DeltaA	17101	2017-09-20	TomoSAR offset 36 meters
12239	DeltaC	17101	2017-09-20	TomoSAR offset 50 meters
30234	DeltaC	17101	2017-09-20	TomoSAR offset 50 meters
12240	DeltaD	17101	2017-09-20	TomoSAR offset 57 meters
30235	DeltaD	17101	2017-09-20	TomoSAR offset 57 meters
12241	DeltaE	17101	2017-09-20	TomoSAR offset 64 meters
30236	DeltaE	17101	2017-09-20	TomoSAR offset 64 meters
12242	DeltaF	17101	2017-09-20	TomoSAR offset 71 meters
30237	DeltaF	17101	2017-09-20	TomoSAR offset 71 meters
12243	DeltaG	17101	2017-09-20	TomoSAR offset 83 meters
30238	DeltaG	17101	2017-09-20	TomoSAR offset 83 meters
30239	DeltaH	17101	2017-09-20	TomoSAR offset 119 meters
12227	DeltaR	17101	2017-09-20	TomoSAR Reference Line 41k
30221	DeltaR	17101	2017-09-20	TomoSAR Reference Line 41k

2.4 Region A4: Southwest Alaska and the Yukon-Kuskokwim Delta

Figure S8 shows the transects for Region A4: Southwest Alaska and the Yukon-Kuskokwim Delta. Details for individual L-band flight lines are given in **Table S13**; the P-band acquisition details are given in **Table S25**. ABoVE surveys in southwest Alaska were anchored by climate monitoring sites from the Southwest Alaska Inventory & Monitoring Network (SWAN). SWAN consists of five parklands in Southwest Alaska: Alagnak National Wild River, Aniakchak National Monument and Preserve, Katmai National Park and Preserve, Kenai Fjords National Park, and Lake Clark National Park and Preserve [Bennett et al. 2006]. Surveys in the Yukon-Kuskokwim Delta were designed to capture field sites where ABoVE researchers were measuring the impacts of fire disturbance on active layer thickness, soil moisture, and other permafrost state variables [Liu et al. 2014; Michaelides et al. 2019] as well as CO2 and CH4 fluxes [Natali et al. 2018]. The Innoko Flats NWR flight line in the lower Yukon Valley surveyed a vast palsa-wetlands complex with permafrost in various stages of degradation [Johnston et al. 2014; Jones et al. 2017]. The Poorman (08911) flight line covered a forested area of the western Interior with extensive tree ring data [Hoy et al. 2018].

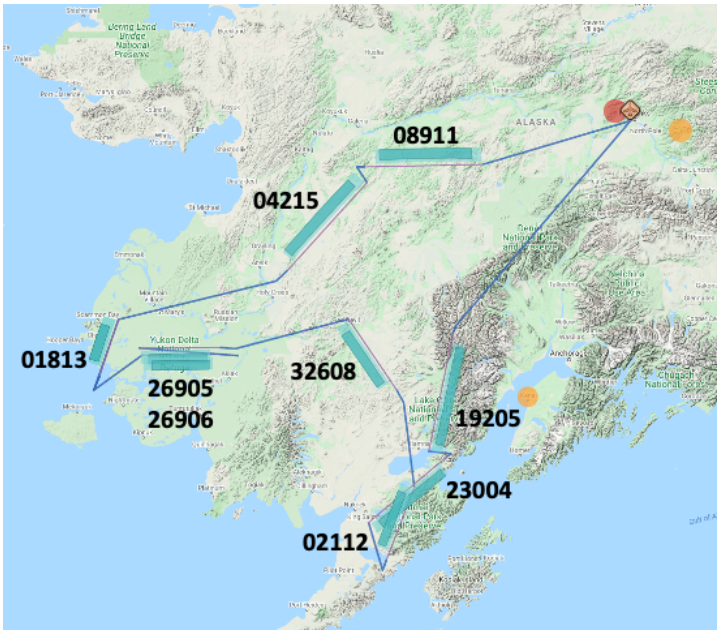

Figure S8. Flight Plan 19066, flown 17 Sep 2019, showing the L-band SAR flight lines in Southwest Alaska and the Yukon-Kuskokwim Delta. Line 28020 (KatmaB) was omitted from this plan due to aircraft endurance limitations. © Google Maps

Line 19205: Lclark The Lake Clark line extends ~200 km from the Chigmit Mountains southwest across the Lake Clark National Park and Preserve to the shores of Iliamna Lake, terminating near Iliamna, AK. The line is anchored by the SWAN/Lake Clark inventory and monitoring sites (LACL) and the U.S. CRN site at Port Alsworth, AK (AK Port Alsworth 1 SW). It is covered by an assortment of conifer forests, sedge meadows, salt marshes and lagoons.

Lines 23004: KatmaA; **28020: KatmaB; 02112: KatmaC** These three lines crisscross the Katmai National Park and Preserve, on the northern portion of the Alaska Peninsula, survey portions of two physiographic provinces—the Aleutian Range and the Nushagak-Bristol Bay Lowlands, and overpass the Naknek Lake. These lines are anchored by ~50 SWAN inventory and monitoring sites (KATM) and the U.S. CRN site at King Salmon, AK (AK King Salmon 42 SE). The 2022 Copper Creek fire destroyed one of the SWAN network sites in July 2022, but observations were continued and the 02112 line captured immediate post-fire conditions in August 2022

Line 32608: Sriver. The Sleetmute line extends ~130 km from the Nushagak Hills of southern Alaska northwest over the Kuskokwim and Holitna Rivers past Sleetmute, AK and terminates near Red Devil Airport. This line is anchored by ~130 tree core sampling sites and supports boreal forest remote sensing studies [Saatchi et al. 2019].

Lines 26905 YKDelA and 26906 YKDelB. The Yukon-Kuskokwim Delta lines extend ~130 km each, surveying east-west transects of discontinuous permafrost in the Bering Tundra ecoregion northwest of Bethel, AK. These lines are specifically designed to map large tundra fire scars from 2015 to evaluate the impacts of fire on the permafrost state and carbon fluxes. The lines are anchored by CO2 and CH4 summer flux and winter respiration measurements [Minions et al. 2019; and Natali et al. 2018]; ground penetrating radar transects [Michaelides et al. 2019]; and vegetation composition across fire history gradients [Frost et al. 2020].

Line 01813: Chevak. The Chevak line extends ~85 km from the Bering Sea coast just west of Hazen Bay north over Chevak, AK across the Yukon-Kuskokwim Delta, ending just east of Scammon Bay. The line is anchored by a 2009 LiDAR survey conducted for the US Fish and Wildlife Service [Airborne Imaging, 2011] and field data collected in 2016 to map sporadic permafrost in the area [Whitley et al. 2018a,b]. This region is defined by its flat coastal plain with elevated permafrost plateaus throughout the floodplain and is a critical waterfowl habitat.

Line 04215: Innoko The Innoko line extends ~175 km northwest from Shageluk, AK across the Innoko Flats National Wildlife Refuge. The line is anchored by field sites established to study permafrost thaw chronosequences [Jorgenson 2013] and carbon fluxes [Johston et al. 2014; Jones et al. 2017]. Much of the area is underlain by permafrost, and over half is covered by wetlands, thermokarst bogs, and fens [Woodward et al. 2011]. Over 100,000 ha of the Lower Innoko River area burned in 2015 [Potter et al. 2018], making this an area for potential long-term study.

Line 08911: Poorma The Poorman line extends ~170km, starting south of the Yukon River near Galena, AK and running west through discontinuous permafrost and boreal forest of the Nowitna National Wildlife Refuge, slightly north of the village of Poorman, AK. This line is anchored by more than 250 tree core sampling sites [Hoy et al. 2018]. It is an acquisition of opportunity, lying along the return route from the Yukon-Kuskokwim Delta back to Fairbanks, AK.

Table S13. Region A4: Southwest Alaska and the Yukon-Kuskokwim Delta L-band Flight Line Summary

Line ID	Short Name	Flight Plan	Date	Comments
19205	Lclark	22038 19066 17099 17066	2022-08-23 2019-09-17 2017-09-17 2017-06-17	National Park Service SWAN ground sites

		17065	2017-06-16	
23004	KatmaA	22038 19066 17099 17065	2022-08-23 2019-09-17 2017-09-17 2017-06-16	National Park Service SWAN ground sites
28020	KatmaB	17099 17065	2017-09-17 2017-06-16	National Park Service SWAN ground sites
02112	KatmaC	22038 19066 17099 17065	2022-08-23 2019-09-17 2017-09-17 2017-06-16	National Park Service SWAN ground sites
32608	Sriver	22038 19066 18052 17099 17066	2022-08-23 2019-09-17 2018-08-28 2017-09-17 2017-06-17	Snake River tree rings sampling
26905	YKDelA	22038 19066 18052 17099 17066	2022-08-23 2019-09-17 2018-08-28 2017-09-17 2017-06-17	YK Delta 2015 fire scars; POLARIS portable flux towers/flux chambers; GPR transects; soil moisture measurements
26906	YKDelB	22038 19066 18052 17099 17066	2022-08-23 2019-09-17 2018-08-28 2017-09-17 2017-06-17	YK Delta 2015 fire scars; POLARIS portable flux towers/flux chambers; GPR transects; soil moisture measurements
01813	Chevak	22038 19066 18052 17099 17066	2022-08-23 2019-09-17 2018-08-28 2017-09-17 2017-06-17	YK Delta wildlife survey; USGS LiDAR survey; ground measurements
04215	Innoko	22038 19066 18052 17099 17066	2022-08-23 2019-09-17 2018-08-28 2017-09-17 2017-06-17	Permafrost surveys; extensive bog/fen/wetland complex
08911	Poorma	22038 19066 18052 17099 17066	2022-08-23 2019-09-17 2018-08-28 2017-09-17 2017-06-17	Interior Alaska, boreal forest

3 Canadian Flight Lines

The Canadian SAR flight lines (**Figure S1**) are broken into six regional collections: C1) Lower Mackenzie Valley and Northern Yukon Territory, C2) Southern Yukon Territory, C3) Upper Mackenzie Valley, C4) Great Slave Lake Region, C5) Transboundary Watershed, and C6) Southern Boreal Forest/BERMS. Legacy L- and P-band flight lines in the BERMS area from the CANEX 2010 campaign [Magagi et al. 2012] and the AirMOSS EV-S1 investigation [Chapin et al. 2012; 2018] provide the potential to establish longer time series.

3.1 Region C1: Lower Mackenzie Valley and Northern Yukon Territory

Figure S9 shows the flight lines for Region C1: Lower Mackenzie Valley and Northern Yukon Territory. Details for individual L-band PolInSAR flight lines are given in **Table S14**; the P-band acquisition details are given in **Table S26**. Region C1 features flight lines that overlap the Mackenzie River Valley transects for the CALM and GTN-P networks, annual GNWT/CFS forest health surveys, megaslumps on the Peel Plateau [Kokelj et al. 2015; Kokelj et al. 2017], and multiple legacy LiDAR surveys. The Mackenzie Delta and the Inuvik-Tuktoyaktuk corridor have been extensively targeted by RadarSat and RadarSat-2 [Touzi et al. 2019] and include the Havipak and Trail Valley Creek [Wilcox et al. 2019; Walker et al. 2020] field sites. The lines in the northern Yukon Territory survey the Old Crow Flats/Porcupine River wetlands complex.

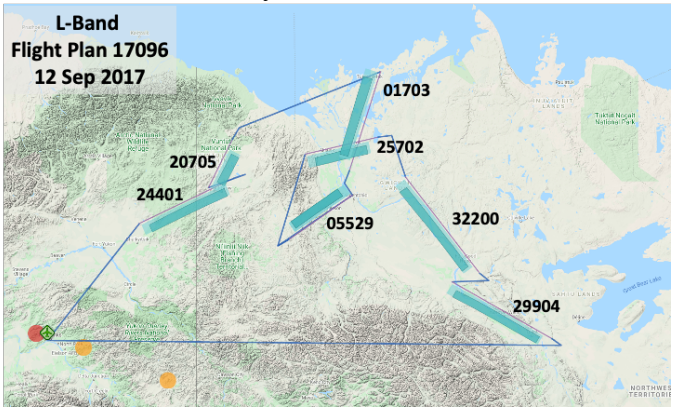

Figure S9. L-band Flight Plan 17096 flown on 12 September, 2017 over Region C1. These lines cover the Lower Mackenzie Valley, the Mackenzie Delta, and the Old Crow/Porcupine River wetlands in the Norther Yukon Territory. © Google Maps

Line 29904: Nwells. The Norman Wells flight line begins about 20 km southeast of Tulita and extends ~225 km northwest along the Mackenzie River past Norman Wells and terminates north of Mountain River. It is anchored by CALM sites at Mountain River (thaw tube, C9A), Pump Station/Norman Wells (C10), Norman Wells grid and thaw tube (C11), and Great Bear River/Tulita (C12) as well as GTN-P boreholes clustered in and around Norman Wells: Pump Station-1 (TSP.257), KP2 offrow (TSP.278), KP5 offrow (TSP.279), Kee Scarp (TSP.276, TSP.288), and Canyon Creek (TSP.258, TSP.259, TSP.260, TSP.261, TSP.262). Oil exploration and production facilities fan out from Norman Wells. The landscape is dominated by coniferous forest atop discontinuous permafrost.

Line 32200: FtGood. The Fort Good Hope flight line begins southeast of Fort Good Hope and then extends ~225 km northwest along the Mackenzie River past the bend at Thunder River. This flight line provides critical coverage of bioclimatic gradients along the lower Mackenzie River Valley even though there are no long-term monitoring sites in this transect. The landscape is dominated by coniferous forest atop discontinuous permafrost.

Line 25702: Aklavik. The Aklavik flight line begins east of Inuvik and extends ~125 km west across the middle of the Mackenzie Delta past Aklavik and then onto the Peel Plateau. It is anchored by a 2008 legacy LiDAR survey [Marsh et al. 2009] which can be used to assess changes over time in the digital elevation map [Whalen et al. 2009], water surface elevation [Hopkinson et al. 2011], and open water masks [Crasto et al. 2015] as well as to characterize vegetation cover gradients across the Delta and into the neighboring tundra environments. Comparisons are also possible with the extensive RadarSat and RadarSat-2 acquisitions.

Line 05529: FtMcPh. The Fort McPherson flight line begins in the Yukon Territory, ~25 km east of Yukon – Northwest Territories border, then extends ~135 km northeast following the Dempster Highway across the Peel Plateau past Fort McPherson to the main channel of the Mackenzie River. It is anchored by a legacy LiDAR survey along the Dempster Highway [NWT Center for Geomatics, personal communication]. This line offers opportunities to quantify mass flow and expansion of the numerous megaslumps – retrogressive thaw slumps greater than 10 ha – that have formed in the Peel Plateau's Stony Creek watershed as a result of catastrophic permafrost degradation [Kokelj et al. 2015; Kokelj et al. 2017]. Additionally, this flight line enables the study of the transition from dense boreal forest in the southern edge of the Mackenzie Delta to the tundra of the Peel Plateau. Of particular interest are the fluvial drainages that extend tree lined tendrils deeper into the Peel Plateau than observed in adjacent terrain. Access from the Dempster Highway to many sites along this flight line offer the potential for future ground-based work to complement the SAR acquisitions.

Line 01703: TukHwy. The Tuktoyaktuk Highway flight line begins ~25 km southwest of Inuvik, NT then extends ~170 km northeast following the Inuvik-Tuktoyaktuk Highway past Tuktoyaktuk, NT to the Arctic Ocean. It is anchored by a series of RadarSat-2 acquisition tiles, a legacy LiDAR survey along the Highway [NWT Center for Geomatics, personal communication], and a legacy LiDAR survey over Trail Valley Creek [Marsh et al. 2010]. Intensive field data collections were conducted by members of the Canada Centre for Remote Sensing (CCRS) along the ITH in 2016 and again in 2017 during the airborne P-band and L-band overflights. iButton temperature data loggers were installed in many sites along the ITH to measure the annual variations of near-surface soil temperature. These measurements enabled estimates of the active layer thickness [Zhang et al. 2021] and were combined with the field data collected in 2017 to validate the ALT retrievals from polarimetric L-band (ALOS2 and UAVSAR) and P-band (AIRMOSS). Preliminary results using the Touzi decomposition (Touzi et al. 2009; 2021a) to analyze these data suggests that polarimetric L-band measurements permit the characterization of permafrost ALT at depths up to 50 cm, while P-band measurements permits the characterization of even deeper permafrost [Touzi et al. 2021b]. Similar results were found for enhanced mapping discontinuous permafrost and peatlands North Alberta [Touzi et al. 2018; 2019b]. The airborne SAR data complement studies of Arctic Ocean shoreline degradation near Tuktoyaktuk [Banks et al. 2012; 2014] and lake drainage events [Marsh et al. 2009]. Tundra vegetation cover on the Tuktoyaktuk Peninsula has also been characterized using multi-frequency X-, C-, and L-bands [Ullmann et al. 2017]. This flight line also captures the Canadian Changing Cold Regions Network (CCRN) site at Trail Valley Creek and the ShrubTundra sites about 28 km north of Inuvik used to study shrub expansion [Myers-Smith et al. 2011]. Access from the Inuvik-Tuktoyaktuk Highway to many

sites along this flight line offer the potential for ground-based work to complement the SAR acquisitions.

Lines 20705: OldCrA and 24401: OldCrB. The Old Crow A flight line travels ~80 km across the Old Crow Flats, a Ramsar wetland of International Importance in the northern Yukon Territory, terminating near the village of Old Crow, YT. This line covers multiple long-term field sites used to assess thermokarst induced changes in lake area [Lantz et al. 2015]. The Old Crow B flight line originates northeast of Old Crow and then extends ~185 km southwest along the Porcupine River towards Chaklyitsik, AK.

Table S14. Region C1: Lower Mackenzie Valley and Northern Yukon Territory L-band Flight Line Summary

Line ID	Short Name	Flight Plan	Date	Comments
29904	Nwells	17096 17068	2017-09-12 2017-06-20	CALM and GTN-P borehole sites; oil exploration and production near Norman Wells
32200	FtGood	22037 19065 17096 17070 17068	2022-08-22 2019-09-16 2017-09-12 2017-06-22 2017-06-20	Boreal forest and fire disturbance; wetlands and water surface elevation (WSE)
25702	Aklavi	22037 19065 18053 17096 17070	2022-08-22 2019-09-16 2018-08-29 2017-09-12 2017-06-22	Legacy LiDAR and RadarSat data; Makenzie Delta WSE
05529	FtMcPh	22037 19065 18053 17096 17070	2022-08-22 2019-09-16 2018-08-29 2017-09-12 2017-06-22	Legacy LiDAR data; retrogressive thaw megaslumps
01703	TukHwy	22037 19065 18053 17096 17068	2022-08-22 2019-09-16 2018-08-29 2017-09-12 2017-06-20	Legacy LiDAR and RadarSat data; Trail Valley Creek site; ShrubTundra sites
20705	OldCrA	22037 19065 18053 17096 17068	2022-08-22 2019-09-16 2018-08-29 2017-09-12 2017-06-20	Long-term monitoring of thermokarst-driven lake change
24401	OldCrB	22037	2022-08-22	Old Crow; Porcupine River

		19065 18053 17096 17068	2019-09-16 2018-08-29 2017-09-12 2017-06-20	

3.2 Region C2: Southern Yukon Territory

Figure S10 shows the flight lines for Region C2: Southern Yukon Territory. Details for individual L-band SAR flight lines are given in **Table S15**; the P-band acquisition details are given in **Table S27**. These lines form a transect across the Boreal Montaigne ecoregion linking Boreal Interior (A3) and Continental Boreal (C3) – an important bioclimatic gradient. They also cover intensively studied field sites at Watson Lake, YT, Wolf Creek, YT, and Kluane Lake, YT. These lines are typically acquired during transit between Yellowknife, NT and Fairbanks, AK.

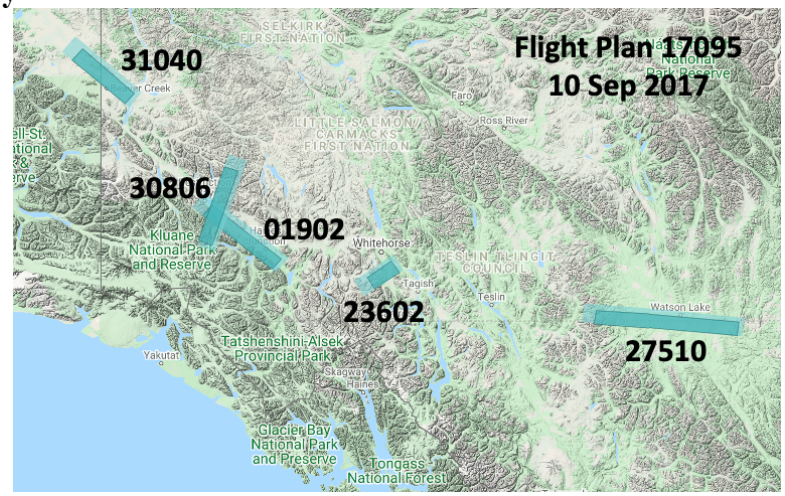

Figure S10. Flight lines across the southern Yukon Territory (Region C2) link the Eastern Interior of Alaska (Region A3) with the upper Mackenzie River Valley in the Northwest Territories (Region C3). © Google Maps

Line 27510: Watson. This ~200 km flight line is centered on Watson Lake, YT and travels east-west along the highway corridor. It is anchored by more than 50 permanent sampling plots from the Yukon Geological Survey Permafrost Monitoring Network [Lipovsky et al. 2014; Smith et al. 2017]. Land cover is predominantly boreal forest over sporadic discontinuous permafrost zone, where 10-50% of the terrain is underlain by permafrost, and permafrost appears to be degrading rapidly (mean annual temperature > -0.5º C) [Lipovsky et al. 2014].

Line 23602: WolfCr. The Wolf Creek flight line extends for ~55 km over the Wolf Creek Research Basin just south of Whitehorse, YT. This line is anchored by the four Wolf Creek flux towers and three permanent sampling plots from the Yukon Geological Survey Permafrost Monitoring Network [Smith et al. 2017]. Surface land cover consists of dense boreal forest at lower elevations, sparse forest, open meadow and shrub tundra at the higher elevations, and exposed alpine areas with mostly bare rock at the highest elevations. The trees in the lower elevation forests are some of the largest in the ABoVE domain (R. Janowicz, personal communication). Similar to Watson Lake, permafrost appears to be degrading rapidly (mean annual temperature > -0.5º C). Drunken forests surrounding the Whitehorse monitoring station are additional visual indicators of thawing or degrading permafrost [Lipovsky et al. 2014].

Lines 30806: KluanA and 01902: KluanB. The Kluane Lake flight lines are anchored by the Kluane Lake Research Station (KLRS) [Danby et al. 2014]. Flight line 30806 extends ~120 km along the length of Kluane Lake along the Alaska Highway past Haines Junction. It captures ~20 permanent sampling plots from the Yukon Geological Survey Permafrost Monitoring Network [Smith et al. 2017] as well as forests recovering after devastating spruce beetle infestation in the 1990s [Campbell et al. 2019]. Flight line 01902 is oriented perpendicular to the southern edge of the lake and extends ~110 km into the

forest on the eastern shore. This line captures Hyperion and Landsat imagery that has been used to study forest structure and treeline dynamics [Danby et al. 2003]. It also captures the Kaskawulsh Glacier as it feeds Slims River and Kluane Lake (**Figure S11**).

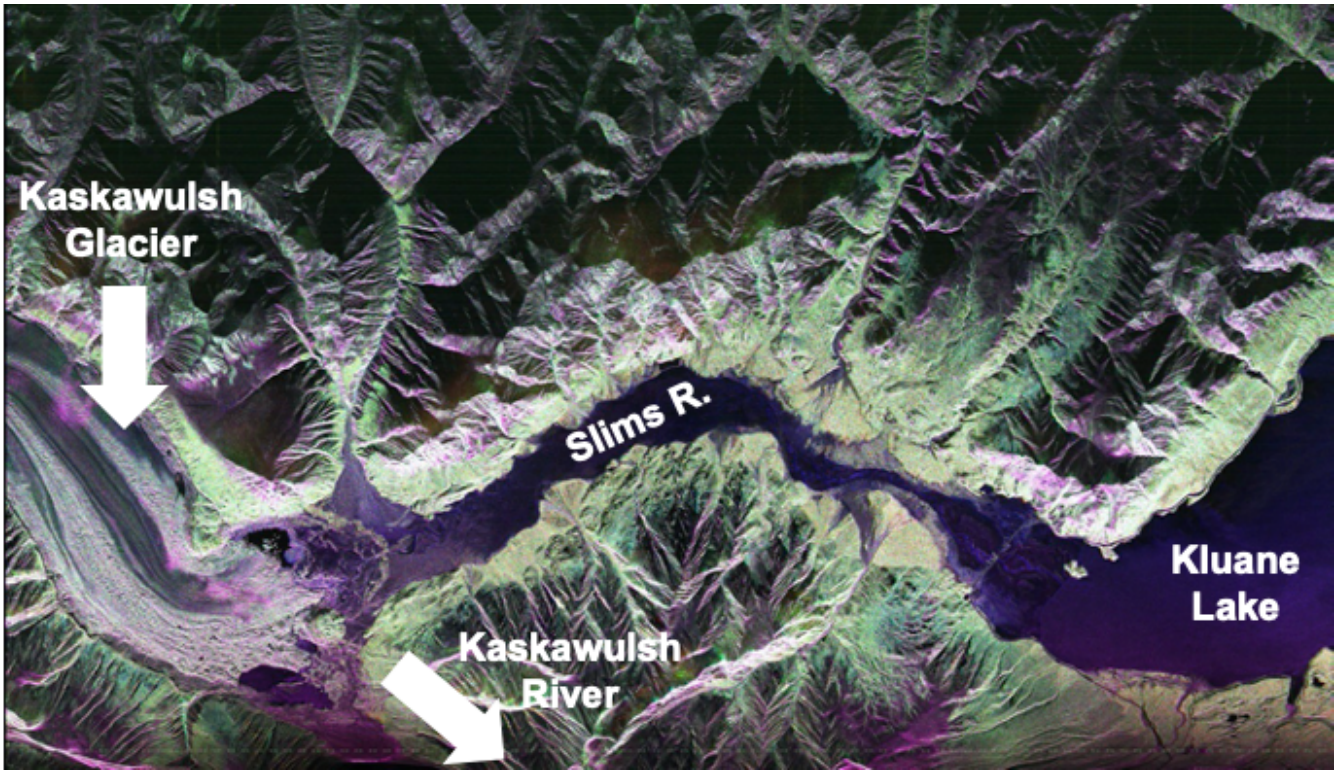

Figure S11. L-band SAR imagery from line 01902 collected 15 June 2017 clearly shows water flowing from the Kaskawulsh Glacier into the Slims River and Kluane Lake. "River Piracy" occurred abruptly in Spring 2016 when the Kaskawulsh Glacier retreated, triggering a shift in its melt which began flowing into the Kaskawulsh River rather than the Slims River. This resulted in a drop of ~1 meter in Kluane Lake level and radically altered the regional drainage pattern [Shugar et al. 2017].

Line 31040: SnagYK. The Snag flight line originates southeast of Snag, YT and travels ~95 km northwest along the Alaska Highway past Beaver Creek and across the border into Alaska. This line is anchored by five permanent sampling plots from the Yukon Geological Survey Permafrost Monitoring Network [Smith et al. 2017]. This line continues the series of flight lines that capture the bioclimatic gradients from Fairbanks, AK to Whitehorse, YT.

Lines 21611: GaribA and 03606 GaribB (new in 2022; not shown in Fig 9?). At the request of The Geological Survey of Canada, we added two new lines in British Columbia as the NASA aircraft transitioned from the ABoVE domain back to AFRC in Palmdale CA (Lines GaribA_21611 and GaribB_03606). These lines run parallel to each other for ~150 km on a NE-SW course which surveys from the Squamish River Delta to Lillooet. These lines characterize a particularly valued corridor in the

Coast Mountains of BC that is defined by varied geology, receding alpine glaciers, active fluvial processes, varied and changing vegetation. SAR imagery will be utilized by a variety of stake holders for the assessment of volcanic risks, active faulting, rapid onset alpine geohazards and ongoing glacier mass balance monitoring. Airborne hyperspectral imagery and LiDAR have been acquired over parts of the corridor to explore glacier change and other active geological processes in the area. The flight path prioritizes the high alpine setting including Warren Glacier, Overlord Glacier, Weart Glacier and Matier Glacier which are presently undergoing rapid retreat as a consequence of recent climate change.

Table S15. Region C2: Southern Yukon Territory L-band Flight Line Summary

Line ID	Short Name	Flight Plan	Date	Comments
27510	Watson	22034 19061 17095 17064	2022-08-18 2019-09-12 2017-09-10 2017-06-15	Watson Lake YT research nexus; YGS Permafrost Monitoring Network
23602	WolfCr	22034 19061 18049 17095 17064	2022-08-18 2019-09-12 2018-08-24 2017-09-10 2017-06-15	Wolf Creek Research Basin; YGS Permafrost Monitoring Network
30806	KluanA	22034 19061 18049 17095 17064	2022-08-18 2019-09-12 2018-08-24 2017-09-10 2017-06-15	Kluane Lake Research Station; legacy Hyperion data
01902	KluanB	17095 17064	2017-09-10 2017-06-15	Kluane Lake Research Station; legacy Hyperion data
31040	SnagYK	22034 18049 17095 17064	2022-08-18 2018-08-24 2017-09-10 2017-06-15	Snag YT and Alaska/Canada border region; YGS Permafrost Monitoring Network
21611	GaribA	22034	2022-08-18	BC Coast Mountains; active faulting; glacier mass balance
03606	GaribB	22034	2022-08-18	BC Coast Mountains; active faulting; glacier mass balance

3.3 Region C3: Upper Mackenzie Valley

Figure S12 shows the flight lines for Region C3: the Upper Mackenzie Valley. Details for individual L-band PolInSAR flight lines are given in **Table S16**; the P-band acquisition details are given in **Table S28**. The Upper Mackenzie Valley region features flight lines over long-term boreal forest inventory data from the Canadian Forestry Service's CIPHA and HELCIA plots; long-term permafrost, hydrology and ecology time series records from the CCRN site at Scotty Creek, NWT; and the Scotty Creek and Smith Creek flux towers. Together, these sites provide data critical to understanding the performance of airborne SAR for investigating boreal forests and peatlands.

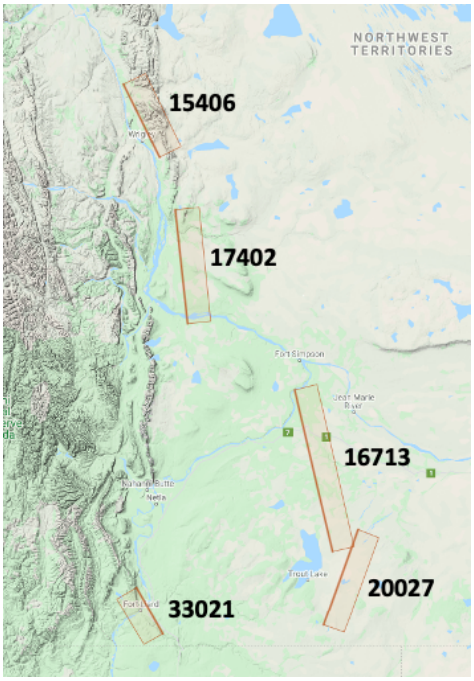

Figure S12. Flight lines for the Upper Mackenzie Valley (Region C3) cover the flux towers at Scotty Creek (16713) and Smith Creek (17402) as well as the boreal forest near Fort Liard (33021), the most productive region in the NWT. © Google Maps

Line 33021: Fliard. This ~60 km flight line is centered on Fort Liard, NT and captures landscapes on either side of the Liard River. It is anchored by ~45 HELCIA and CFS NWT inventory plots. This line enables studies of boreal forest structure and above ground biomass in the most productive forests in the Northwest Territories [R. Hall, personal communication].

Lines 20027: ScottyIOP and 16713: Scotty. These flight lines sample the Scotty Creek Research Watershed [Quinton et al. 2019] and the surrounding taiga plains. Flight line 20027 extends northeast ~95 km from the British Columbia border and terminates east of Trout Lake, NT. It overflies remote sensing areas of interest (AOI) 9, 7, 6, and 5 established by the Consortium for Permafrost Ecosystems in Transition (CPET). Each of the AOIs has a 6 x 6 km^2 footprint. Imagery stacking over these sites includes recent Landsat (30 m resolution) and World View 1,2 (50 cm resolution) datasets and historical aerial photographs acquired in 1970/71 (1.2 m resolution). Detailed statistical characterization of the land covers within these AOIs is being developed at high resolutions, providing information on proportions of major land cover types and changes to the land cover types over a 40-year period. Flight line 16713 begins east of Trout Lake and extends northwest ~165 km towards Fort Simpson, NT overflying AOIs 6, 5, 4, 3, and 2 as well as the Scotty Creek watershed and flux towers (Scotty Creek Landscape, CA-SCC, and Scotty Creek Bog, CA-SCB). These lines will enable multi-disciplinary investigations into permafrost ecosystem vulnerability and change [Quinton et al. 2016].

Lines 17402: FtSimp and 15406: Wrigle. Flight line 17402 starts north of Fort Simpson, NT, crosses the Mackenzie River between Miles 255 and 270, then extends north parallel to the river on the eastern bank to Mile 326. It is anchored by the Willowlake River CALM sites (C14A,B). Flight line 15406 starts near Mile 336 and proceeds ~75 km northwest over Wrigley, NT. It is anchored by the Smith Creek flux tower (CA-SMC) and the Ochre River CALM site (C13). These lines link the Upper and

Lower Mackenzie Valley (Region C1), defining a transect between the Taiga Plains and the Subarctic Tundra ecoregions.

Table S16. Region C3: Upper Mackenzie Valley L-band Flight Line Summary

Line ID	Short Name	Flight	Date	Comments
33021	Fliard	22034 19061 17099 17066 17065	2022-08-18 2019-09-11 2017-09-17 2017-06-17 2017-06-16	Fort Liard NT; HELCIA plots; highly productive boreal forest
16713	Scotty	22033 19061 17099 17065	2022-08-16 2019-09-11 2017-09-17 2017-06-16	Scotty Creek Research Watershed; permafrost monitoring; flux towers
20027	ScottyIOP	22034 17099 17065	2022-08-18 2017-09-17 2017-06-16	Scotty Creek Intensive Observation sites near Trout Lake
17402	FtSimp	19066 18052 17099 17066	2019-09-17 2018-08-28 2017-09-17 2017-06-17	Fort Simpson NT area; HELCIA and CALM site
15406	Wrigle	19066 17099 17065	2019-09-17 2017-09-17 2017-06-16	Wrigley NT area; Smith Creek flux tower; CALM site

3.4 Region C4: Great Slave Lake Region

Figure S13 shows the flight lines for Region C4: the Great Slave Lake Region. Details for individual L-band SAR flight lines are given in **Table S17**; the P-band acquisition details are given in **Table S29**. Many of these lines are anchored to road-accessible ground sites where research is being conducted on fire severity and the post-fire recovery of areas burned during the 2014-15 wildfire seasons [Walker et al. 2018a,b; 2019a,b; Bourgeau-Chavez et al. 2016, 2017, 2019a,b, French et al. 2020a,b] as well as soil moisture, ALT, peatland mapping and biomass [Bourgeau-Chavez et al. 2016, 2017, 2019a,b], and long-term boreal forest inventory data from the Canadian Forestry Service's CIPHA and HELCIA plots. Soil moisture was sampled for both L- and P-band at 6, 12, 20 and 50 cm depths [Bourgeau-Chavez et al. 2019, Schaefer XXX]. Other research in this area focuses on wetland inundation monitoring [French et al. 2018], lake and river WSE, studies of the tundra-taiga ecotone, and exploiting long term flux measurements at Daring Lake, NT (CA-DL1, CA-DL2) [Lafleur et al. 2018; Meyer et al. 2020].

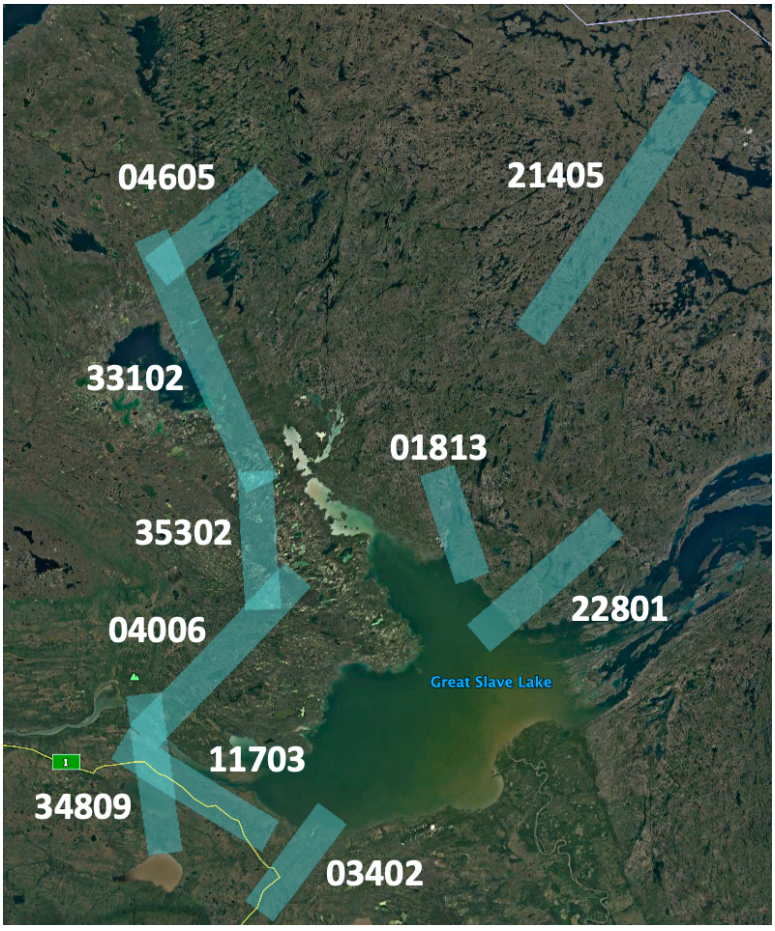

Figure S13. L-band SAR lines in the Great Slave Lake Region (C4) sample fire disturbance, long-term forest inventory plots, the tundra-taiga ecotone (TTE), and water surface elevation in the boreal forest and onto the Canadian Shield. Extensive ground-based measurements are available to validate the airborne SAR collections. Multiple flight days are required to acquire all of these lines. © Google Earth

Line 03402: HayRiv. The Hay River line begins southwest of Enterprise, NT, then follows the Mackenzie Highway and the river northeast for ~60 km, terminating at Hay River, NT on the shores of Great Slave Lake. It is anchored by numerous CIPHA and HELCIA plots, and caribou tracking data [Serrouya et al. 2021]. This line was added in 2019 to complement intensive field work [G. Castilla, private communication] and LiDAR acquisitions [C. Hopkinson, private communication] along the Hay River corridor.

Lines 11703: Kakisa1 and 34809: Kakisa2. The Kakisa Lake lines were designed to cover sites where field work was conducted in peatlands and 2014-15 burn scars [Bourgeau-Chavez et al. 2016; 2017; 2019a,b; Walker et al. 2019a,b]. Line 11703 follows NT Highway 1 from Enterprise, NT northwest for

~110 km towards Fort Providence, NT. Line 34809 extends ~100 km north from the northern shore of Tathlina Lake over Kakisa Lake and ends north of Fort Providence. These lines overfly areas severely burned in the 2014 wildfire season. Ground sites include CFS HELCIA plots and burn study sites from various ABoVE. Preliminary analyses show changes in ALT and soil moisture within the burn scars compared to adjacent unburned areas [Schaefer et al. 2019].

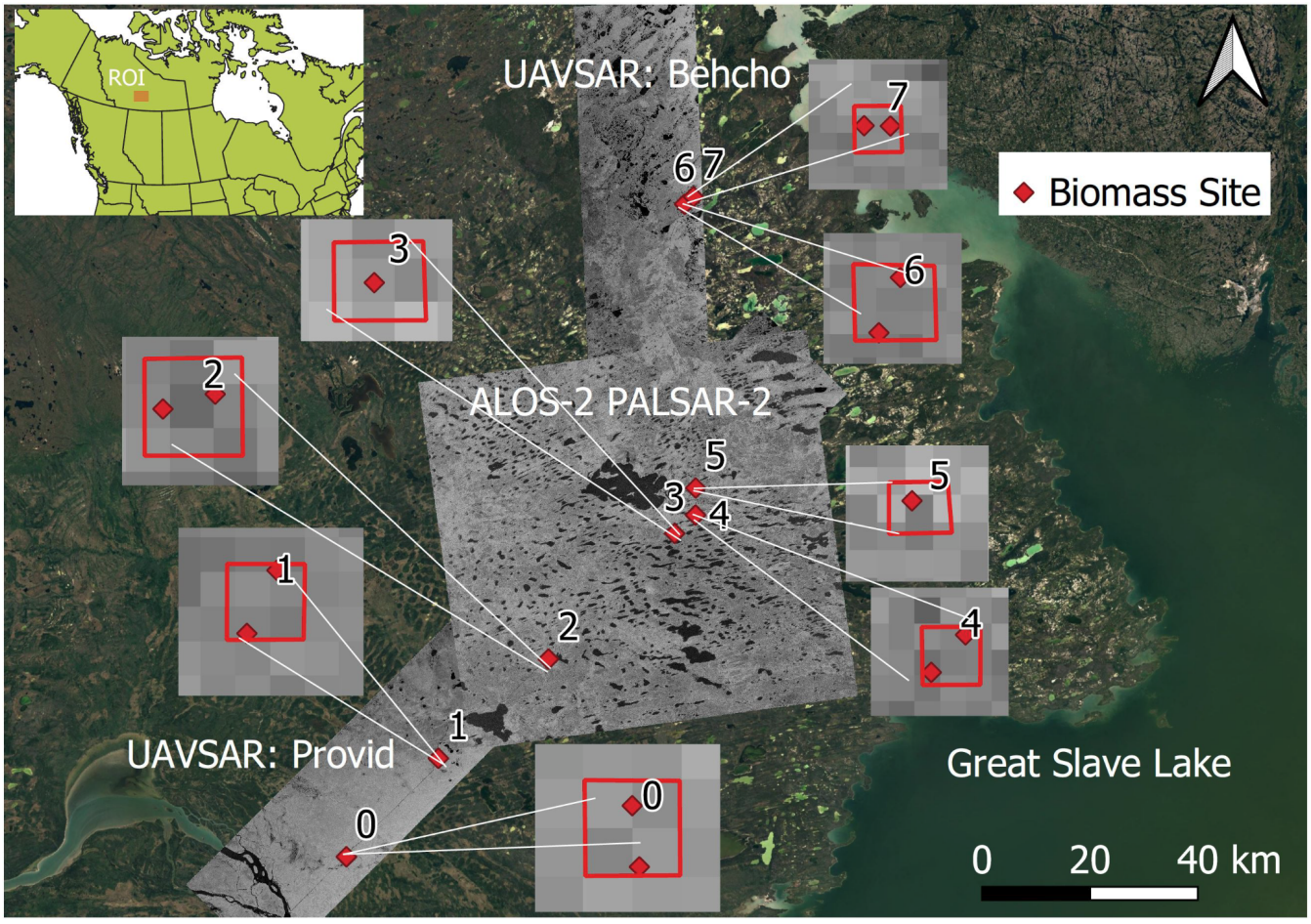

Figure S14. The western extent of the Great Slave Lake region between Fort Providence (Line 0406) and Behchoko (Line 35302) was the focus of coordinated ground, satellite and airborne activities. This image shows the location of ground-validation sites for biomass and soil moisture with overlapping imagery obtained from ALOS-2 and UAVSAR L-band SAR observations. © Google Earth

Line 04006: FtProv. This line originates southwest of Fort Providence, NT and extends ~140 km northeast along the Mackenzie Highway. It is anchored by numerous CFS long term forest inventory sites [Hoy et al. 2018] and electrical resistivity tomography (ERT) transects [M. Turretsky, private communication]. **Figure S14** shows that this line overflies areas severely burned in the 2014 wildfire season and was extensively sampled by ABoVE research teams [Bourgeau-Chavez et al. 2016, 2017,

2019a,b, 2021; Walker et al. 2019a,b]. Post fire vegetation changes have made this an attractive area for wintering woodland caribou [A. Kelly, private communication].

Line 35302: Behcho. The Behchoko line extends ~85 km on a north-south axis along the Mackenzie Highway to the west of Behchoko, NT. It overflies two severely burned areas from the 2014 wildfire season (**Figure S14**). It is anchored by ERT transects and long term forest inventory plots, and was extensively sampled by ABoVE research teams [Bourgeau-Chavez et al. 2016, 2017, 2019a,b, 2021; Walker et al. 2019a,b].

Line 33102: SnareR. This line follows the Snare River northwest for ~170 km from Great Slave Lake over the village of Whati, NT. Water surface elevation (WSE) investigations in this region inform hydroelectric power potential for Yellowknife, NT [A. Applejohn, private communication] and complement AirSWOT acquisitions [Pitcher et al. 2019a,b; Kyzivat et al. 2020]. In situ measurements have been collected to validate ABoVE SAR soil moisture and ALT products [Schaefer et al. 2019]. The Snare River line was not acquired in 2018.

Line 04605: FaberL. The Faber Lake line extends ~90 km across two large 2014 burned areas on the northern shore of Great Slave Lake. Field work by ABoVE research teams assessed the severity of the burns [Walker et al. 2019a,b]. The Faber Lake line was acquired only in 2017; it was replaced by higher priority acquisitions.

Line 21405: Daring. The Daring Lake flight line extends nearly 200 km southwest from the Daring Lake Tundra Ecosystem Research Station (TERS) across the Canadian Shield. It is anchored by TERS field sites and flux towers (CA-DL1, CA-DL2) [Lafleur et al. 2018; Meyer et al. 2020]. This line complements AirSWOT acquisitions [Pitcher et al. 2019a,b; Kyzivat et al. 2020] and creates a transect across the tundra-taiga transition. The Daring Lake line was not acquired in 2018.

Line 22801: Yellow. This line southeast of Yellowknife extends ~110 km from Great Slave Lake northeast. It is anchored by a number of Northern Contaminated Sites Program (INAC) mine remediation sites [Hoy et al. 2018] as well as peatland and fire disturbance ground sites [Bourgeau-Chavez et al. 2016, 2017, 2019a,b, 2021; Walker et al. 2019a,b; French et al. 2020a,b]. These sites are accessible via helicopter, floatplane, or boat. The Yellowknife line was not acquired in 2018.

Line 16008: BakerC. This line begins north of the Yellowknife airport and extends ~60 km to the southeast. It is anchored by long-term hydrological monitoring sites associated with the Baker Creek Research Watershed [Spence et al. 2018], as well as a short-term study of water-inundated vegetation [B. Chapman, personal communication, French et al. 2018]. Acquisitions for the Baker Creek line began in 2018; it was not acquired in 2017 and, therefore, has no P-band counterpart.

82 **Table S17. Region C4: Great Slave Lake Region L-band Flight Line Summary**

Line ID	Short Name	Flight Plan	Sortie Date	Comments
03402	HayRiv	22032 19060	2022-08-15 2019-09-05	Canadian Forest Service Permanent Sampling Plots near Highway NT 2 along the Hay River
11703	KakisA	22033 19060 18048 17094 17063	2022-08-16 2019-09-05 2017-08-22 2017-09-09 2017-06-14	Burn study sites near Kakisa Lake
34809	KakisaB	22032 19060 18048 17094 17063	2022-08-15 2019-09-05 2017-08-22 2017-09-09 2017-06-14	Burn study sites near Kakisa Lake
04006	Provid	22032 19060 19059 18048 18047 17094 17063	2022-08-15 2019-09-05 2019-09-04 2017-08-22 2017-08-21 2017-09-09 2017-06-14	Burn study sites accessible from Highway NT 3 near Fort Providence
35302	Behcho	22032 19060 18048 17094 17063	2022-08-15 2019-09-05 2017-08-22 2017-09-09 2017-06-14	Burn study sites accessible from Highway NT 3 near Behchoko
33102	SnareR	19060 17094 17063	2019-09-05 2017-09-09 2017-06-14	Snare River hydrology and water surface elevation
04605	FaberL	17094 17063	2017-09-09 2017-06-14	Faber Lake burn study sites
21405	Daring	22033 19060 17094 17063	2022-08-16 2019-09-05 2017-09-09 2017-06-14	Taiga-tundra transition from Yellowknife to the Daring Lake Research Station
22801	Yellow	22033 19059 17094 17063	2022-08-16 2019-09-04 2017-09-09 2017-06-14	Burn study sites southeast of Yellowknife

16008	BakerC	22032 19060 19059 18048 18047	2022-08-15 2019-09-05 2019-09-04 2018-08-22 2018-08-21	Baker Creek Watershed sites north of the Yellowknife Airport

3.5 Region C5: Peace-Athabasca Delta (PAD) and the Trans-Boundary Watershed

Figure S15 shows the L-band SAR flight lines for the Peace-Athabasca Delta and Transboundary Watershed (Region C5). These flight lines extend from the Peace-Athabasca Delta in northern Alberta to the Slave River Delta near Fort Resolution, NT on the southern shore of Great Slave Lake. Details for individual L-band SAR flight lines are given in **Table S18**; the P-band acquisition details are given in **Table S30**.

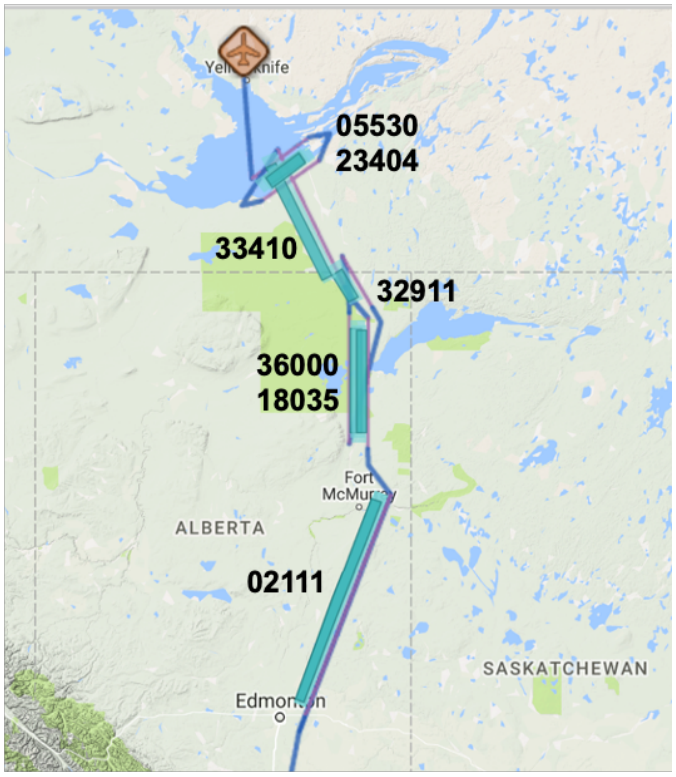

Figure S15. L-band flight lines in the Transboundary Watershed sample from the Peace-Athabasca Delta along the Slave River to the Slave Delta on the on the southern shore of Great Slave Lake. These flight lines help characterize wetlands extent and type as well as water surface elevations. © Google Maps

Multiple ABoVE research groups and Canadian partner organizations engage in research projects across the Peace-Athabasca Delta (PAD) and the Slave River watershed. The PAD has been declared a Ramsar Convention Wetland and a UNESCO World Heritage site based on its high biological diversity. The Slave River and Delta are monitored under the NWT Water Stewardship Strategy, in which Traditional Knowledge and western science are merged to create state of the art understanding of the hydrology, ecology, and biodiversity of the Slave River watershed. The ABoVE flight lines were designed in close consultation with the GNWT Science Advisor to help quantify and understand trans-boundary water flow. The L-band SAR acquisitions described here complement the LVIS LiDAR and AirSWOT Ka-band, thermal and optical data acquired in 2017 to study trans-boundary WSE and hydrologic dynamics in detail [Fayne et al. 2019; Kyzivat et al. 2019] (See Section 8).

Lines 36000: PADelE and 18035: PADelW. The Peace-Athabasca Delta (PAD), a 5200 km^2 freshwater delta at the confluence of the Peace and Athabasca Rivers with Lake Athabasca (58.7N, 111.5W; **Figure S16**), is the largest inland river delta in the world, among the world's most globally significant boreal wetlands, and a critical habitat for millions of water fowl. Aside from some exposed bedrock features in the northern sector, the PAD consists of hundreds of interconnected wetlands, shallow lakes (<2 m depth), and active and relict distributary channels. [Pavelsky and Smith 2008]. The SAR flight lines are centered on the PAD and run north-south for ~180 km. Both L-band and P-band swaths were designed to overlap with AirSWOT Ka-band WSE data acquired in June and August 2017 [Miller et al. 2019; Fayne et al. 2019; Kyzivat et al. 2019]. The L-band swaths overlap substantially as they were placed for optimized near-field coverage of the narrower P-band and Ka-band swaths. ABoVE researchers coordinated on-water WSE and optical property measurements with the SAR swaths. **Figure S16** shows overlap of L-band image with on the water measurements made in August 2018. ABoVE researchers are also using the PAD L-Band SAR imagery to develop wetland waterfowl habitat classification methods [French et al. 2018].

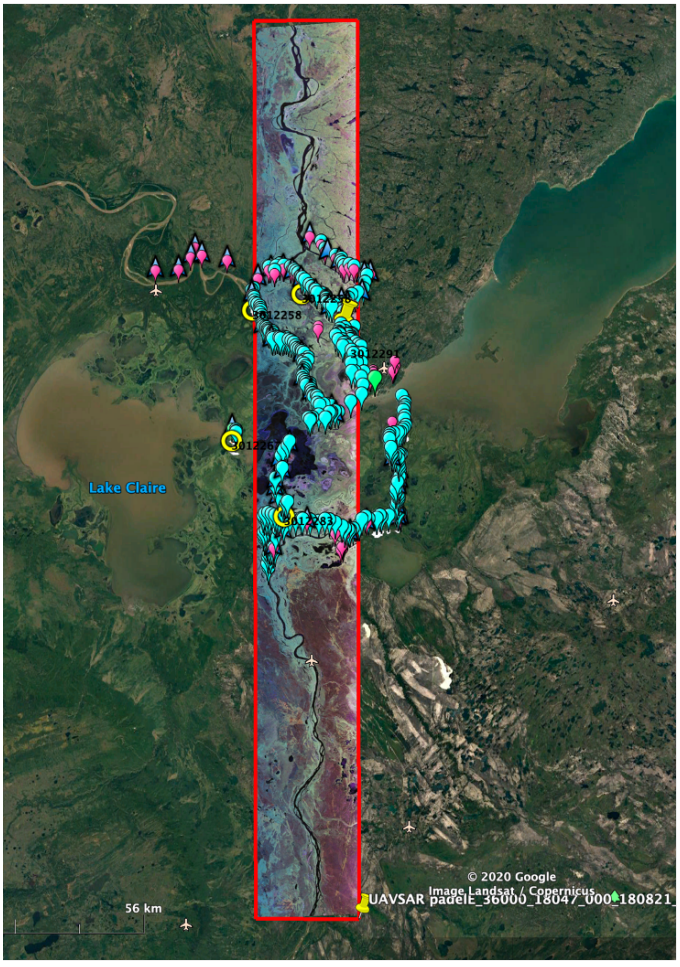

Figure S16. L-band SAR flight line 36000 (PADelE) overlaps with on-water measurements made by ABoVE ecohydrology researchers [Smith-Pavelsky-Butman]. SAR data will help quantify water surface elevations (WSE) and provide wetlands classifications for the world's largest inland delta. © Google Earth

Lines 32911: FSmithS and 33410: FSmithN. The Fort Smith flight lines provide imagery of the Slave River from northern Alberta to the Great Slave Lake. Flight line 32911 starts about 40 km south of the Alberta-Northwest Territories border and follows the river north past Fort Smith, NT. Flight line 33410 continues the survey from the border to the Slave River Delta near Fort Resolution, NT, extending several kilometers into the Great Slave Lake to characterize Slave River outflow into the lake. These lines are anchored by numerous river gauges to calibrate WSE, and also a part of wetland waterfowl habitat assessment for ABoVE [French et al. 2018].

Lines 05530: FtResS and Line 23404: FtResN. The Fort Resolution flight lines are parallel transects designed to map the Slave River Delta. Each extends ~80 km perpendicular to the Slave River to map

the entire Fort Resolution Peninsula. As with the PAD flight lines 36000 and 18035, the spatial offset in flight lines 05530 and 23404 optimizes overlap for the narrower P-band swath. The Slave River Delta is a critical waterfowl habitat, and the SAR imagery will deliver important information on its structure and interannual variability [French et al. 2018].

Table S18. Region C5: Peace-Athabasca Delta and Trans-Boundary Watershed L-band Flight Line Summary

Line ID	Short Name	Flight	Date	Comments
36000	PADelE	22033 22032 19059 18047 17093 17062	2022-08-16 2022-08-15 2019-09-04 2018-08-21 2017-09-08 2017-06-13	Water Surface Elevation (WSE) and habitat classification in the Peace-Athabasca Delta; overlap with AirSWOT Ka-band acquisitions
18035	PADelW	22033 18047 17093 17062	2022-08-16 2018-08-21 2017-09-08 2017-06-13	Water Surface Elevation (WSE) and habitat classification in the Peace-Athabasca Delta; overlap with AirSWOT Ka-band acquisitions
32911	FSmitS	17093 17062	2017-09-08 2017-06-13	Water Surface Elevation (WSE) for the Slave River trans-boundary watershed
33410	FSmitN	22033 19059 17093 17062	2022-08-16 2019-09-04 2017-09-08 2017-06-13	Water Surface Elevation (WSE) for the Slave River trans-boundary watershed
05530	FtResN	22033 19059 18047 17093 17062	2022-08-16 2019-09-04 2018-08-21 2017-09-08 2017-06-13	Water Surface Elevation (WSE) and habitat classification in the Slave River Delta
23404	FtResS	22033 19059 17093 17062	2022-08-16 2019-09-04 2017-09-08 2017-06-13	Water Surface Elevation (WSE) and habitat classification in the Slave River Delta

3.6 Region C6: Southern Boreal Forest/BERMS

Figure S17 shows the flight lines for Region C6: Southern Boreal Forest/BERMS. Details for individual L-band SAR flight lines are given in **Table S19**; the P-band acquisition details are given in **Table S31**.

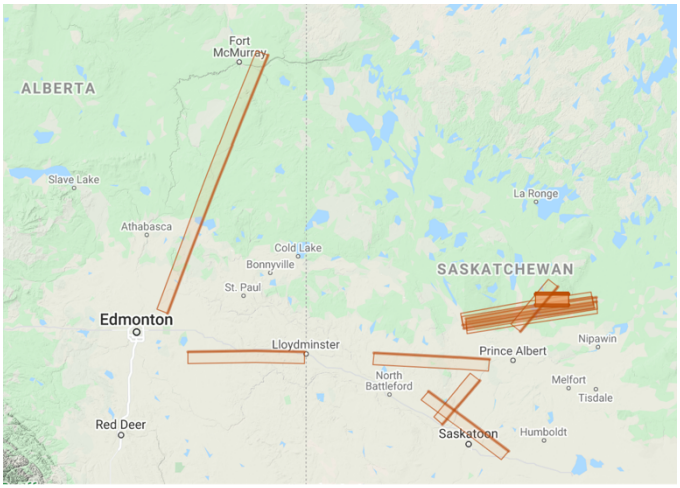

Figure S17. L-band SAR flight lines in Region C6 sample the southern boreal forest, including the BOREAS-era BERMS sites. Both NASA's L-band SAR and DLR's multi-frequency F-SAR flew tomoSAR grids over the BERMS site in 2018. Legacy data from CANEX 2010 (L-band) and the AIRMOSS EV-S investigation (P-band, 2013-2015) provide the opportunity to investigate decadal-scale ecosystem change. © Google Maps

Region C6 covers the southern edge of the boreal plains ecozone which was intensively studied during NASA's BOREAS field campaigns in the 1990s [Sellers et al. 1994; 1997]. Revisits to the area during ABoVE allow for an assessment of change over the last 20 years. This region features the Boreal Ecosystem Research and Monitoring Sites (BERMS) covering flux towers at Old Jack Pine (OJP), Old Black Spruce (OBS), and Old Aspen (OAS) vegetation types [Barr 2006]. 'Old' refers to the monitoring site being located within a mature stand of trees. The Old Aspen site ended operations in 2017 shortly after the ABoVE flights that year. The BERMS area has been the target of previous L- and P-band SAR campaigns. Legacy acquisitions from CanEx 2010 [Magagi et al. 2012] and AirMOSS (2013-2015) [Tabatabaeenejad et al. 2020] provide the opportunity to extend the ABoVE time series and investigate decadal-scale ecosystem change. ABoVE SAR flight lines also leverage the extensive forest inventory plots, HELCIA, and CIPHA sites maintained by the Canadian Forestry Service, as well as legacy LiDAR acquisitions. The region also spatially overlaps with extensive PALS airborne L-band retrievals acquired during the NASA SMAPVEX-16 campaign [McNairn et al. 2017; Colliander et al. 2019] and tower mounted L-band radiometer acquisitions at the OBS site [Roy et al. 2020]; these data provide opportunities to investigate L-band active/passive microwave synergy for mapping vegetation biomass, freeze-thaw, and soil moisture conditions.

Since this region lacks permafrost, there was no reason to acquire an early season baseline and all acquisitions have been acquired near DOY 240 (late-August to early-September). In 2018 L-band tomoSAR data were acquired over the BERMS grid in conjunction with DLR's F-SAR multi-frequency airborne SAR (see Section 6 for additional details).

Line 30704: Redber. The Redberry Lake flight line starts southeast of Saskatoon and travels ~130 km northwest and terminates north of Hafford, SK. It is anchored by the Redberry Lake WSE calibration site [Pietroniro et al. 2019] and is an important line for cross calibration with AirSWOT Ka-band radar acquisitions [Smith et al. 2017]. It includes Environment & Climate Change Canada monitoring sites;

GPS water level surveys of prairie pothole wetlands; and geomorphic changes along the North Saskatchewan River.

Line 04016: SaskS. The Saskatoon South flight line begins northeast of Radisson, SK then travels ~70 km northeast over Blaine Lake to end near Leask, SK. It is anchored by several CFS plots and also captures large agricultural areas. It includes ECCC sites; GPS water level surveys; prairie pothole wetlands; and geomorphic changes along the North Saskatchewan River.

Line 04018: SaskN. The Saskatoon North flight line begins ~20 km southwest of Candle Lake, SK, then travels ~70 km northeast over Candle Lake and the BERMS research area. It is anchored by the Old Black Spruce (OBS) flux tower and numerous CFS/HELICA plots.

Lines 26107 BERMSA, 26106: BERMSB, 08111: BERMSC, and 08108: BERMSD. The BERMS area flight lines BERMSA-D create a 30 km x 175 km grid over the OBS, OJP, FEN, and OAS flux towers and Candle Lake. These lines overlap substantially with the legacy L-band lines from the CANEX 2010 campaign [Magagi et al. 2012] and the P-band lines from the AirMOSS EV-S1 investigation (2012-2015) [Chapin et al. 2018].

Line 27037: BERMSR. The BERMSR (reference) flight line covers an east-west transect of ~55 km and is anchored by the OBS and OJP flux towers. It is a reference acquisition for the tomoSAR experiment performed in August 2018 (Flight Plan 18046) in conjunction with the German Space Agency's multi-frequency F-SAR [Pichierri et al. 2018]. Flight line details are given in **Table S20** and the results are described in Section 6 of the main text. Line 27037 was reacquired in 2019 to evaluate interannual variability.

Lines 27304 LloydE and 27304 LloydW. The two Llyodminster flight lines establish a long east-west transect across the prairie in an area known to be permafrost free and provide a critical test for water mask and water surface elevation retrieval algorithms adapted for permafrost ecosystems [L. Smith, private communication]. The Llyodminster East flight line begins near Sherbrook, SK and travels ~150 km west to Edam, SK. After a gap of ~100 km, data collection was restarted for the Llyodminster West line and continued for another ~150 km along the same heading.

Line 02111: FtMacM. The Fort McMurray flight line originates north of Edmonton and travels nearly 400 km north, terminating north of Fort McMurray. It is anchored by multiple clusters of CFS long-term plots, studies of boreal forest reclamation, and provides a south-north transect through the 2016 Horse River burn scar. Field data on fire severity and pre-fire biomass were sampled at several sites in the 2016 fire [Bourgeau-Chavez et al. 2017]. This flight line covers the prairie-boreal forest ecotone.

Table S19. Region C6: Southern Boreal Forest/BERMS L-band Flight Line Summary

Line ID	Short Name	Flight	Date	Comments
30704	Redber	19057 17092	2019-08-16 2017-09-07	Calibration for AirSWOT and Water Surface Elevation (WSE) at Redberry Lake
04016	SaskaS	19057 17092	2019-08-16 2017-09-07	AirSWOT field sites
04018	SaskaN	19057 17092	2019-08-16 2017-09-07	Transect through the BERMS research area, BOREAS Old Black Spruce (OBS) flux tower, HELICA sites
26107	BERMSA	17093	2017-09-08	BERMS area grid; OBS, OJP, FEN, and OAS flux towers
26106	BERMSB	17093	2017-09-08	BERMS area grid; OBS, OJP, FEN, and OAS flux towers
08111	BERMSC	17093	2017-09-08	BERMS area grid; OBS, OJP, FEN, and OAS flux towers
08108	BERMSD	17093	2017-09-08	BERMS area grid; OBS, OJP, FEN, and OAS flux towers
27037	BERMSR	19057	2019-08-16	TomoSAR reference line; interannual variability
27304	LloydE	17092	2017-09-07	Test for ecohydrology algorithms (permafrost free zone)
27304	LloydW	17092	2017-09-07	Test for ecohydrology algorithms (permafrost free zone)
02111	FtMacM	17093 17062	2017-09-08 2017-06-13	Horse River burn transect; prairie – boreal forest ecotone

Table S20. BERMS L-band TomoSAR Flight Lines

Line ID	Short Name	Flight Plan	Date	Comments
09041	BERMSA	22031 18046	2022-08-14 2018-08-19	TomoSAR 40m Baseline
26107	BERMSA	22031 18046	2022-08-14 2018-08-19	TomoSAR 40m Baseline
09043	BERMSB	22031 18046	2022-08-14 2018-08-19	TomoSAR 80m Baseline
27043	BERMSB	22031 18046	2022-08-14 2018-08-19	TomoSAR 80m Baseline
09039	BERMSC	22031 18046	2022-08-14 2018-08-19	TomoSAR 120m Baseline
27039	BERMSC	22031 18046	2022-08-14 2018-08-19	TomoSAR 120m Baseline
09044	BERMSD	22031 18046	2022-08-14 2018-08-19	TomoSAR 160m Baseline
27044	BERMSD	22031 18046	2022-08-14 2018-08-19	TomoSAR 160m Baseline
09040	BERMSE	22031	2022-08-14	TomoSAR 200m Baseline

		18046	2018-08-19	
27040	BERMSE	22031 18046	2022-08-14 2018-08-19	TomoSAR 200m Baseline
09042	BERMSF	22031 18046	2022-08-14 2018-08-19	TomoSAR 240m Baseline
27042	BERMSF	22031 18046	2022-08-14 2018-08-19	TomoSAR 240m Baseline
09038	BERMSG	22031 18046	2022-08-14 2018-08-19	TomoSAR 280m Baseline
27038	BERMSG	22031 18046	2022-08-14 2018-08-19	TomoSAR 280m Baseline
09037	BERMSR	22031 18046	2022-08-14 2018-08-19	TomoSAR Reference Line
27037	BERMSR	22031 18046	2022-08-14 2018-08-19	TomoSAR Reference Line
TM090	BERMSR	18046	2018-08-19	TomoSAR 280m Baseline
TM270	BERMSR	18046	2018-08-19	TomoSAR 80m Baseline

4 ABoVE P-band Flight Lines

The ABoVE P-band SAR data were acquired during campaigns in May/June, August, and October of 2017 (**Tables S6-S8**). **Tables S21-S31** provide the details for individual flight lines for the Alaskan and Canadian Sectors.

Table S21. Region A1 (North Slope Alaska) P-band Flight Line Summary

P-band Line ID	Short Name	Flight Plan	Date	Comments
03107	Ivotuk	17109 17079 17056	2017-10-09 2017-08-13 2017-05-29	Legacy line; Ivotuk flux tower, CALM site, GTN-P boreholes Matches L-band line 03111
34505	Atqasu	17109 17079 17058	2017-10-09 2017-08-13 2017-06-06	Legacy line; Atqasuk flux tower; CALM site Matches L-band line 34509
15010	Barrow	17109 17079 17058	2017-10-09 2017-08-13 2017-06-06	Legacy line; NGEE-Artic, NEON, BEO flux towers, CALM sites Matches L-band line 15018
04600	Inigok	17079 17058	2017-08-13 2017-06-06	North Slope CALM sites, boreholes Matches L-band line 04603
33410	AnaktE	17079 17058	2017-08-13 2017-06-06	Anaktuvuk River fire scar, eastern transect Matches L-band line 33408
16404	AnaktW	17079 17058	2017-08-13 2017-06-06	Anaktuvuk River fire scar, western transect Matches L-band line 16405
18517	Dhorse	17109 17079 17058	2017-10-09 2017-08-13 2017-06-06	North-South transect running from the Arctic Ocean coast through Deadhorse and south along the Dalton Highway; covers numerous calibration sites Matches L-band line 18519
05406	Toolik	17109 17079 17056	2017-10-09 2017-08-13 2017-05-29	Toolik Lake Research Station, Arctic LTER, NEON box Matches L-band line 04300
28608	Noatak	17079 17056	2017-08-13 2017-05-29	Fire disturbance/recovery

Table S22. Region A2 (Seward Peninsula and Northwestern Interior P-band Flight Line Summary

Line ID	Short Name	Flight	Date	Comments
25507	Huslia	17109 17082 17055	2017-10-09 2017-08-17 2017-05-27	Interior Alaska, Huslia village Matches L-band line 25516
25508	Koyukk	17110 17082 17055	2017-10-10 2017-08-17 2017-05-27	AirMOSS legacy line; Koyuk village, boreal forest, coastal mountains Matches L-band line 25517
32510	Counci	17110 17082 17056	2017-10-10 2017-08-17 2017-05-29	Legacy line; NGEE-Artic Council watershed and flux tower, Kougarok watershed Matches L-band line 32519
04900	Teller	17110 17082 17056	2017-10-10 2017-08-17 2017-05-29	NGEE-Arctic Teller watershed, Kougarok watershed, Kougarok area fire disturbance/recovery Matches L-band lines 04806, 04901
08509	Kougar	17110 17082 17056	2017-10-10 2017-08-17 2017-05-29	AirMOSS legacy line; Seward Peninsula CALM sites, boreholes Matches L-band line 08502
03106	Ambler	17109 17082 17055	2017-10-09 2017-08-17 2017-05-27	AirMOSS legacy line; boreholes, boreal forest-foothills gradient Matches L-band line 03101
28608	Noatak	17079 17056	2017-08-13 2017-05-29	Fire disturbance/recovery Matches L-band line 28508

Table S23. Region A3: Eastern Interior P-band Flight Line Summary

Line ID	Short Name	Flight Plan	Date	Comments
20007	Coldfo	17109 17082 17079 17055	2017-10-09 2017-08-17 2017-08-13 2017-05-27	CALM and GTN-P sites; tundra-taiga ecotone Matches L-band line 20026
21507	YflatW	17082 17056	2017-08-17 2017-05-29	Overlap with AEM surveys, AirSWOT and in situ water surface elevation measurements
21608	YflatE	17082 17056	2017-08-17 2017-05-29	Overlap with AEM surveys, AirSWOT and in situ water surface elevation measurements
04707	FtYuko	17082 17056	2017-08-17 2017-05-29	Overlap with AEM surveys, AirSWOT and in situ water surface elevation measurements
00100	DJNEON	17078	2017-08-11	NEON D19 taiga field site near Delta Junction, AK
30406	DeltJA	17078	2017-08-11	Delta Junction, AK boreal forest

10203	DeltJB	17078	2017-08-11	Delta Junction, AK boreal forest
30203	DeltJC	17078	2017-08-11	Delta Junction, AK boreal forest

*** Interior Alaska P-band lines forbidden due to radar keep out zone at Clear AK – See Fig 4 in Main Text. Therefore, there are no P-band lines corresponding to the BonanW, BonanE, DenalN, DenalS L-band lines ****

Table S24. Delta Junction, AK P-band tomoSAR Flight Line Summary

Line ID	Short Name	Flight Plan	Date	Comments
12216	DeltaR	17081	2017-08-15	TomoSAR Reference Line 9000 mASL
30210	DeltaR	17081	2017-08-15	TomoSAR Reference Line 9000 mASL
12217	DeltaA	17081	2017-08-15	TomoSAR offset 120 meters
30211	DeltaA	17081	2017-08-15	TomoSAR offset 120 meters
12218	DeltaB	17081	2017-08-15	TomoSAR offset 135 meters
30212	DeltaB	17081	2017-08-15	TomoSAR offset 135 meters
12219	DeltaC	17081	2017-08-15	TomoSAR offset 105 meters
30213	DeltaC	17081	2017-08-15	TomoSAR offset 105 meters
12220	DeltaD	17081	2017-08-15	TomoSAR offset 150 meters
30214	DeltaD	17081	2017-08-15	TomoSAR offset 150 meters
12221	DeltaE	17081	2017-08-15	TomoSAR offset 75 meters
30215	DeltaE	17081	2017-08-15	TomoSAR offset 75 meters
12222	DeltaF	17081	2017-08-15	TomoSAR offset 175 meters
30216	DeltaF	17081	2017-08-15	TomoSAR offset 175 meters
12223	DeltaG	17081	2017-08-15	TomoSAR offset 250 meters
30217	DeltaG	17081	2017-08-15	TomoSAR offset 250 meters
12224	DeltaH	17081	2017-08-15	TomoSAR offset 90 meters
30218	DeltaH	17081	2017-08-15	TomoSAR offset 90 meters
12216	DeltaR	17081	2017-08-15	TomoSAR Reference Line 9000 mASL, Take 2
30210	DeltaR	17081	2017-08-15	TomoSAR Reference Line 9000 mASL. Take 2

Table S25. Region A4: Southwest Alaska and the Yukon-Kuskokwim Delta P-band Flight Line Summary

Line ID	Short Name	Flight Plan	Date	Comments
19204	Lclark	17080 17054	2017-08-14 2017-05-26	National Park Service SWAN ground sites Matches L-band line 19205
23002	KatmaA	17080 17054	2017-08-14 2017-05-26	National Park Service SWAN ground sites Matches L-band line 23004
28019	KatmaB	17080 17054	2017-08-14 2017-05-26	National Park Service SWAN ground sites Matches L-band line 28020
02110	KatmaC	17080 17054	2017-08-14 2017-05-26	National Park Service SWAN ground sites Matches L-band line 02112
32607	Sriver	17080 17054	2017-08-14 2017-05-26	Snake River tree rings sampling Matches L-band line 32608
27030	YKDelA	17080 17055	2017-08-14 2017-05-27	YK Delta 2015 fire scars; POLARIS portable flux towers/flux chambers; GPR transects; soil moisture measurements; Matches L-band line 26905
27031	YKDelB	17080 17055	2017-08-14 2017-05-27	YK Delta 2015 fire scars; POLARIS portable flux towers/flux chambers; GPR transects; soil moisture measurements; Matches L-band line 26906
01811	Chevak	17080 17055	2017-08-14 2017-05-27	YK Delta wildlife survey; USGS LiDAR survey; ground measurements; Matches L-band line 01813
04214	Innoko	17080 17055	2017-08-14 2017-05-27	Permafrost surveys; extensive bog/fen/wetland complex Matches L-band line 04215
08919	Poorma	17080 17054	2017-08-14 2017-05-26	Interior Alaska, boreal forest Matches L-band line 08911

Table S26. Region C1: Lower Mackenzie Valley and Northern Yukon Territory P-band Flight Line Summary

Line ID	Short Name	Flight Plan	Date	Comments
30013	Nwells	17083 17057	2017-08-18 2017-06-06	CALM and GTN-P borehole sites; oil exploration and production near Norman Wells; Matches L-band line 29904
32203	GdHope	17083	2017-08-18	Boreal forest and fire disturbance; wetlands and water surface elevation (WSE) Matches L-band line 32200
31616	GdHope	17057	2017-06-06	Boreal forest and fire disturbance; wetlands and water surface elevation (WSE) Matches L-band line 32200
25701	Aklavi	17083 17057	2017-08-18 2017-06-06	Legacy LiDAR and RadarSat data; Makenzie Delta WSE Matches L-band line 25702
05604	McPher	17083 17057	2017-08-18 2017-06-06	Legacy LiDAR data; retrogressive thaw megaslumps Matches L-band line 05529
01812	TukHwy	17083 17057	2017-08-18 2017-06-06	Legacy LiDAR and RadarSat data; Trail Valley Creek site; ShrubTundra sites; Matches L-band line 01703
20605	OldCrA	17083 17057	2017-08-18 2017-06-06	Long-term monitoring of thermokarst-driven lake change Matches L-band line 20705
24400	OldCrB	17083 17057	2017-08-18 2017-06-06	Old Crow; Porcupine River Matches L-band line 24401

Table S27. Region C2: Southern Yukon Territory P-band Flight Line Summary

Line ID	Short Name	Flight Plan	Date	Comments
27509	Watson	17078 17053	2017-08-11 2017-05-25	Watson Lake YT research nexus; YGS Permafrost Monitoring Network; Matches L-band line 27510
23601	WolfCr	17078 17053	2017-08-11 2017-05-25	Wolf Creek Research Basin; YGS Permafrost Monitoring Network; Matches L-band line 23602
30805	KluanA	17078	2017-08-11	Kluane Lake Research Station; legacy Hyperion data Matches L-band line 30806
01901	KluanB	17078 17053	2017-08-11 2017-05-25	Kluane Lake Research Station; legacy Hyperion data Matches L-band line 01902
31030	SnagYK	17078 17053	2017-08-11 2017-05-25	Snag YT and Alaska/Canada border region; YGS Permafrost Monitoring Network; Matches L-band line 31040

Table S28. Region C3: Upper Mackenzie Valley P-band Flight Line Summary

Line ID	Short Name	Flight	Date	Comments
33020	Fliard	17077 17053	2017-08-09 2017-05-25	Fort Liard NT; HELCIA plots; highly productive boreal forest; Matches L-band line 33021
16712	Scotty	17077 17052	2017-08-09 2017-05-23	Scotty Creek Research Watershed; permafrost monitoring; flux towers; Matches L-band line 16713
20025	ScoAOI	17077 17053	2017-08-09 2017-05-25	Scotty Creek Intensive Observation sites near Trout Lake Matches L-band line 20027
17401	WriglS	17077 17052	2017-08-09 2017-05-23	Fort Simpson NT area; HELCIA and CALM site Matches L-band line 17402
15405	WriglN	17077 17052	2017-08-09 2017-05-23	Wrigley NT area; Smith Creek flux tower; CALM site Matches L-band line 15406

Table S29. Region C4: Great Slave Lake Region P-band Flight Line Summary

Line ID	Short Name	Flight Plan	Sortie Date	Comments
11702	KakisA	17077 17052	2017-08-09 2017-05-23	Burn study sites near Kakisa Lake Matches L-band line 11703
34808	KakisaB	17077 17053	2017-08-09 2017-05-25	Burn study sites near Kakisa Lake Matches L-band line 34809
04005	Provid	17077 17052	2017-08-09 2017-05-23	Burn study sites accessible from Highway NT 3 near Fort Providence; Matches L-band line 04006
35301	Behcho	17076 17052	2017-08-08 2017-05-23	Burn study sites accessible from Highway NT 3 near Behchoko; Matches L-band line 35302
33101	SnareR	17077 17052	2017-08-09 2017-05-23	Snare River hydrology and water surface elevation Matches L-band line 33102
04601	FaberL	17077 17052	2017-08-09 2017-05-23	Faber Lake burn study sites Matches L-band line 04605
21404	Daring	17078 17052	2017-08-11 2017-05-23	Taiga-tundra transition from Yellowknife to the Daring Lake Research Station; Matches L-band line 21405
22800	Yellow	17076 17052	2017-08-08 2017-05-23	Burn study sites southeast of Yellowknife Matches L-band line 22801

Table S30. Region C5: Peace-Athabasca Delta and Trans-Boundary Watershed P-band Flight Line Summary

Line ID	Short Name	Flight	Date	Comments
00026	PADelE	17076 17051	2017-08-08 2017-05-22	Water Surface Elevation (WSE) and habitat classification in the Peace-Athabasca Delta; overlap with AirSWOT Ka-band acquisitions; Matches L-band line 36000
18034	PADelW	17076 17051	2017-08-08 2017-05-22	Water Surface Elevation (WSE) and habitat classification in the Peace-Athabasca Delta; overlap with AirSWOT Ka-band acquisitions; Matches L-band line 18035
32910	FSmitS	17076 17051	2017-08-08 2017-05-22	Water Surface Elevation (WSE) for the Slave River trans-boundary watershed; Matches L-band line 32911
33409	FSmitN	17076 17053	2017-08-08 2017-05-25	Water Surface Elevation (WSE) for the Slave River trans-boundary watershed; Matches L-band line 33410
05528	FtResN	17076 17053	2017-08-08 2017-05-25	Water Surface Elevation (WSE) and habitat classification in the Slave River Delta; Matches L-band line 05530
23403	FtResS	17076 17053	2017-08-08 2017-05-25	Water Surface Elevation (WSE) and habitat classification in the Slave River Delta; Matches L-band line 23404

Table S31. Region C6: Southern Boreal Forest/BERMS P-band Flight Line Summary

Line ID	Short Name	Flight	Date	Comments
30703	Redber	17075	2017-08-07	Calibration for AirSWOT and Water Surface Elevation (WSE) at Redberry Lake; Matches L-band line 30704
04011	SaskaS	17075	2017-08-07	AirSWOT field sites Matches L-band line 04016
04015	SaskaN	17075	2017-08-07	Transect through the BERMS research area, BOREAS Old Black Spruce (OBS) flux tower, HELICA sites Matches L-band line 04018
26105	BERMSA	17075	2017-08-07	BERMS area grid; OBS, OJP, FEN, and OAS flux towers Matches L-band line 26107
26104	BERMSB	17075	2017-08-07	BERMS area grid; OBS, OJP, FEN, and OAS flux towers Matches L-band line 26106
08107	BERMSC	17075	2017-08-07	BERMS area grid; OBS, OJP, FEN, and OAS flux towers Matches L-band line 08111
08106	BERMSD	17075	2017-08-07	BERMS area grid; OBS, OJP, FEN, and OAS flux towers Matches L-band line 08108
27303	LloydE	17075	2017-08-07	Test for ecohydrology algorithms (permafrost free zone) Matches L-band line 27304
27303	LloydW	17075	2017-08-07	Test for ecohydrology algorithms (permafrost free zone) Matches L-band line 27304
02109	FtMacM	17076 17051	2017-08-08 2017-05-22	Horse River burn transect; prairie – boreal forest ecotone Matches L-band line 02111

*** No permafrost in this region, so early season lines not acquired, except for FtMacM, which exists in an area of sporadic permafrost ***

5 Legacy Flight Lines

Numerous legacy flight lines for both L- and P-band SAR were available prior to the ABoVE Airborne Campaigns. Most notably, the SMAP CANEX 2010 validation experiment acquired an intensive L-band time series over the BERMS site in northern Saskatchewan during June 2017. These lines were revisited with P-band acquisitions during the AIRMOSS EV-S1 investigation (2012-2015). Additionally, the AIRMOSS team executed 1 L-band and 4 P-band campaigns in Alaska during the 2014-15 period.

Table S32. Legacy L-band SAR Flight Plans

Flight Plan	Date	Regions Sampled (hyperlink to flight line map)
15147	2015-10-05	Seward Peninsula, NW Alaska, & North Slope
10051	2010-06-17	BERMS-C flight line; SMAP CanEx 2010 Campaign
10050	2010-06-16	BERMS boreal forest grid; SMAP CanEx 2010 Campaign
10049	2010-06-15	Kenaston SK Daily Time Series; SMAP CanEx 2010 Campaign
10048	2010-06-14	Kenaston SK Daily Time Series; SMAP CanEx 2010 Campaign
10047	2010-06-13	Kenaston SK Daily Time Series; SMAP CanEx 2010 Campaign
10046	2010-06-09	Kenaston SK Daily Time Series; SMAP CanEx 2010 Campaign
10045	2010-06-06	Kenaston SK Daily Time Series; SMAP CanEx 2010 Campaign
10044	2010-06-05	Kenaston SK Daily Time Series; SMAP CanEx 2010 Campaign
10043	2010-06-02	Kenaston SK Daily Time Series; SMAP CanEx 2010 Campaign

Table S33. Legacy P-band SAR Flight Plans

Flight Plan	Date	Regions Sampled (hyperlink to flight line map)
PLAN_15142	2015-10-01	Seward Peninsula, NW Alaska, & North Slope
PLAN_15124	2015-08-29	Seward Peninsula, NW Alaska, & North Slope
PLAN_15039	2015-04-08	Seward Peninsula, NW Alaska, & North Slope
PLAN_14144	2014-10-09	Seward Peninsula, NW Alaska, & North Slope
PLAN_14117	2014-08-16	North Slope
PLAN_14116	2014-08-16	Seward Peninsula, NW Alaska, & North Slope
PLAN_15139	2015-09-28	BERMSA-D
PLAN_15137	2015-09-25	BERMSA-D
PLAN_15135	2015-09-22	BERMSA-D
PLAN_15121	2015-08-26	BERMSA-D
PLAN_15119	2015-08-23	BERMSA-D
PLAN_15117	2015-08-19	BERMSA-D
PLAN_15102	2015-07-05	BERMS & SAFIRE, Northern Saskatchewan
PLAN_15101	2015-07-02	BERMSA-D
PLAN_15101	2015-07-02	BERMSA-D
PLAN_15099	2015-06-29	BERMSA-D
PLAN_14141	2014-10-07	BERMSA-D
PLAN_14138	2014-10-04	BERMSA-D
PLAN_14136	2014-10-01	BERMSA-D
PLAN_14114	2014-08-15	BERMSA-D
PLAN_14111	2014-08-12	BERMSA-D
PLAN_14084	2014-06-14	BERMSA-D
PLAN_14080	2014-06-11	BERMSA-D
PLAN_14078	2014-06-08	BERMSA-D
PLAN_13141	2013-08-02	BERMSA-D
PLAN_13139	2013-07-29	BERMSA-D
PLAN_13137	2013-07-27	BERMSA-D
PLAN_13084	2013-05-01	BERMSA-D
PLAN_13078	2013-04-26	BERMSA-D
PLAN_13070	2013-04-22	BERMSA-D
PLAN_12101	2012-10-11	BERMSA-D
PLAN_12095	2012-10-07	BERMSA-D
PLAN_12090	2012-10-04	BERMSA-D

5.1 Alaska SAR Legacy Flight Lines

The Alaska P-band SAR legacy data (**Figure S19**) are available via the ORNL DAAC [Lou et al. 2019; https://doi.org/10.3334/ORNLDAAC/1678]. This data set provides level 1 (L1) polarimetric radar backscattering coefficient (sigma-0), multi-look complex, polarimetrically calibrated, and georeferenced data products from the Airborne Microwave Observatory of Subcanopy and Subsurface (AirMOSS) radar instrument collected over 10 study sites across Northern Alaska, USA. Flight campaigns took place in August 2014, October 2014, April 2015, August 2015, September 2015, and October 2015 (**Table S34**). The L1 P-band radar backscatter data can be used to derive estimates of soil water content and permafrost state. P-band flights over the North Slope during the early cold season (~DOY 280) have the promise of retrieving zero curtain layer and increasing understanding of non-growing season CO2 and CH4 fluxes [Zona et al. 2016; Natali et al. 2021]

Corresponding L-band legacy data were acquired during a single sortie on 5 October 2015 (**Figure S18**, **Table S35**).

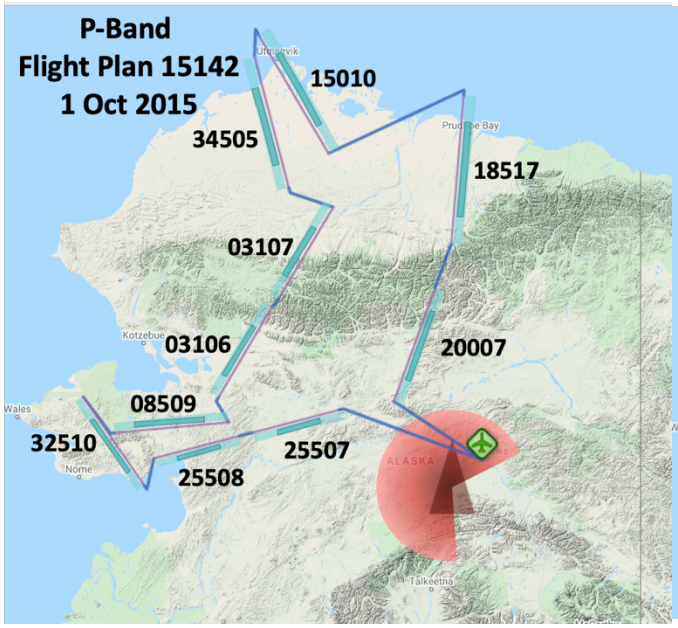

Figure S19. Alaska P-band SAR legacy lines from flight plan 15142 flown on 1 October 2015. Line IDs are given next to the lines. The large red areas in the Interior show P-band radar keep-out zones associated with the military radar at Clear, AK. © Google Maps

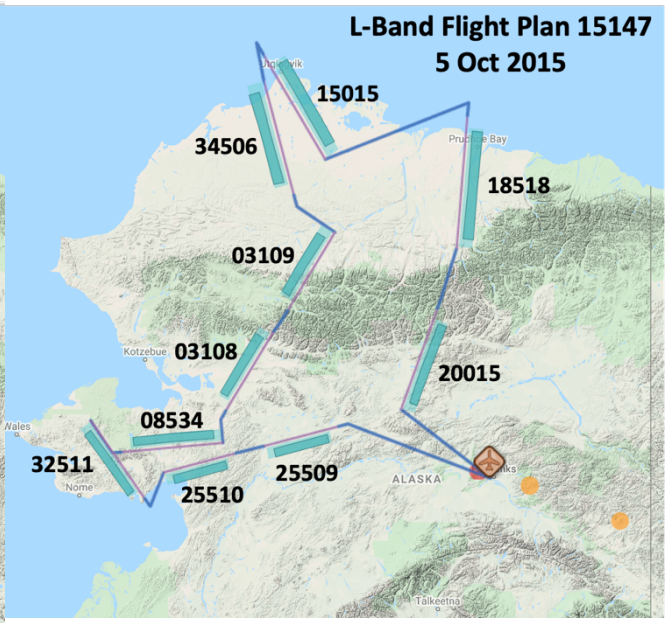

Figure S18. Alaska L-band legacy Flight Plan 15147 flown on 5 October, 2015. Flight line IDs are given next to each line. See Figure S19 for the corresponding P-band legacy flight lines. © Google Maps

79 **Table S34. Alaska Legacy P-band SAR Data**

Line ID	Short Name	Flight Plan	Date	Comments
25507	huslia	15142 15124 15039 14144 14117	2015-10-05 2015-08-29 2015-04-08 2014-10-09 2014-08-16	Legacy P-band line; Matches L-band legacy line 25509
27059	permaf	14116	2014-08-16	Legacy P-band line; Matches L-band legacy line 25509
25508	koyukk	15142 15124 15039 14144 14117	2015-10-05 2015-08-29 2015-04-08 2014-10-09 2014-08-16	Legacy P-band line; Matches L-band legacy line 25510
25504	permaf	14116	2014-08-16	Legacy P-band line; Matches L-band legacy line 25510
32510	counci	15142 15124 15039 14144 14117	2015-10-05 2015-08-29 2015-04-08 2014-10-09 2014-08-16	Legacy P-band line; Matches L-band legacy line 32511
33008	permaf	14116	2014-08-16	Legacy P-band line; Matches L-band legacy line 32511
08509	kougar	15142 15124 15039 14144 14117	2015-10-05 2015-08-29 2015-04-08 2014-10-09 2014-08-16	Legacy P-band line; Matches L-band legacy line 08534
08601	permaf	14116	2014-08-16	Legacy P-band line; Matches L-band legacy line 08534
03106	ambler	15142 15124 15039 14144 14117	2015-10-05 2015-08-29 2015-04-08 2014-10-09 2014-08-16	Legacy P-band line; Matches L-band legacy line 03108
03101	permaf	14116	2014-08-16	Legacy P-band line; Matches L-band legacy line 03108
03107	ivotuk	15142 15124 15039	2015-10-05 2015-08-29 2015-04-08	Legacy P-band line; Matches L-band legacy line 03109

		14144	2014-10-09	
03102	permaf	14116	2014-08-16	Legacy P-band line; Matches L-band legacy line 03109
34505	atqasu	15142 15124 15039 14144 14117	2015-10-05 2015-08-29 2015-04-08 2014-10-09 2014-08-16	Legacy P-band line; Matches L-band legacy line 34506
34503	permaf	14116	2014-08-16	Legacy P-band line; Matches L-band legacy line 34506
15010	barrow	15142 15124 15039 14144 14117	2015-10-05 2015-08-29 2015-04-08 2014-10-09 2014-08-16	Legacy P-band line; Matches L-band legacy line 15015
18517	dhorse	15142 15124 15039 14144 14117	2015-10-05 2015-08-29 2015-04-08 2014-10-09 2014-08-16	Legacy P-band line; Matches L-band legacy line 18518
20007	coldfo	15142 15124 15039 14144 14117	2015-10-05 2015-08-29 2015-04-08 2014-10-09 2014-08-16	Legacy P-band line; Matches L-band legacy line 20015

Table S35. Alaska Legacy L-band Flight Line Summary Data

Line ID	Short Name	Flight Plan	Date	Comments
25509	Permaf	15147	2015-10-05	Legacy L-band line; Matching P-band legacy line 25507
25510	Permaf	15147	2015-10-05	Legacy L-band line; Matching P-band legacy line 25508
32511	Permaf	15147	2015-10-05	Legacy L-band line; Matching P-band legacy line 32510
08534	Permaf	15147	2015-10-05	Legacy L-band line; Matching P-band legacy line 08509
03108	Permaf	15147	2015-10-05	Legacy L-band line; Matching P-band legacy line 03106
03109	Permaf	15147	2015-10-05	Legacy L-band line; Matching P-band legacy line 03107
34506	Permaf	15147	2015-10-05	Legacy L-band line; Matching P-band legacy line 34505
15015	Permaf	15147	2015-10-05	Legacy L-band line; Matching P-band legacy line 15010
18518	Permaf	15147	2015-10-05	Legacy L-band line; Matching P-band legacy line 18517
20015	Permaf	15147	2015-10-05	Legacy L-band line; Matching P-band legacy line 20007

5.2 L-band SAR Legacy Flight Lines - BERMS

Legacy L-band boreal forest sampling over BERMS and Kenaston SK (**Figure S20**) was performed during the CanEx 2010 boreal forest field campaign for SMAP [Maggai et al. 2012; Djamai et al. 2015] and as one of the AirMOSS regular sampling sites [Moghaddam et al. 2016].

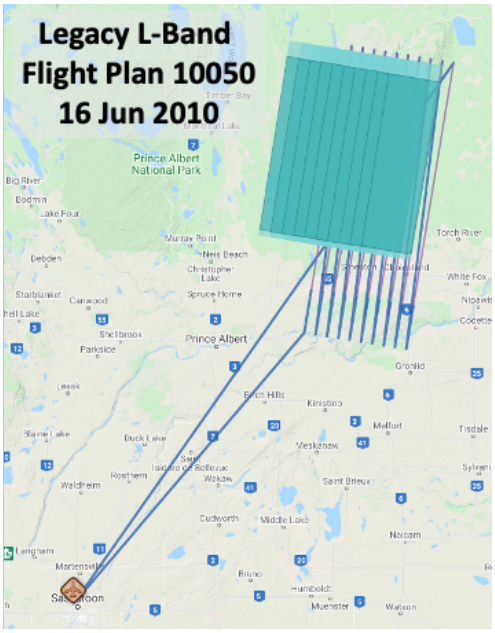

Figure S20. Legacy L-band flight lines acquired over the BERMS site during the SMAP CANEX-2010 campaign. These lines link L-band SAR acquired during ABoVE to BOREAS era measurements [Sellars et al. 1994; 1997]. See Table S3 for flight line details. © Google Maps

Table S36. BERMS-C Grid Legacy L-band Flight Line Summary Data

Line ID	Short Name	Flight Plan	Date	Comments
00901	bermsC	10050	2010-06-16	BERMS boreal forest grid; SMAP CanEx 2010 Campaign
00902	bermsC	10050	2010-06-16	BERMS boreal forest grid; SMAP CanEx 2010 Campaign
00903	bermsC	10050	2010-06-16	BERMS boreal forest grid; SMAP CanEx 2010 Campaign
00904	bermsC	10050	2010-06-16	BERMS boreal forest grid; SMAP CanEx 2010 Campaign
00905	bermsC	10050	2010-06-16	BERMS boreal forest grid; SMAP CanEx 2010 Campaign
00906	bermsC	10050	2010-06-16	BERMS boreal forest grid; SMAP CanEx 2010 Campaign
00907	bermsC	10050	2010-06-16	BERMS boreal forest grid; SMAP CanEx 2010 Campaign
00908	bermsC	10050	2010-06-16	BERMS boreal forest grid; SMAP CanEx 2010 Campaign
00909	bermsC	10050	2010-06-16	BERMS boreal forest grid; SMAP CanEx 2010 Campaign
00910	bermsC	10050	2010-06-16	BERMS boreal forest grid; SMAP CanEx 2010 Campaign

6 Acronyms and Abbreviations

Table S37. List of Acronyms and Abbreviations

Acronym	Name	Description
ABoVE	Arctic Boreal Vulnerability Experiment (ABoVE)	NASA Terrestrial Ecology Program's 10-year community field experiment designed to evaluate the vulnerability/resilience of Arctic ecosystems to change
AirMOSS	Airborne Microwave Observatory of Subcanopy and Subsurface (AirMOSS)	An EV-S1 investigation deploying an airborne P-band SAR based on the UAVSAR/L-band system (PI M. Moghaddam). AirMOSS made flights over BERMS (2012-2015) and Alaska (2014, 2015) providing legacy data for ABoVE.
AirSWOT	Airborne instrument for supporting the SWOT mission (AirSWOT)	AirSWOT is an airborne instrument for supporting the SWOT mission. AirSWOT is designed to make interferometric measurements similar to those that will be made in space by SWOT. AirSWOT data will also be used to help calibrate and validate SWOT data and can be used additionally for science studies in their own right.
ALT	Active Layer Thickness (ALT)	Active Layer Thickness (ALT), defined as the maximum depth of seasonally thawed soil overlying permafrost, is critical for understanding the effects of climate warming, disturbance, and hydrologic changes on permafrost degradation in cold regions
BERMS	Boreal Ecosystem Research and Monitoring Sites (BERMS)	The Boreal Ecosystem Research and Monitoring Sites (BERMS) are located in the southern edge of the boreal plains ecozone in Saskatchewan, Canada. The four BERMS sites, covering 4 different forest vegetation types common to the Boreal Plains are: Fen, Old Jack Pine (OJP), Old Black Spruce (OBS), and Old Aspen (OA). 'Old' refers to the monitoring site being located within a mature stand of trees.
BIOMASS	BIOMASS (mission name)	Carrying a novel P-band synthetic aperture radar, the Biomass mission is designed to deliver crucial information about the state of our forests and how they are changing, and to further our knowledge of the role forests play in the carbon cycle. planned for launch by the European Space Agency (ESA) in August 2023.
BOREAS	Boreal Ecosystem–Atmosphere Study (BOREAS)	The Boreal Ecosystem-Atmosphere Study (BOREAS) was a large-scale international interdisciplinary experiment in the boreal forests of central Canada. Its focus was improving our understanding of the exchanges of radiative energy, sensible heat, water, CO2 and trace gases between the boreal forest and the lower atmosphere.
CALM	Circumpolar Active Layer Monitoring network (CALM)	The primary goal of the Circumpolar Active Layer Monitoring (CALM) program is to observe the response of the active layer and near-surface permafrost to climate change over long (multi-decadal) time scales.
CanEx	SMAP CanEx 2010	2010 Canadian soil moisture field campaign run by the SMAP team over the BERMS sites [Magagi 2012]
CCRN	Canadian Changing Cold Regions Network (CCRN)	CCRN's overall aims were to integrate existing and new sources of data with improved predictive and observational tools to understand, diagnose and predict interactions amongst the cryospheric, ecological, hydrological, and climatic components of the changing Earth system at multiple scales, with a geographic focus on Western Canada's rapidly changing cold interior. CCRN operated from 2013-2018.
CFS	Canadian Forest Service (CFS)	The Canadian Forest Service is the national and international voice for Canada's forest sector. We are part of Natural Resources Canada, a federal government department, and have an office in Ottawa and 6 research centres across the country. We collaborate closely with Canada's provinces and territories to ensure our forests are sustainable and healthy

CIPHA	Climate Impacts on Productivity and Health of Aspen (CIPHA)	The Canadian Forest Service's Climate Impacts on Productivity and Health of Aspen (CIPHA) study includes a network of 180 research plots aimed at tracking dieback and changes in the growth of aspen forests across the boreal forest. Trembling aspen, also known locally as "white poplar," is the most abundant deciduous tree in Canada's boreal forest, where it is important both ecologically and commercially. Recent severe droughts have led to widespread dieback and decline of aspen and other types of forests across large areas of west-central Canada, prompting concerns for the future in a changing climate.
DAAC	Distributed Active Archive Center	The NASA TE program data, including ABoVE data, are archived at the ORNL DAAC
DLR	German Space Agency (DLR)	DLR is the Federal Republic of Germany's research centre for aeronautics and space. We conduct research and development activities in the fields of aeronautics, space, energy, transport, security and digitalisation.
DOY	Day of Year (DOY)	The Day-of-Year (DOY) numbering system is a common format used in research data and by the military. The Day-of-Year system ignores the existence of months and numbers each day of the year consecutively.
EV-S1	Earth Ventures Sub-orbital (EV-1)	The EV-S1 airborne-science investigations are Principal Investigator-led, temporally-sustained, airborne-science investigations. They are broader in scope than typical airborne-science missions due to multiple deployments, sustained science data collection and operations spanning several years. The AirMOSS EV-S1 mission and ABoVE precursor ran from 2010-2015
F-SAR	F-SAR – DLR's New Airborne SAR System	DLR's advanced airborne SAR testbed for technology and remote sensing applications. F-SAR operates fully polarimetric at X-, C-, S-, L- and P-bands and features single-pass polarimetric interferometric SAR (PolInSAR) capabilities in X- and S-bands [Reigber 2013].; flew over the ABoVE domain in August 2018
FMS	Flight Management System (FMS)	A Flight Management System (FMS) is an on-board multi-purpose navigation, performance, and aircraft operations computer designed to provide virtual data and operational harmony between closed and open elements associated with a flight from pre-engine start and take-off, to landing and engine shut-down.
GeoSAR	Geographic Synthetic Aperture Radar (GeoSAR)	GeoSAR was an airborne state-of-the-art, dual-band (P-band and X-band), dual-sided, single-pass interferometric mapping radar, designed to efficiently map wide-area, both top vegetation canopies and the terrain beneath the canopy. GeoSAR was a precursor of the UAVSAR instrument.
GNWT	Government of the Northwest Territories (GNWT)	GNWT supports ABoVE activities in the NWT, especially via its Climate and Environment & Energy programs. See the 2030 NWT Climate Change Strategic Framework
GPS	Global Positioning System (GPS)	The Global Positioning System (GPS) is a U.S.-owned utility that provides users with positioning, navigation, and timing (PNT) services. This system consists of three segments: the space segment, the control segment, and the user segment. The U.S. Space Force develops, maintains, and operates the space and control segments.
GTN-P	Global Terrestrial Network for Permafrost (GTN-P)	The Global Terrestrial Network for Permafrost (GTN-P) is the primary international programme concerned with monitoring permafrost parameters. GTN-P was developed in the 1990s by the International Permafrost Association (IPA) under the Global Climate observing System (GCOS) and the Global Terrestrial Observing Network (GTOS), with the long-term goal of obtaining a comprehensive view of the spatial structure, trends and variability of changes in the active layer thickness and permafrost temperature.
HELCIA	High Elevation & Latitude Climate Change Impacts & Adaptation (HELCIA)	A collaborative initiative under the NRCAN-CFS Forest Change Program

InSAR	Interferometric Synthetic Aperture Radar (InSAR)	Interferometric Synthetic Aperture Radar (InSAR) is an effective way to measure changes in land surface altitude. InSAR makes high-density measurements over large areas by using radar signals from Earth-orbiting satellites to measure changes in land-surface altitude at high degrees of measurement resolution and spatial detail. Synthetic Aperture Radar (SAR) imagery is produced by reflecting radar signals off a target area and measuring the two-way travel time back to the satellite. The SAR interferometry technique uses two SAR images of the same area acquired at different times and "interferes" (differences) them, resulting in maps called interferograms that show ground-surface displacement (range change) between the two time periods.
ISRO	Indian Space Research Organization (ISRO)	ISRO's vision is to harness space technology for national development, while pursuing space science research and planetary exploration. ISRO owns the LS-ASAR airborne instrument and is NASA's partner in the NISAR mission.
KaSPAR	Ka-band SWOT Phenomenology Airborne Radar (KaSPAR)	The core of AirSWOT is the Ka-band SWOT Phenomenology Airborne Radar (KaSPAR). It collects two swaths of across-track interferometry data - between nadir and 1 km and between 1 km and 5 km, respectively - which can be used to obtain centimeter-level topographic maps of water surfaces. In addition, KaSPAR has an along-track interferometer that can be used to measure the temporal decorrelation of water surfaces, as well as the water radial velocity.
LiDAR	Light Detection and Ranging (lidar)	Lidar is a remote sensing method that uses light in the form of a pulsed laser to measure ranges (variable distances) to the Earth. These light pulses—combined with other data recorded by the airborne system — generate precise, three-dimensional information about the shape of the Earth and its surface characteristics.
LS-ASAR	L- and S-Band-Airborne SAR (LS-ASAR)	As a precursor to the NISAR mission, ISRO has developed a L- and S-Band-Airborne SAR (LS-ASAR) to prepare the community to maximize the scientific and societal benefits of NISAR data [Ramanujam 2016; 2019; Mehra 2019]. LS-ASAR operates in Dual, Quad, and Hybrid and Polarization modes in both L- and S-bands. It covers incidence angles from 24°-77°
LTER	Long Term Ecological Research (LTER)	The LTER Network was founded in 1980 by the National Science Foundation with the recognition that long-term research could help unravel the principles and processes of ecological science, which frequently involves long-lived species, legacy influences, and rare events. LTER's mission is to provide the scientific community, policy makers, and society with the knowledge and predictive understanding necessary to conserve, protect, and manage the nation's ecosystems, their biodiversity, and the services they provide.
LVIS	Land, Vegetation, and Ice Sensor (LVIS)	LVIS is an airborne, full waveform scanning laser altimeter which produces topographic maps with decimeter accuracy as well as vegetation vertical height and structure measurements [Blair 1999a,b]. LVIS became a NASA Facility Instrument in 2019.
NEON	National Ecological Observatory Network (NEON)	NSF's National Ecological Observatory Network (NEON) program provides open, continental-scale data across the United States that characterize and quantify complex, rapidly changing ecological processes. Its Tundra (D-19) and Taiga (D-18) observatories in Alaska are key ground truth sites for ABoVE airborne SAR data collections
NGEE-Arctic	Next Generation Ecological Experiment-Arctic (NGEE-Arctic)	The Next-Generation Ecosystem Experiments (NGEE Arctic) is a 10-year project (2012—2022) to improve our predictive understanding of carbon (C)-rich Arctic system processes and feedbacks to climate. This is achieved through experiments, observations, and synthesis of existing datasets that strategically inform model process representation and parameterization, and that enhance the knowledge base required for model initialization, calibration, and evaluation. The NGEE-Arctic Seward Peninsula and Barrow area sites provide critical ground truth data for ABoVE airborne SAR data

NISAR	NASA-ISRO SAR (NISAR) mission	NISAR is a joint Earth-observing mission between NASA and the Indian Space Research Organization (ISRO) with the goal to make global measurements of the causes and consequences of land surface changes using advanced radar imaging. To be launched in early 2023, NISAR will employ L- and S-band SARs to measure Earth's changing ecosystems, dynamic surfaces, and ice masses. NISAR will observe Earth's land and ice-covered surfaces globally with 12-day regularity on ascending and descending passes, sampling Earth on average every 6 days for a baseline 3-year mission [Rosen 2017]
NoFC	Northern Forestry Centre (NoFC)	The Northern Forestry Centre is one of five research centres operated by the Canadian Forest Service. It is located in Edmonton, Alberta. It's primary research areas are: Boreal ecosystem ecology, Climate Change and forests research, Land reclamation, and Wildland fire. ABoVE SAR flight lines target many of its forest inventory, CIPHA and HELCIA sites for ground truth measurements
NWT	Northwest Territories (NWT)	Northwest Territories, region of northern and northwestern Canada encompassing ~1.35 Mkm2 of forests and tundra. The NWT are bordered by Nunavut to the east, the provinces of Saskatchewan, Alberta, and British Columbia to the south, and Yukon to the west. NWT lands are a focal point for ABoVE airborne SAR campaigns, with Yellowknife serving as a base of operations
OAS	Old Aspen (OAS)	BERMS Flux tower site; CA-Oas: Saskatchewan - Western Boreal, Mature Aspen; 53.62889° N, 106.19779° W, elevation of 600.63 m, BOREAS 1994, 1996, BERMS climate and flux measurements began Dec. 1996. The Old Aspen site ended operations in 2017 and has since been decommissioned.
OBS	Old Black Spruce (OBS)	BERMS Flux tower site; CA-Obs: Saskatchewan - Western Boreal, Mature Black Spruce; 53.98717° N, 105.11779° W, elevation of 628.94 m, BOREAS 1994, 1996, BERMS climate measurements began Dec. 1996 and flux measurements in Apr. 1999
OJP	Old Jack Pine (OJP)	BERMS Flux tower site; CA-Ojp: Saskatchewan - Western Boreal, Mature Jack Pine; 53.91634° N, 104.69203° W, elevation of 579.27 m, BOREAS 1994, BERMS climate measurements began Mar. 1997 and flux measurements Aug. 1999
ORNL	Oak Ridge National Laboratory (ORNL)	Home of the ABoVE DAAC and NGEE-Arctic leadership
PALSAR	Phased Array type L-band Synthetic Aperture Radar (PALSAR)	The Phased Array type L-band Synthetic Aperture Radar (PALSAR, launched in 2006) is an active microwave sensor using L-band frequency to achieve cloud-free and day-and-night land observation. PALSAR provides 10m resolution in a conventional mode, but can acquire a 250 to 350 km width of SAR images (depending on the number of scans) at the expense of spatial resolution. The development of the PALSAR is a joint project between JAXA and the Japan Resources Observation System Organization (JAROS). PALSAR acquisitions across the ABoVE domain provide a valuable baseline for ABoVE airborne SAR comparisons.
PALSAR-2	Phased Array type L-band Synthetic Aperture Radar 2 (PALSAR-2)	PALSAR-2 (launched in 2014 aboard ALOS-2) is the successor to JAXA's Phased Array type L-band Synthetic Aperture Radar (PALSAR). ALOS-2/PALSAR-2 has a spotlight mode (1m×3m resolution in azimuth×range direction) as well as right and left viewing capabilities.
PDO	Permafrost Dynamics Observatory (PDO)	The PDO algorithm uses L-band InSAR to measure seasonal surface subsidence due to the thawing of the active layer and the P-band backscatter to measure soil moisture. The combined PDO algorithm estimates seasonal subsidence, ALT, and the vertical soil moisture profile [Michaelides 2021; Chen 2021a,b]
PermASAR	permafrost airborne SAR experiment (PermASAR)	DLR's permafrost airborne SAR experiment (PermASAR) deployed F-SAR to northern Canada in August 2018 and April 2019. F-SAR flight lines sampled many ABoVE L-band transects

POLAR	Polar Knowledge Canada (POLAR)	Polar Knowledge Canada (POLAR) is responsible for advancing Canada's knowledge of the Arctic, strengthening Canadian leadership in polar science and technology, and promoting the development and distribution of knowledge of other circumpolar regions, including Antarctica. POLAR operates the Canadian High Arctic Research Station (CHARS) campus and conducts world-class cutting edge Arctic research out of this extraordinary facility. POLAR is ABoVE's primary Canadian partner.
PolInSAR	Polarimetric Interferometric Synthetic Aperture Radar (PolInSAR)	Known by the unwieldy acronym, POLinSAR, the technique combines varying the orientation, or polarisation, of radar signals (POLarimetry) with the analysis of the phase differences in the signal to produce differential range and range-change measurements (interferometry) from two or more images captured by synthetic aperture radars (SARs). Taken together, polarimetry and interferometry offers the potential to see the Earth in three dimensions.
PPA	Platform Precision Autopilot (PPA)	The real-time platform control system that confines the repeat flight path to within a 10 m tube over a 200 km course in conditions of calm to light turbulence; enables repeat-pass SAR interferometry for the airborne L- and P-band sensors
RADARSAT	RADARSAT (mission name)	RADASAT-1 (launched 4 November 1995 by the Canadian Space Agency) was a C-band radar with 8m x 8m spatial resolution. RADASAT-2 (launched 14 December 2007) was a C-band radar with 1m x 3m spatial resolution in spotlight mode. It has routine left- and right-looking operation and increased re-visit frequency for improved monitoring efficiencies. It offers enhanced marine surveillance, ice monitoring, disaster management, environmental monitoring, resource management and mapping in the Arctic.
RCM	RADARSAT Constellation Mission (RCM)	The RADARSAT Constellation Mission (RCM) is Canada's new generation of Earth observation C-band radars. Launched on June 12, 2019 by the Canadian Space Agency, the three identical satellites are capable of scanning Earth day or night and in any weather conditions with 1m x 3m spatial resolution in spotlight mode. The three-satellite configuration allows for daily revisits of Canada's vast territory and maritime approaches, as well as access to the Arctic up to four times a day.
ReSALT	remotely sensed active layer thickness (ReSALT)	An algorithm which uses spaceborne InSAR measurements of the seasonal deformation of the thawing active layer to estimate the total active layer thickness [Schaefer 2015]
RH100	Relative Height 100th percentile (RH100)	LVIS canopy height is provided as the mean height (in meters) above ground of the received waveform signal that was the first reflection off the top of the canopy (RH100). RH100 or relative height is the 100th percentile of waveform energy relative to ground elevation. Derived from the L2B LIDAR metric RH100 data product.
ROSE-L	Copernicus Radar Observation System for Europe in L-band (ROSE-L)	With launch planned in 2028, the new high-priority Copernicus Radar Observation System for Europe in L-band (ROSE-L) environmental monitoring mission will provide information for monitoring forest type and cover in support of biomass estimation, as well as soil moisture, vegetation and land ice – as part of Europe's Copernicus programme. The mission will automatically map and monitor sea and land ice, greatly helping climate change research. ROSE-L will provide continuous day-and-night all-weather monitoring of Earth's land, oceans and ice, and offer frequent images at a high spatial resolution.
SAR	Synthetic Aperture Radar (SAR)	Synthetic-aperture radar (SAR) remote sensing is usually implemented by mounting, on a moving platform such as an aircraft or spacecraft, a single beam-forming antenna from which a target scene is repeatedly illuminated with pulses of microwaves at wavelengths anywhere from a meter down to millimeters. A sequence of acquisitions from a shorter antenna are combined to simulate a much larger antenna (the synthetic aperture), thus increasing the spatial resolution data

SDC	Surface Deformation and Change (SDC)	The Surface Deformation and Change (SDC) Targeted Observable will use deformation measurements, such as Synthetic Aperture Radar Interferometry (InSAR), to understand the dynamics of earthquakes, volcanoes, landslides, glaciers, groundwater and the deep interior; for quantifying the rates and driving processes of sea-level change and landscape change; and for supporting hazard forecasts and disaster impact assessments. SDC architectures are being studied for a potential launch in the late 2020s.
Sentinel-1	Sentinel-1 (mission name)	The Sentinel-1 mission is the European Radar Observatory for the Copernicus joint initiative of the European Commission (EC) and the European Space Agency (ESA). The Sentinel-1 mission comprises a constellation of two polar-orbiting satellites, operating day and night performing C-band synthetic aperture radar imaging, enabling them to acquire imagery regardless of the weather. The Sentinel-1 mission includes C-band imaging operating in four exclusive imaging modes with different resolution (down to 5 m) and coverage (up to 400 km). It provides dual polarisation capability, very short revisit times and rapid product delivery. Sentinel-1A was launched on 3 April 2014. Sentinel-1B was launched on 25 April 2016. Each has an operational lifespan of seven years with consumables for 12 years. Sentinel-1C and Sentinel-1D are planned to replace the first two satellites at the end of their operational lifespan.
SMAP	Soil Moisture Active/Passive (SMAP)	SMAP is an Earth satellite mission designed to measure and map Earth's soil moisture and freeze/thaw state to better understand terrestrial water, carbon and energy cycles
SnowEx	Snow Experiment (SnowEx)	SnowEx is a five-year program initiated and funded by the NASA Terrestrial Hydrology Program to address the most important gaps in snow remote sensing knowledge. A joint SnowEx-ABoVE tundra-taiga snowscapes campaign is planned for Alaska during the January – May 2023 period.
SWOT	Surface Water and Ocean Topography (SWOT)	The SWOT mission will be NASA's first global survey of Earth's surface water. SWOT is being jointly developed by NASA and Centre National D'Etudes Spatiales (CNES) with contributions from the Canadian Space Agency (CSA) and United Kingdom Space Agency.
TomoSAR	tomographic SAR (tomoSAR)	Synthetic aperture radar tomography (TomoSAR) at lower frequencies allows the reconstruction of the 3-D radar reflectivity of volume scatterers allowing access to their physical 3-D structure by means of multiangular SAR acquisitions. The performance of the reconstruction critically depends on the number and (spatial) distribution of the tomographic acquisitions (tracks).
UAVSAR	Uninhabited Aerial Vehicle Synthetic Aperture Radar (UAVSAR)	NASA's airborne L-band SAR; a compact pod-mounted polarimetric instrument for interferometric repeat-track observations
VWC	Volumetric Water Content (VWC)	The volumetric water content is the ratio of the volume of water to the unit volume of soil. Volumetric water content can be expressed as ratio, percentage or depth of water per depth of soil (assuming a unit surface area), such as inches of water per foot of soil.

7 Acknowledgments

The L- and P-band SAR data acquisitions would not have been possible without the indefatigable support of our NASA pilots and flight crews. We thank John McGrath and the NASA AFRC C-20 (N30502) team as well as Derek Rutovic and the NASA JSC G-III (N995NA) team. We also thank the instrument scientists, operators, and data processing team from the JPL Subortbital Radar Science and Engineering Team (334F) who were essential to the successful execution of these experiments and rapid processing of the resulting data products. The field work supporting the SAR campaigns was made possible by the excellent support from Dan Hodkinson, Sarah Sackett, and the ABoVE Logistics Office. Finally, we thank the data curation team at the Oak Ridge Distributed Active Archive Center for their support and expert advice.

This work was supported by the NASA Terrestrial Ecology Program's Arctic-Boreal Vulnerability Experiment (ABoVE). A portion of this work was performed at the Jet Propulsion Laboratory, California Institute of Technology, under contract with National Aeronautics and Space Administration (80NM0018D0004).

8 References

Abe, T., Iwahana, G., Efremov, P. V., Desyatkin, A. R., Kawamura, T., Fedorov, A., Zhegusov, Y., Yanagiya, K., and Tadono, T.: Surface displacement revealed by L-band InSAR analysis in the Mayya area, Central Yakutia, underlain by continuous permafrost, Earth Planets Space, 72, 138, https://doi.org/10.1186/s40623-020-01266-3, 2020.

Airborne Imaging: Final LiDAR processing & vertical accuracy report: Prepared for the U.S. Fish and Wildlife Service, in: LiDAR Imagery & DEM Model for Yukon Delta National Wildlife Refuge—Near Angyaravak Bay, Alaska, Airborne Imaging, Calgary, AB, Canada, 28, 2011.

Allen, B. D., Braun, S. A., Crawford, J. H., Jensen, E. J., Miller, C. E., Moghaddam, M., and Maring, H.: Proposed investigations from NASA's Earth Venture-1 (EV-1) airborne science selections, in: 2010 IEEE International Geoscience and Remote Sensing Symposium, 2010 IEEE International Geoscience and Remote Sensing Symposium, 2575–2578, https://doi.org/10.1109/IGARSS.2010.5651920, 2010.

Alonzo, M., Dial, R. J., Schulz, B. K., Andersen, H.-E., Lewis-Clark, E., Cook, B. D., and Morton, D. C.: Mapping tall shrub biomass in Alaska at landscape scale using structure-from-motion photogrammetry and lidar, Remote Sens. Environ., 245, 111841, https://doi.org/10.1016/j.rse.2020.111841, 2020.

Altenau, E. H., Pavelsky, T. M., Moller, D., Lion, C., Pitcher, L. H., Allen, G. H., Bates, P. D., Calmant, S., Durand, M., and Smith, L. C.: AirSWOT measurements of river water surface elevation and slope: Tanana River, AK, Geophys. Res. Lett., 44, 181–189, https://doi.org/10.1002/2016GL071577, 2017.

Kenaston / Brightwater Creek Mesonet Site, SK - CCRNetwork: http://www.ccrnetwork.ca/science/WECC/prairie/brightwater-creek.php, last access: 30 April 2021.

Bakian-Dogaheh, K., Chen, R. H., Moghaddam, M., and Tabatabaeenejad, A.: Electromagnetic scattering behavior of a new organic soil dielectric model for long-wavelength radar retrieval of permafrost active layer soil properties, 2020 IEEE International Geoscience and Remote Sensing Symposium, 2020.

Bakian-Dogaheh, K., R.H. Chen, M. Moghaddam, Y. Yi, and A. Tabatabaeenejad. 2020. ABoVE: Active Layer Soil Characterization of Permafrost Sites, Northern Alaska, 2018. ORNL DAAC, Oak Ridge, Tennessee, USA. https://doi.org/10.3334/ORNLDAAC/1759

Banks, S. N., Ullmann, T., Duffe, J., Roth, A., King, D., Demers, A.-M., Hogg, A., Schmitt, A., Baumhauer, R., and Dech, S.: Multi-frequency analysis of high resolution quad-pol Radarsat-2 and dual-pol TerraSAR-X data for land cover classification in Arctic Coastal Ecosystems, Mackenzie Delta, beaufort sea, 3548–3551, https://doi.org/10.1109/IGARSS.2012.6350653, 2012.

Banks, S. N., King, D. J., Merzouki, A., and Duffe, J.: Characterizing Scattering Behaviour and Assessing Potential for Classification of Arctic Shore and Near-Shore Land Covers with Fine Quad-Pol RADARSAT-2 Data, Can. J. Remote Sens., 40, 291–314, https://doi.org/10.1080/07038992.2014.979487, 2014.

Barr, A. G., Morgenstern, K., Black, T. A., McCaughey, J. H., and Nesic, Z.: Surface energy balance closure by the eddy-covariance method above three boreal forest stands and implications for the measurement of the CO2 flux, Agric. For. Meteorol., 140, 322–337, https://doi.org/10.1016/j.agrformet.2006.08.007, 2006.

Bennett, A. J., Thompson, W. L., and Mortenson, D. C.: Vital Signs Monitoring Plan Southwest Alaska Network: Inventory and Monitoring Program, Natl. Park Serv., 2006.

Blair, J. B and Hofton, M.: ABoVE LVIS L2 Geolocated Surface Elevation Product, Version 1, https://doi.org/10.5067/IA5WAX7K3YGY, 2018.

Blomberg, E., Ulander, L. M. H., Tebaldini, S., and Ferro-Famil, L.: Evaluating P-Band TomoSAR for Biomass Retrieval in Boreal Forest, IEEE Trans. Geosci. Remote Sens., 59, 3793–3804, https://doi.org/10.1109/TGRS.2020.3020775, 2021.

Bourgeau-Chavez, L. L., French, N. H. F., Grelick, S. E., Jenkins, L., Battaglia, M., Serocki, E., and Billmire, M.: ABoVE: Burn Severity, Fire Progression, Landcover and Field Data, NWT, Canada, 2014, ORNL DAAC, https://doi.org/10.3334/ORNLDAAC/1307, 2016.

Bourgeau-Chavez, L. L., Grelick, S. E., Jenkins, L., Battaglia, M., Serocki, E., and Billmire, M.: ABoVE: Burn Severity, Fire Progression, and Field Data, NWT, Canada, 2015-2016, ORNL DAAC, https://doi.org/10.3334/ORNLDAAC/1548, 2017.

Bourgeau-Chavez, L. L., Graham, J. A., Grelick, S. E., French, N. H. F., Battaglia, M., Hansen, D., and Tanzer, D.: ABoVE: Ecosystem Map, Great Slave Lake Area, Northwest Territories, Canada, 1997-2011, ORNL DAAC, https://doi.org/10.3334/ORNLDAAC/1695, 2019a.

Bourgeau-Chavez, L. L., Battaglia, M., Kane, E. S., Cohen, L. M., and Tanzer, D.: ABoVE: Post-Fire and Unburned Vegetation Community and Field Data, NWT, Canada, 2018, ORNL DAAC, https://doi.org/10.3334/ORNLDAAC/1703, 2019b.

Burns, L. E., Fugro Airborne Survey Corp., and Stevens Exploration Management Corp.: Final processed database for the airborne geophysical surveys of the Alaska Highway corridor, east-central Alaska: Alaska Division of Geological & Geophysical Surveys Geophysical Report 2006-8, 1 DVD., https://doi.org/10.14509/17761, 2008.

Campbell, E. M., Antos, J. A., and vanAkker, L.: Resilience of southern Yukon boreal forests to spruce beetle outbreaks, For. Ecol. Manag., 433, 52–63, https://doi.org/10.1016/j.foreco.2018.10.037, 2019.

Chapin, E., Chau, A., Chen, J., Heavey, B., Hensley, S., Lou, Y., Machuzak, R., and Moghaddam, M.: AirMOSS: An Airborne P-band SAR to measure root-zone soil moisture, in: 2012 IEEE Radar Conference, 2012 IEEE Radar Conference, 0693–0698, https://doi.org/10.1109/RADAR.2012.6212227, 2012.

Chapin, E., Flores, S., Harcke, L., Hawkins, B. P., Hensley, S., Michel, T. R., Muellerschoen, R. J., Shimada, J. G., Tung, W. W., and Veeramachaneni, C.: AirMOSS: L1 S-0 Polarimetric Data from AirMOSS P-band SAR, BERMS, Canada, 2012-2015, ORNL DAAC, https://doi.org/10.3334/ORNLDAAC/1406, 2018.

Chen, A. C., Parsekian, A. D., Schaefer, K., Jafarov, E. E., Panda, S. K., Liu, L., Zhang, T., and Zebker, H. A.: Pre-ABoVE: Ground-penetrating Radar Measurements of ALT on the Alaska North Slope, ORNL DAAC, https://doi.org/10.3334/ORNLDAAC/1265, 2015.

Chen, R. H., Tabatabaeenejad, A., and Moghaddam, M.: A time-series active layer thickness retrieval algorithm using P- and L-band SAR observations, 2016 IEEE International Geoscience and Remote Sensing Symposium (IGARSS), 3672–3675, https://doi.org/10.1109/IGARSS.2016.7729951, 2016.

Chen, R. H., Tabatabaeenejad, A., and Moghaddam, M.: Retrieval of permafrost active layer properties using P-band airmoss and L-band UAVSAR data, 2017 IEEE International Geoscience and Remote Sensing Symposium (IGARSS), 1415–1418, https://doi.org/10.1109/IGARSS.2017.8127230, 2017.

Chen, R. H., Tabatabaeenejad, A., and Moghaddam, M.: P-Band Radar Retrieval of Permafrost Active Layer Properties: Time-Series Approach and Validation with In-Situ Observations, IGARSS 2018 - 2018 IEEE International Geoscience and Remote Sensing Symposium, 6777–6779, https://doi.org/10.1109/IGARSS.2018.8518179, 2018.

Chen, R. H., Tabatabaeenejad, A., and Moghaddam, M.: ABoVE: Active Layer and Soil Moisture Properties from AirMOSS P-band SAR in Alaska, ORNL DAAC, https://doi.org/10.3334/ORNLDAAC/1657, 2019a.

Chen, R. H., Bakian-Dogaheh, K., Tabatabaeenejad, A., and Moghaddam, M.: Modeling and Retrieving Soil Moisture and Organic Matter Profiles in the Active Layer of Permafrost Soils From P-Band Radar Observations, IGARSS 2019 - 2019 IEEE International Geoscience and Remote Sensing Symposium, 10095–10098, https://doi.org/10.1109/IGARSS.2019.8899802, 2019b.

Chen, R. H., Tabatabaeenejad, A., and Moghaddam, M.: Retrieval of Permafrost Active Layer Properties Using Time-Series P-Band Radar Observations, IEEE Trans. Geosci. Remote Sens., 57, 6037–6054, https://doi.org/10.1109/TGRS.2019.2903935, 2019c.

Chen, R. H., Michaelides, R. J., Sullivan, T. D., Parsekian, A. D., Zebker, H. A., Moghaddam, M., and Schaefer, K. M.: Joint Retrieval of Soil Moisture and Permafrost Active Layer Thickness Using L-Band Insar and P-Band Polsar, IGARSS 2020 - 2020 IEEE International Geoscience and Remote Sensing Symposium, 4606–4609, https://doi.org/10.1109/IGARSS39084.2020.9324660, 2020a.

Chen, R. H., Pinto, N., Duan, X., Tabatabaeenejad, A., and Moghaddam, M.: Mapping Tree Canopy Cover and Canopy Height with L-Band SAR Using LiDAR Data and Random Forests, IGARSS 2020 - 2020 IEEE International Geoscience and Remote Sensing Symposium, 4136–4139, https://doi.org/10.1109/IGARSS39084.2020.9323738, 2020b.

Chen, R. H., Michaelides, R. J., Sullivan, T. D., Parsekian, A. D., Zebker, H. A., Moghaddam, M., & Schaefer, K. M. (2021a). Joint retrieval of soil moisture and activere layer thickness in the northern circumpolar permafrost region using l-band InSAR and p-band polsar. Earth and Space Science.

Chen, Richard H., Roger J. Michaelides, Yuhuan Zhao, Lingcao Huang, Elizabeth Wig, Taylor D. Sullivan, Andrew D. Parsekian, Howard A. Zebker, Mahta Moghaddam, and Kevin M. Schaefer. "Permafrost Dynamics Observatory: Retrieval of Active Layer Thickness and Soil Moisture from Airborne Insar and Polsar Data." In *2021 IEEE International Geoscience and Remote Sensing Symposium IGARSS*, pp. 1444-1447. IEEE, 2021b. DOI: 10.1109/IGARSS47720.2021.9554288

Colliander, A., Cosh, M. H., Misra, S., Jackson, T. J., Crow, W. T., Powers, J., McNairn, H., Bullock, P., Berg, A., Magagi, R., Gao, Y., Bindlish, R., Williamson, R., Ramos, I., Latham, B., O'Neill, P., and Yueh, S.: Comparison of high-resolution airborne soil moisture retrievals to SMAP soil moisture during the SMAP validation experiment 2016 (SMAPVEX16), Remote Sens. Environ., 227, 137–150, https://doi.org/10.1016/j.rse.2019.04.004, 2019.

Cooley, S. W., Smith, L. C., Stepan, L., and Mascaro, J.: Tracking Dynamic Northern Surface Water Changes with High-Frequency Planet CubeSat Imagery, Remote Sens., 9, 1306, https://doi.org/10.3390/rs9121306, 2017.

Crasto, N., Hopkinson, C., Forbes, D. L., Lesack, L., Marsh, P., Spooner, I., and van der Sanden, J. J.: A LiDAR-based decision-tree classification of open water surfaces in an Arctic delta, Remote Sens. Environ., 164, 90–102, https://doi.org/10.1016/j.rse.2015.04.011, 2015.

Danby, R.: A Muniscale Study of Tree-Line Dynamics in Southwestern Yukon, Arctic, 56, 427–429, 2003.

Danby, R. K., Williams, A., and Hik, D. S.: Fifty Years of Science at the Kluane Lake Research Station, Arctic, 67, iii–viii, https://doi.org/10.14430/arctic4398, 2014.

Davey, C. A., Redmond, K. T., and Simeral, D. B.: Weather and Climate Inventory National Park Service Southwest Alaska Network, National Park Service, Fort Collins, Colorado, 2007.

Davidson, S. J., Santos, M. J., Sloan, V. L., Watts, J. D., Phoenix, G. K., Oechel, W. C., and Zona, D.: Mapping Arctic Tundra Vegetation Communities Using Field Spectroscopy and Multispectral Satellite Data in North Alaska, USA, Remote Sens., 8, 978, https://doi.org/10.3390/rs8120978, 2016.

Davidson, S. J., Santos, M. J., Sloan, V. L., Reuss-Schmidt, K., Phoenix, G. K., Oechel, W. C., and Zona, D.: Upscaling CH4 Fluxes Using High-Resolution Imagery in Arctic Tundra Ecosystems, Remote Sens., 9, 1227, https://doi.org/10.3390/rs9121227, 2017.

Dengel, S. and Torn, M.: NGEE Arctic CO2, CH4 and Energy Eddy-Covariance (EC) Flux Tower Auxiliary Measurements, Council Road Mile Marker 71, Seward Peninsula, Alaska, 2017 - Ongoing, https://doi.org/10.5440/1526749, 2020.

Djamai, N., Magagi, R., Goïta, K., Hosseini, M., Cosh, M.H., Berg, A. and Toth, B., 2015. Evaluation of SMOS soil moisture products over the CanEx-SM10 area. *Journal of hydrology*, *520*, pp.254-267. https://doi.org/10.1016/j.jhydrol.2014.11.026

Douglas, T.A., Jorgenson, M.T., Brown, D.N., Hiemstra, C.A., Liljedahl, A.K., Downer, C., Pradhan, N., Marchenko, S., Campbell, S., Senseman, G. and Olson, K., 2016. *Addressing the Impacts of Climate Change*

on US Army Alaska with Decision Support Tools Developed Through Field Work and Modeling. US Army Cold Regions Research and Engineering Laboratory Fort Wainwright United States. https://apps.dtic.mil/sti/pdfs/AD1030958.pdf

Douglas, T. A.: ABoVE: Soil Active Layer Thaw Depths at CRREL sites near Fairbanks, Alaska, 2014-2018, ORNL DAAC, https://doi.org/10.3334/ORNLDAAC/1701, 2019.

Douglas, T. A., Hiemstra, C. A., and Barker, A. J.: ABoVE: End of Season Snow Depth at CRREL sites near Fairbanks, Alaska, 2014-2019, ORNL DAAC, https://doi.org/10.3334/ORNLDAAC/1702, 2019.

Douglas, T. A., Turetsky, M. R., and Koven, C. D.: Increased rainfall stimulates permafrost thaw across a variety of Interior Alaskan boreal ecosystems, Npj Clim. Atmospheric Sci., 3, 1–7, https://doi.org/10.1038/s41612-020-0130-4, 2020.

Douglas, T. A., Hiemstra, C. A., Anderson, J. E., Barbato, R. A., Bjella, K. L., Deeb, E. J., Gelvin, A. B., Nelsen, P. E., Newman, S. D., Saari, S. P., and Wagner, A. M.: Recent degradation of Interior Alaska permafrost mapped with ground surveys, geophysics, deep drilling, and repeat airborne LiDAR, Cryosphere Discuss., 1–39, https://doi.org/10.5194/tc-2021-47, 2021.

Du, J., Kimball, J. S., and Moghaddam, M.: Theoretical Modeling and Analysis of L- and P-band Radar Backscatter Sensitivity to Soil Active Layer Dielectric Variations, Remote Sens., 7, 9450–9472, https://doi.org/10.3390/rs70709450, 2015.

Engstrom, R., Hope, A., Kwon, H., Stow, D., and Zamolodchikov, D.: Spatial distribution of near surface soil moisture and its relationship to microtopography in the Alaskan Arctic coastal plain, Hydrol. Res., 36, 219–234, https://doi.org/10.2166/nh.2005.0016, 2005.

Euskirchen, E. S. and Edgar, C.: FLUXNET-CH4 US-BZB Bonanza Creek Thermokarst Bog, , https://doi.org/10.18140/FLX/1669668, 2014a.

Euskirchen, E. S. and Edgar, C.: FLUXNET-CH4 US-BZF Bonanza Creek Rich Fen, , https://doi.org/10.18140/FLX/1669669, 2014b.

Euskirchen, E. S. and Edgar, C.: FLUXNET-CH4 US-BZS Bonanza Creek Black Spruce, , https://doi.org/10.18140/FLX/1669670, 2015.

Euskirchen, E. S., Bret-Harte, M. S., Scott, G. J., Edgar, C., and Shaver, G. R.: Seasonal patterns of carbon dioxide and water fluxes in three representative tundra ecosystems in northern Alaska, Ecosphere, 3, art4, https://doi.org/10.1890/ES11-00202.1, 2012.

Fayne, J. V., Smith, L. C., Pitcher, L. H., Kyzivat, E. D., Cooley, S. W., Cooper, M. G., Denbina, M. W., Chen, A. C., Chen, C. W., and Pavelsky, T. M.: Airborne observations of arctic-boreal water surface elevations from AirSWOT Ka-Band InSAR and LVIS LiDAR, Environ. Res. Lett., 15, 105005, https://doi.org/10.1088/1748-9326/abadcc, 2020.

French, N. H. F., Bourgeau-Chavez, L. L., and Chapman, B.: Wetland monitoring in high northern latitudes for carbon and habitat assessment using synthetic aperture radar, in: AGU Fall Meeting Abstracts, H31N-1951, 2019.

French, N. H. F., Graham, J. A., Bourgeau-Chavez, L. L., and Whitman, E.: ABoVE: Burn Severity of Soil Organic Matter, Northwest Territories, Canada, 2014-2015, ORNL DAAC, https://doi.org/10.3334/ORNLDAAC/1694, 2020a.

French, N. H. F., Graham, J., Whitman, E., Bourgeau-Chavez, L. L., French, N. H. F., Graham, J., Whitman, E., and Bourgeau-Chavez, L. L.: Quantifying surface severity of the 2014 and 2015 fires in the Great Slave Lake area of Canada, Int. J. Wildland Fire, 29, 892–906, https://doi.org/10.1071/WF20008, 2020b.

Frost, G. V., Loehman, R. A., Nelson, P. R., and Paradis, D. P.: ABoVE: Vegetation Composition across Fire History Gradients on the Y-K Delta, Alaska, ORNL DAAC, https://doi.org/10.3334/ORNLDAAC/1772, 2020.

Gamon, J. A., Huemmrich, K. F., Peddle, D. R., Chen, J., Fuentes, D., Hall, F. G., Kimball, J. S., Goetz, S., Gu, J., McDonald, K. C., Miller, J. R., Moghaddam, M., Rahman, A. F., Roujean, J.-L., Smith, E. A., Walthall, C. L., Zarco-Tejada, P., Hu, B., Fernandes, R., and Cihlar, J.: Remote sensing in BOREAS: Lessons learned, Remote Sens. Environ., 89, 139–162, https://doi.org/10.1016/j.rse.2003.08.017, 2004.

Goetz, SJ, Miller, CE, Griffith, PC, et al., An overview of NASA's Arctic Boreal Vulnerability Experiment (ABoVE): An integrated research campaign to assess ecosystem vulnerability and its implications within the Arctic and boreal domain, *Environmental Research Letters* (ABoVE Special Collection), Manuscript ERL-112259, submitted, 2021

Greaves, H. E., Vierling, L., Eitel, J., Boelman, N., Magney, T., Prager, C., and Griffin, K.: High-Resolution Shrub Biomass and Uncertainty Maps, Toolik Lake Area, Alaska, 2013, ORNL DAAC, https://doi.org/10.3334/ORNLDAAC/1573, 2018.

Gusmeroli, A., Liu, L., Schaefer, K., Zhang, T., Schaefer, T., and Grosse, G.: Active Layer Stratigraphy and Organic Layer Thickness at a Thermokarst Site in Arctic Alaska Identified Using Ground Penetrating Radar, Arct. Antarct. Alp. Res., 47, 195–202, https://doi.org/10.1657/AAAR00C-13-301, 2015.

He, J., Loboda, T. V., Jenkins, L., and Chen, D.: Mapping fractional cover of major fuel type components across Alaskan tundra, Remote Sens. Environ., 232, 111324, https://doi.org/10.1016/j.rse.2019.111324, 2019.

He, J., Loboda, T. V., Jenkins, L., and Chen, D.: ABoVE: Distribution Maps of Wildland Fire Fuel Components across Alaskan Tundra, 2015, ORNL DAAC, https://doi.org/10.3334/ORNLDAAC/1761, 2020.

He, J., Chen, D., Jenkins, L., and Loboda, T. V.: Impacts of wildfire and landscape factors on organic soil properties in Arctic tussock tundra. Environmental Research Letters., Environ. Res. Lett., in review, n.d.

Hensley, S., Oveisgharan, S., Saatchi, S., Simard, M., Ahmed, R. and Haddad, Z., 2014. An error model for biomass estimates derived from polarimetric radar backscatter. *IEEE Transactions on Geoscience and Remote Sensing*, *52*(7), pp.4065-4082.

Hensley, S., Lou, Y., Michel, T., Muellerschoen, R., Hawkins, B., Lavalle, M., Pinto, N., Reigber, A. and Pardini, M., 2016, July. UAVSAR PolInSAR and tomographic experiments in Germany. In *Geoscience and Remote Sensing Symposium (IGARSS), 2016 IEEE International* (pp. 7517-7520). IEEE.

Hensley, S., Chapman, B., Lavalle, M., Hawkins, B., Riel, B., Michel, T., Muellerschoen, R., Lou, Y., and Simard, M.: UAVSAR L-Band and P-Band Tomographic Experiments in Boreal Forests, IGARSS 2018 - 2018 IEEE International Geoscience and Remote Sensing Symposium, 8679–8682, https://doi.org/10.1109/IGARSS.2018.8518784, 2018.

Hensley, S., Ahmed, R., Chapman, B., Hawkins, B., Lavalle, M., Pinto, N., Pardini, M., Papathanassiou, K., Siqueria, P., and Treuhaft, R.: Boreal Forest Radar Tomography at P, L and S-Bands at Berms and Delta Junction, IGARSS 2020 - 2020 IEEE International Geoscience and Remote Sensing Symposium, 96–99, https://doi.org/10.1109/IGARSS39084.2020.9323337, 2020.

Higuera, P. E., Barnes, J., Chipman, M. L., Urban, M., and Hu, F. S.: The Burning Tundra: A Look Back at the Last 6,000 Years of Fire in the Noatak National Preserve, Northwestern Alaska (U.S. National Park Service), Alsk. Park Sci., 10, 36–41, 2011.

Hinzman, L. D., Deal, C. J., McGuire, A. D., Mernild, S. H., Polyakov, I. V., and Walsh, J. E.: Trajectory of the Arctic as an integrated system, Ecol. Appl., 23, 1837–1868, https://doi.org/10.1890/11-1498.1, 2013.

Hogg, E. H., Michaelian, M., Hook, T. I., and Undershultz, M. E.: Recent climatic drying leads to age-independent growth reductions of white spruce stands in western Canada, Glob. Change Biol., 23, 5297–5308, https://doi.org/10.1111/gcb.13795, 2017.

Hogg, E. H. (Ted) H. H., Brandt, J. P. B. P., and Michaelian, M. M.: Impacts of a regional drought on the productivity, dieback, and biomass of western Canadian aspen forests, Can. J. For. Res., https://doi.org/10.1139/X08-001, 2008.

Holloway, J. E., Lewkowicz, A. G., Douglas, T. A., Li, X., Turetsky, M. R., Baltzer, J. L., and Jin, H.: Impact of wildfire on permafrost landscapes: A review of recent advances and future prospects, Permafr. Periglac. Process., 31, 371–382, https://doi.org/10.1002/ppp.2048, 2020.

Hopkinson, C., Crasto, N., Marsh, P., Forbes, D., and Lesack, L.: Investigating the spatial distribution of water levels in the Mackenzie Delta using airborne LiDAR, Hydrol. Process., 25, 2995–3011, https://doi.org/10.1002/hyp.8167, 2011.

Horn, R., Jaeger, M., Keller, M., Limbach, M., Nottensteiner, A., Pardini, M., Reigber, A., and Scheiber, R.: F-SAR - recent upgrades and campaign activities, in: 2017 18th International Radar Symposium (IRS), 2017 18th International Radar Symposium (IRS), 1–10, https://doi.org/10.23919/IRS.2017.8008092, 2017.

Hoy, E. E., Griffith, P., Miller, C. E., and Team, A. S.: ABoVE: Directory of Field Sites Associated with 2017 ABoVE Airborne Campaign, ORNL DAAC, https://doi.org/10.3334/ORNLDAAC/1582, 2018.

Hu, F. S., Higuera, P. E., Walsh, J. E., Chapman, W. L., Duffy, P. A., Brubaker, L. B., and Chipman, M. L.: Tundra burning in Alaska: Linkages to climatic change and sea ice retreat, J. Geophys. Res. Biogeosciences, 115, https://doi.org/10.1029/2009JG001270, 2010.

Iwahana, G., Harada, K., Uchida, M., Tsuyuzaki, S., Saito, K., Narita, K., Kushida, K., and Hinzman, L. D.: Geomorphological and geochemistry changes in permafrost after the 2002 tundra wildfire in Kougarok, Seward Peninsula, Alaska, J. Geophys. Res. Earth Surf., 121, 1697–1715, https://doi.org/10.1002/2016JF003921, 2016a.

Iwahana, G., Uchida, M., Liu, L., Gong, W., Meyer, F. J., Guritz, R., Yamanokuchi, T., and Hinzman, L.: InSAR Detection and Field Evidence for Thermokarst after a Tundra Wildfire, Using ALOS-PALSAR, Remote Sens., 8, 218, https://doi.org/10.3390/rs8030218, 2016b.

Jafarov, E. E., Parsekian, A. D., Schaefer, K., Liu, L., Chen, A. C., Panda, S. K., and Zhang, T.: Estimating active layer thickness and volumetric water content from ground penetrating radar measurements in Barrow, Alaska, Geosci. Data J., 4, 72–79, https://doi.org/10.1002/gdj3.49, 2017.

Jenkins, L. K., Bourgeau-Chavez, L. L., French, N. H. F., Loboda, T. V., and Thelen, B. J.: Development of Methods for Detection and Monitoring of Fire Disturbance in the Alaskan Tundra Using a Two-Decade Long Record of Synthetic Aperture Radar Satellite Images, Remote Sens., 6, 6347–6364, https://doi.org/10.3390/rs6076347, 2014.

Johnston, C. E., Ewing, S. A., Harden, J. W., Varner, R. K., Wickland, K. P., Koch, J. C., Fuller, C. C., Manies, K., and Jorgenson, M. T.: Effect of permafrost thaw on CO2 and CH4 exchange in a western Alaska peatland chronosequence, Environ. Res. Lett., 9, 085004, https://doi.org/10.1088/1748-9326/9/8/085004, 2014.

Jones, B. M., Kolden, C. A., Jandt, R., Abatzoglou, J. T., Urban, F., and Arp, C. D.: Fire Behavior, Weather, and Burn Severity of the 2007 Anaktuvuk River Tundra Fire, North Slope, Alaska, Arct. Antarct. Alp. Res., 41, 309–316, https://doi.org/10.1657/1938-4246-41.3.309, 2009.

Jones, B. M., Grosse, G., Arp, C. D., Miller, E., Liu, L., Hayes, D. J., and Larsen, C. F.: Recent Arctic tundra fire initiates widespread thermokarst development, Sci. Rep., 5, 15865, https://doi.org/10.1038/srep15865, 2015.

Jones, M. C., Harden, J., O'Donnell, J., Manies, K., Jorgenson, T., Treat, C., and Ewing, S.: Rapid carbon loss and slow recovery following permafrost thaw in boreal peatlands, Glob. Change Biol., 23, 1109–1127, https://doi.org/10.1111/gcb.13403, 2017.

Jorgenson, M. T., Harden, J., Kanevskiy, M., O'Donnell, J., Wickland, K., Ewing, S., Manies, K., Zhuang, Q., Shur, Y., Striegl, R., and Koch, J.: Reorganization of vegetation, hydrology and soil carbon after permafrost degradation across heterogeneous boreal landscapes, Environ. Res. Lett., 8, 035017, https://doi.org/10.1088/1748-9326/8/3/035017, 2013.

Karion, A., Sweeney, C., Miller, J. B., Andrews, A. E., Commane, R., Dinardo, S., Henderson, J. M., Lindaas, J., Lin, J. C., Luus, K. A., Newberger, T., Tans, P., Wofsy, S. C., Wolter, S., and Miller, C. E.: Investigating Alaskan methane and carbon dioxide fluxes using measurements from the CARVE tower, Atmospheric Chem. Phys., 16, 5383–5398, https://doi.org/10.5194/acp-16-5383-2016, 2016.

Kobayashi, H., Hiroki, I., and Suzuki, R.: AmeriFlux US-Prr Poker Flat Research Range Black Spruce Forest, Ver. 3-5, https://doi.org/10.17190/AMF/1246153, 2019.

Kokelj, S. V., Lacelle, D., Lantz, T. C., Tunnicliffe, J., Malone, L., Clark, I. D., and Chin, K. S.: Thawing of massive ground ice in mega slumps drives increases in stream sediment and solute flux across a range of watershed scales, J. Geophys. Res. Earth Surf., 118, 681–692, https://doi.org/10.1002/jgrf.20063, 2013.

Kokelj, S. V., Tunnicliffe, J., Lacelle, D., Lantz, T. C., Chin, K. S., and Fraser, R.: Increased precipitation drives mega slump development and destabilization of ice-rich permafrost terrain, northwestern Canada, Glob. Planet. Change, 129, 56–68, https://doi.org/10.1016/j.gloplacha.2015.02.008, 2015.

Kokelj, S. V., Lantz, T. C., Tunnicliffe, J., Segal, R., and Lacelle, D.: Climate-driven thaw of permafrost preserved glacial landscapes, northwestern Canada, Geology, 45, 371–374, https://doi.org/10.1130/G38626.1, 2017.

Kyzivat, E. D., Smith, L. C., Pitcher, L. H., Fayne, J. V., Cooley, S. W., Cooper, M. G., Topp, S. N., Langhorst, T., Harlan, M. E., Horvat, C., Gleason, C. J., and Pavelsky, T. M.: A High-Resolution Airborne Color-Infrared Camera Water Mask for the NASA ABoVE Campaign, Remote Sens., 11, 2163, https://doi.org/10.3390/rs11182163, 2019.

Kyzivat, E. D., Smith, L. C., Pitcher, L. H., Fayne, J. V., Cooley, S. W., Cooper, M. G., Topp, S., Langhorst, T., Harlan, M. E., Gleason, C. J., and Pavelsky, T. M.: ABoVE: AirSWOT Water Masks from Color-Infrared Imagery over Alaska and Canada, 2017, ORNL DAAC, https://doi.org/10.3334/ORNLDAAC/1707, 2020.

Lafleur, P. M. and Humphreys, E. R.: Tundra shrub effects on growing season energy and carbon dioxide exchange, Environ. Res. Lett., 13, 055001, https://doi.org/10.1088/1748-9326/aab863, 2018.

Lantz, T. C. and Turner, K. W.: Changes in lake area in response to thermokarst processes and climate in Old Crow Flats, Yukon, J. Geophys. Res. Biogeosciences, 120, 513–524, https://doi.org/10.1002/2014JG002744, 2015.

Lavalle, M., Hawkins, B., and Hensley, S.: Tomographic imaging with UAVSAR: Current status and new results from the 2016 AfriSAR campaign, 2017 IEEE International Geoscience and Remote Sensing Symposium (IGARSS), 2485–2488, https://doi.org/10.1109/IGARSS.2017.8127498, 2017.

Le Toan, T., Quegan, S., Davidson, M. W. J., Balzter, H., Paillou, P., Papathanassiou, K., Plummer, S., Rocca, F., Saatchi, S., Shugart, H., and Ulander, L.: The BIOMASS mission: Mapping global forest biomass to better understand the terrestrial carbon cycle, Remote Sens. Environ., 115, 2850–2860, https://doi.org/10.1016/j.rse.2011.03.020, 2011.

Liljedahl, A., Hinzman, L., Busey, R., and Yoshikawa, K.: Physical short-term changes after a tussock tundra fire, Seward Peninsula, Alaska, J. Geophys. Res. Earth Surf., 112, https://doi.org/10.1029/2006JF000554, 2007.

Lindsay, C., Zhu, J., Miller, A. E., Kirchner, P., and Wilson, T. L.: Deriving Snow Cover Metrics for Alaska from MODIS, Remote Sens., 7, 12961–12985, https://doi.org/10.3390/rs71012961, 2015.

Lipovsky, P. S.: Summary of Yukon Geological Survey permafrost monitoring network results, 2008-2013, in: Yukon Exploration and Geology 2014, edited by: MacFarlane, K. E., Nordling, M. G., and Sack, P. J., Yukon Geological Survey, 113–122, 2015.

Liu, L., Schaefer, K., Zhang, T., and Wahr, J.: Estimating 1992–2000 average active layer thickness on the Alaskan North Slope from remotely sensed surface subsidence, J. Geophys. Res. Earth Surf., 117, https://doi.org/10.1029/2011JF002041, 2012.

Liu, L., Jafarov, E. E., Schaefer, K. M., Jones, B. M., Zebker, H. A., Williams, C. A., Rogan, J., and Zhang, T.: InSAR detects increase in surface subsidence caused by an Arctic tundra fire, Geophys. Res. Lett., 41, 3906–3913, https://doi.org/10.1002/2014GL060533, 2014.

Liu, L., Schaefer, K., Chen, A. C., Gusmeroli, A., Jafarov, E. E., Panda, S. K., Parsekian, A. D., Schaefer, T., Zebker, H. A., and Zhang, T.: Pre-ABoVE: Remotely Sensed Active Layer Thickness, Barrow, Alaska, 2006-2011, ORNL DAAC, https://doi.org/10.3334/ORNLDAAC/1266, 2015a.

Liu, L., Schaefer, K., Chen, A. C., Gusmeroli, A., Jafarov, E. E., Panda, S. K., Parsekian, A. D., Schaefer, T., Zebker, H. A., and Zhang, T.: Pre-ABoVE: Remotely Sensed Active Layer Thickness, Prudhoe Bay, Alaska, 1992-2000, ORNL DAAC, https://doi.org/10.3334/ORNLDAAC/1267, 2015b.

Loboda, T. V., French, N. H. F., Hight-Harf, C., Jenkins, L., and Miller, M. E.: Mapping fire extent and burn severity in Alaskan tussock tundra: An analysis of the spectral response of tundra vegetation to wildland fire, Remote Sens. Environ., 134, 194–209, https://doi.org/10.1016/j.rse.2013.03.003, 2013.

Loboda, T. V., Chen, D., He, J., and Baer, A.: ABoVE: Unburned and Burned Sites and Alaskan Tundra, ORNL DAAC, Submitted 1 May 2021, n.d.

Lopez-Sanchez, J. M., Ballester-Berman, J. D., Vicente-Guijalba, F., Cloude, S. R., McNairn, H., Shang, J., Skriver, H., Jagdhuber, T., Hajnsek, I., Pottier, E., Marechal, C., Hubert-Moy, L., Corgne, S., Wdowinski, S., Touzi, R., Gosselin, G., Brooks, R., Yamaguchi, Y., and Singh, G.: Agriculture and Wetland Applications, in: Polarimetric Synthetic Aperture Radar: Principles and Application, vol. 25, edited by: Hajnsek, I. and Desnos, Y.-L., Springer International Publishing, Cham, 119–178, https://doi.org/10.1007/978-3-030-56504-6_3, 2021.

Lou, Y., Shimada, J. G., Michel, T. R., Muellerschoen, R. J., Zheng, Y., and Moghaddam, M.: Pre-ABoVE: L1 S-0 Polarimetric Data from AirMOSS P-band SAR, Alaska, 2014-2015, ORNL DAAC, https://doi.org/10.3334/ORNLDAAC/1678, 2019.

Mack, M. C., Bret-Harte, M. S., Hollingsworth, T. N., Jandt, R. R., Schuur, E. A. G., Shaver, G. R., and Verbyla, D. L.: Carbon loss from an unprecedented Arctic tundra wildfire, Nature, 475, 489–492, https://doi.org/10.1038/nature10283, 2011.

Magagi, R., Berg, A. A., Goita, K., Belair, S., Jackson, T. J., Toth, B., Walker, A., McNairn, H., O'Neill, P. E., Moghaddam, M., Gherboudj, I., Colliander, A., Cosh, M. H., Burgin, M., Fisher, J. B., Kim, S.-B., Mladenova, I., Djamai, N., Rousseau, L.-P. B., Belanger, J., Shang, J., and Merzouki, A.: Canadian Experiment for Soil Moisture in 2010 (CanEx-SM10): Overview and Preliminary Results, IEEE Trans. Geosci. Remote Sens., 51, 347–363, https://doi.org/10.1109/TGRS.2012.2198920, 2013.

Malone, T., Liang, J., and Packee, E. C.: Cooperative Alaska Forest Inventory, Gen Tech Rep PNW-GTR-785 Portland US Dep. Agric. For. Serv. Pac. Northwest Res. Stn. 42 P, 785, https://doi.org/10.2737/PNW-GTR-785, 2009.

Marsh, P., Russell, M., Pohl, S., Haywood, H., and Onclin, C.: Changes in thaw lake drainage in the Western Canadian Arctic from 1950 to 2000, Hydrol. Process., 23, 145–158, https://doi.org/10.1002/hyp.7179, 2009a.

Marsh, P., Lesack, L., Hicks, F., Roberts, A., Hopkinson, C., Solomon, S., Forbes, D., Russell, M., and Haywood, H.: Hydrology of the Mackenzie Delta: off-channel water storage and delta interaction with the Beaufort Sea, 2009b.

Marsh, P., Bartlett, P., MacKay, M., Pohl, S., and Lantz, T.: Snowmelt energetics at a shrub tundra site in the western Canadian Arctic, Hydrol. Process., 24, 3603–3620, https://doi.org/10.1002/hyp.7786, 2010.

McCune, B., Arup, U., Breuss, O., Di Meglio, J., Esslinger, T. L., Magain, N., Miadlikowska, J., Miller, A. E., Muggia, L., Nelson, P. R., Rosentreter, R., Schultz, M., Sheard, J. W., Tønsberg, T., and Walton, J.: Biodiversity and ecology of lichens of Katmai and Lake Clark National Parks and Preserves, Alaska, Mycosphere, 9, 859–930, 2018.

McGuire, A. D., Anderson, L. G., Christensen, T. R., Dallimore, S., Guo, L., Hayes, D. J., Heimann, M., Lorenson, T. D., Macdonald, R. W., and Roulet, N.: Sensitivity of the carbon cycle in the Arctic to climate change, Ecol. Monogr., 79, 523–555, https://doi.org/10.1890/08-2025.1, 2009.

Meddens, A. J. H., Vierling, L. A., Eitel, J. U. H., Jennewein, J. S., White, J. C., and Wulder, M. A.: Developing 5 m resolution canopy height and digital terrain models from WorldView and ArcticDEM data, Remote Sens. Environ., 218, 174–188, https://doi.org/10.1016/j.rse.2018.09.010, 2018.

Mehra, R. and Ramanujam, V. M.: L S Band Airborne SAR Data Products Calibration, in: 2019 URSI Asia-Pacific Radio Science Conference (AP-RASC), 2019 URSI Asia-Pacific Radio Science Conference (AP-RASC), 1–1, https://doi.org/10.23919/URSIAP-RASC.2019.8738681, 2019.

Meyer, G., Humphreys, E. R., Melton, J. R., Cannon, A. J., and Lafleur, P. M.: Simulating shrubs and their energy and carbon dioxide fluxes in Canada's Low Arctic with the Canadian Land Surface Scheme Including biogeochemical Cycles (CLASSIC), Biogeosciences Discuss., 1–34, https://doi.org/10.5194/bg-2020-458, 2020.

Michaelian, M., Hogg, E. H., Hall, R. J., and Arsenault, E.: Massive mortality of aspen following severe drought along the southern edge of the Canadian boreal forest, Glob. Change Biol., 17, 2084–2094, https://doi.org/10.1111/j.1365-2486.2010.02357.x, 2011.

Michaelides, R. J., Schaefer, K., Zebker, H. A., Parsekian, A., Liu, L., Chen, J., Natali, S., Ludwig, S., and Schaefer, S. R.: Inference of the impact of wildfire on permafrost and active layer thickness in a discontinuous permafrost region using the remotely sensed active layer thickness (ReSALT) algorithm, Environ. Res. Lett., 14, 035007, https://doi.org/10.1088/1748-9326/aaf932, 2019.

Michaelides, R. J., Chen, R. H., Zhao, Y., Schaefer, K., Parsekian, A. D., Sullivan, T., et al. (2021). Permafrost Dynamics Observatory—part I: Postprocessing and calibration methods of UAVSAR L-band InSAR data for seasonal subsidence estimation. Earth and Space Science, 8, e2020EA001630. https://doi.org/10.1029/2020EA001630

Miller, C. E., Griffith, P. C., Goetz, S. J., Hoy, E. E., Pinto, N., McCubbin, I. B., Thorpe, A. K., Hofton, M., Hodkinson, D., Hansen, C., Woods, J., Larson, E., Kasischke, E. S., and Margolis, H. A.: An overview of ABoVE airborne campaign data acquisitions and science opportunities, Environ. Res. Lett., 14, 080201, https://doi.org/10.1088/1748-9326/ab0d44, 2019.

Minions, C., Natali, S., Watts, J. D., Ludwig, S., and Risk, D.: ABoVE: Year-Round Soil CO2 Efflux in Alaskan Ecosystems, Version 2, ORNL DAAC, https://doi.org/10.3334/ORNLDAAC/1762, 2020.

Minsley, B. J., Abraham, J. D., Smith, B. D., Cannia, J. C., Voss, C. I., Jorgenson, M. T., Walvoord, M. A., Wylie, B. K., Anderson, L., Ball, L. B., Deszcz-Pan, M., Wellman, T. P., and Ager, T. A.: Airborne electromagnetic imaging of discontinuous permafrost, Geophys. Res. Lett., 39, https://doi.org/10.1029/2011GL050079, 2012.

Moghaddam, M., Tabatabaeenejad, A., Chen, R. H., Saatchi, S. S., Jaruwatanadilok, S., Burgin, M., Duan, X., and Truong-Loi, M. L.: AirMOSS: L2/3 Volumetric Soil Moisture Profiles Derived From Radar, 2012-2015, ORNL DAAC, https://doi.org/10.3334/ORNLDAAC/1418, 2016.

Montesano, P. M., Sun, G., Dubayah, R. O., and Ranson, K. J.: Spaceborne potential for examining taiga–tundra ecotone form and vulnerability, Biogeosciences, 13, 3847–3861, https://doi.org/10.5194/bg-13-3847-2016, 2016.

Myers-Smith, I. H., Forbes, B. C., Wilmking, M., Hallinger, M., Lantz, T., Blok, D., Tape, K. D., Macias-Fauria, M., Sass-Klaassen, U., Lévesque, E., Boudreau, S., Ropars, P., Hermanutz, L., Trant, A., Collier, L. S., Weijers, S., Rozema, J., Rayback, S. A., Schmidt, N. M., Schaepman-Strub, G., Wipf, S., Rixen, C., Ménard, C. B., Venn, S., Goetz, S., Andreu-Hayles, L., Elmendorf, S., Ravolainen, V., Welker, J., Grogan, P., Epstein,

H. E., and Hik, D. S.: Shrub expansion in tundra ecosystems: dynamics, impacts and research priorities, Environ. Res. Lett., 6, 045509, https://doi.org/10.1088/1748-9326/6/4/045509, 2011.
Natali, S. M., Schuur, E. A. G., Webb, E. E., Pries, C. E. H., and Crummer, K. G.: Permafrost degradation stimulates carbon loss from experimentally warmed tundra, Ecology, 95, 602–608, https://doi.org/10.1890/13-0602.1, 2014.
National Research Council: Opportunities to Use Remote Sensing in Understanding Permafrost and Related Ecological Characteristics: Report of a Workshop, The National Academies Press, Washington, DC, 2014.
Oechel, W. C., Vourlitis, G. L., Hastings, S. J., Zulueta, R. C., Hinzman, L., and Kane, D.: Acclimation of ecosystem CO 2 exchange in the Alaskan Arctic in response to decadal climate warming, Nature, 406, 978–981, https://doi.org/10.1038/35023137, 2000.
Pan, C. G., Kirchner, P. B., Kimball, J. S., and Du, J.: A Long-Term Passive Microwave Snowoff Record for the Alaska Region 1988–2016, Remote Sens., 12, 153, https://doi.org/10.3390/rs12010153, 2020.
Pavelsky, T. M. and Smith, L. C.: Remote sensing of hydrologic recharge in the Peace-Athabasca Delta, Canada, Geophys. Res. Lett., 35, https://doi.org/10.1029/2008GL033268, 2008.
Pietroniro, A., Peters, D. L., Yang, D., Fiset, J.-M., Saint-Jean, R., Fortin, V., Leconte, R., Bergeron, J., Siles, G. L., Trudel, M., Garnaud, C., Matte, P., Smith, L. C., Gleason, C. J., and Pavelsky, T. M.: Canada's Contributions to the SWOT Mission – Terrestrial Hydrology(SWOT-C TH), Can. J. Remote Sens., 45, 116–138, https://doi.org/10.1080/07038992.2019.1581056, 2019.
Pitcher, L. H., Smith, L. C., Pavelsky, T. M., Fayne, J. V., Cooley, S. W., Altenau, E. H., Moller, D. K., and Arvesen, J.: ABoVE: AirSWOT Radar, Orthomosaic, and Water Masks, Yukon Flats Basin, Alaska, 2015, ORNL DAAC, https://doi.org/10.3334/ORNLDAAC/1655, 2019a.
Pitcher, L. H., Pavelsky, T. M., Smith, L. C., Moller, D. K., Altenau, E. H., Allen, G. H., Lion, C., Butman, D., Cooley, S. W., Fayne, J. V., and Bertram, M.: AirSWOT InSAR Mapping of Surface Water Elevations and Hydraulic Gradients Across the Yukon Flats Basin, Alaska, Water Resour. Res., 55, 937–953, https://doi.org/10.1029/2018WR023274, 2019b.
Pitcher, L. H., Smith, L. C., Cooley, S. W., Zaino, A., Carlson, R., Pettit, J., Gleason, C. J., Minear, J. T., Fayne, J. V., Willis, M. J., Hansen, J. S., Easterday, K. J., Harlan, M. E., Langhorst, T., Topp, S. N., Dolan, W., Kyzivat, E. D., Pietroniro, A., Marsh, P., Yang, D., Carter, T., Onclin, C., Hosseini, N., Wilcox, E., Moreira, D., Berge-Nguyen, M., Cretaux, J.-F., and Pavelsky, T. M.: Advancing Field-Based GNSS Surveying for Validation of Remotely Sensed Water Surface Elevation Products, Front. Earth Sci., 8, https://doi.org/10.3389/feart.2020.00278, 2020.
Plaza, C., Pegoraro, E., Bracho, R., Celis, G., Crummer, K. G., Hutchings, J. A., Hicks Pries, C. E., Mauritz, M., Natali, S. M., Salmon, V. G., Schädel, C., Webb, E. E., and Schuur, E. A. G.: Direct observation of permafrost degradation and rapid soil carbon loss in tundra, Nat. Geosci., 12, 627–631, https://doi.org/10.1038/s41561-019-0387-6, 2019.
Porter, C., Morin, P., Howat, I., Noh, M.-J., Bates, B., Peterman, K., Keesey, S., Schlenk, M., Gardiner, J., Tomko, K., Willis, M., Kelleher, C., Cloutier, M., Husby, E., Foga, S., Nakamura, H., Platson, M., Wethington, M., Williamson, C., Bauer, G., Enos, J., Arnold, G., Kramer, W., Becker, P., Doshi, A., D'Souza, C., Cummens, P., Laurier, F., and Bojesen, M.: ArcticDEM, https://doi.org/10.7910/DVN/OHHUKH, 2018.
Potter, C.: Ecosystem carbon emissions from 2015 forest fires in interior Alaska, Carbon Balance Manag., 13, 2, https://doi.org/10.1186/s13021-017-0090-0, 2018.
Quegan, S., Le Toan, T., Chave, J., Dall, J., Exbrayat, J.-F., Minh, D. H. T., Lomas, M., D'Alessandro, M. M., Paillou, P., Papathanassiou, K., Rocca, F., Saatchi, S., Scipal, K., Shugart, H., Smallman, T. L., Soja, M. J., Tebaldini, S., Ulander, L., Villard, L., and Williams, M.: The European Space Agency BIOMASS mission:

Measuring forest above-ground biomass from space, Remote Sens. Environ., 227, 44–60, https://doi.org/10.1016/j.rse.2019.03.032, 2019.
Quinton, W., Berg, A., Braverman, M., Carpino, O., Chasmer, L., Connon, R., Craig, J., Devoie, É., Hayashi, M., Haynes, K., Olefeldt, D., Pietroniro, A., Rezanezhad, F., Schincariol, R., and Sonnentag, O.: A synthesis of three decades of hydrological research at Scotty Creek, NWT, Canada, Hydrol. Earth Syst. Sci., 23, 2015–2039, https://doi.org/10.5194/hess-23-2015-2019, 2019.
Quinton, W. L., Adams, J. R., Baltzer, J. L., Berg, A. A., Craig, J. R., and Johnson, E.: Permafrost Ecosystems in Transition: Understanding and Predicting Hydrological and Ecological Change in the Southern Taiga Plains, Northeastern British Columbia and Southwestern Northwest Territories, 6, 2015.
Ramanujam, V. M. and Mehra, R.: L S Band SAR Data Processing and Products, in: 2019 URSI Asia-Pacific Radio Science Conference (AP-RASC), 2019 URSI Asia-Pacific Radio Science Conference (AP-RASC), 1–1, https://doi.org/10.23919/URSIAP-RASC.2019.8738235, 2019.
Ramanujam, V. M., Suneela, T. J. V. D., and Bhan, R.: ISRO's dual frequency airborne SAR pre-cursor to NISAR, in: Earth Observing Missions and Sensors: Development, Implementation, and Characterization IV, Earth Observing Missions and Sensors: Development, Implementation, and Characterization IV, 98810A, https://doi.org/10.1117/12.2228086, 2016.
Rocha, A. V. and Shaver, G. R.: Burn severity influences postfire CO2 exchange in arctic tundra, Ecol. Appl., 21, 477–489, https://doi.org/10.1890/10-0255.1, 2011a.
Rocha, A. V. and Shaver, G. R.: Postfire energy exchange in arctic tundra: the importance and climatic implications of burn severity, Glob. Change Biol., 17, 2831–2841, https://doi.org/10.1111/j.1365-2486.2011.02441.x, 2011b.
Rosen, P.A., Kim, Y., Kumar, R., Misra, T., Bhan, R. and Sagi, V.R., 2017, May. Global persistent SAR sampling with the NASA-ISRO SAR (NISAR) mission. In *Radar Conference (RadarConf), 2017 IEEE* (pp. 0410-0414). IEEE.
Roy, A., Toose, P., Mavrovic, A., Pappas, C., Royer, A., Derksen, C., Berg, A., Rowlandson, T., El-Amine, M., Barr, A., Black, A., Langlois, A., and Sonnentag, O.: L-Band response to freeze/thaw in a boreal forest stand from ground- and tower-based radiometer observations, Remote Sens. Environ., 237, 111542, https://doi.org/10.1016/j.rse.2019.111542, 2020.
Saatchi, S. S. and Moghaddam, M.: Estimation of crown and stem water content and biomass of boreal forest using polarimetric SAR imagery, IEEE Trans. Geosci. Remote Sens., 38, 697–709, https://doi.org/10.1109/36.841999, 2000.
Saatchi, S., Xu, L., Yang, Y., and Yu, Y.: Evaluation of NISAR Biomass Algorithm in Temperate and Boreal Forests, IGARSS 2019 - 2019 IEEE International Geoscience and Remote Sensing Symposium, 7363–7366, https://doi.org/10.1109/IGARSS.2019.8898657, 2019.
Sadeghi, M., Tabatabaeenejad, A., Tuller, M., Moghaddam, M., and Jones, S. B.: Advancing NASA's AirMOSS P-Band Radar Root Zone Soil Moisture Retrieval Algorithm via Incorporation of Richards' Equation, Remote Sens., 9, 17, https://doi.org/10.3390/rs9010017, 2017.
Schaefer, K., Chen, A. C., Chen, J., Chen, R. H., Dogaheh, K., Jafarov, E., Liu, L., Michaelides, R. J., Moghaddam, M., Parsekian, A. D., Sullivan, T. D., Tabatabaeenejad, A., Thompson, J., and Zebker, H.: The Permafrost Dynamics Observatory, 2018a.
Schaefer, K., Chen, A. C., Chen, J., Chen, R. H., Dogaheh, K., Jafarov, E., Liu, L., Michaelides, R. J., Moghaddam, M., Parsekian, A. D., Sullivan, T. D., Tabatabaeenejad, A., Thompson, J., and Zebker, H.: The Permafrost Dynamics Observatory (PDO), 2018b.
Schaefer, K., Michaelides, R. J., Chen, R. H., Sullivan, T. D., Parsekian, A. D., Bakian-Dogaheh, K., Tabatabaeenejad, A., Moghaddam, M., Chen, J., Chen, A. C., Liu, L., and Zebker, H. A.: ABoVE: Active

Layer Thickness Derived from Airborne L- and P-band SAR, Alaska, 2017, ORNL DAAC, https://doi.org/10.3334/ORNLDAAC/1676, 2019.
Schaefer, K., R.J. Michaelides, R.H. Chen, T.D. Sullivan, A.D. Parsekian, Y. Zhao, K. Bakian-Dogaheh, A. Tabatabaeenejad, M. Moghaddam, J. Chen, A.C. Chen, L. Liu, and H.A. Zebker. 2021. ABoVE: Active Layer Thickness Derived from Airborne L- and P-band SAR, Alaska, 2017. ORNL DAAC, Oak Ridge, Tennessee, USA. https://doi.org/10.3334/ORNLDAAC/1796
Schuur, E. A. G., Vogel, J. G., Crummer, K. G., Lee, H., Sickman, J. O., and Osterkamp, T. E.: The effect of permafrost thaw on old carbon release and net carbon exchange from tundra, Nature, 459, 556–559, https://doi.org/10.1038/nature08031, 2009.
Schuur, T.: AmeriFlux US-EML Eight Mile Lake Permafrost thaw gradient, Healy Alaska (3.5), https://doi.org/10.17190/AMF/1418678, 2019.
Sellers, P., Hall, F., Margolis, H., Kelly, B., Baldocchi, D., Hartog, G. den, Cihlar, J., Ryan, M. G., Goodison, B., Crill, P., Ranson, K. J., Lettenmaier, D., and Wickland, D. E.: The Boreal Ecosystem–Atmosphere Study (BOREAS): An Overview and Early Results from the 1994 Field Year, Bull. Am. Meteorol. Soc., 76, 1549–1577, https://doi.org/10.1175/1520-0477(1995)076<1549:TBESAO>2.0.CO;2, 1995.
Sellers, P. J., Hall, F. G., Kelly, R. D., Black, A., Baldocchi, D., Berry, J., Ryan, M., Ranson, K. J., Crill, P. M., Lettenmaier, D. P., Margolis, H., Cihlar, J., Newcomer, J., Fitzjarrald, D., Jarvis, P. G., Gower, S. T., Halliwell, D., Williams, D., Goodison, B., Wickland, D. E., and Guertin, F. E.: BOREAS in 1997: Experiment overview, scientific results, and future directions, J. Geophys. Res. Atmospheres, 102, 28731–28769, https://doi.org/10.1029/97JD03300, 1997.
Serrouya, R., Dickie, M., Lamb, C., van Oort, H., Kelly, A. P., DeMars, C., McLoughlin, P. D., Larter, N. C., Hervieux, D., Ford, A. T., and Boutin, S.: Trophic consequences of terrestrial eutrophication for a threatened ungulate, Proc. R. Soc. B Biol. Sci., 288, 20202811, https://doi.org/10.1098/rspb.2020.2811, 2021.
Sherriff, R. L., Miller, A. E., Muth, K., Schriver, M., and Batzel, R.: Spruce growth responses to warming vary by ecoregion and ecosystem type near the forest-tundra boundary in south-west Alaska, J. Biogeogr., 44, 1457–1468, https://doi.org/10.1111/jbi.12968, 2017.
Shugar, D. H., Clague, J. J., Best, J. L., Schoof, C., Willis, M. J., Copland, L., and Roe, G. H.: River piracy and drainage basin reorganization led by climate-driven glacier retreat, Nat. Geosci., 10, 370–375, https://doi.org/10.1038/ngeo2932, 2017.
Silva, C. A., Duncanson, L., Hancock, S., Neuenschwander, A., Thomas, N., Hofton, M., Fatoyinbo, L., Simard, M., Marshak, C. Z., Armston, J., Lutchke, S., and Dubayah, R.: Fusing simulated GEDI, ICESat-2 and NISAR data for regional aboveground biomass mapping, Remote Sens. Environ., 253, 112234, https://doi.org/10.1016/j.rse.2020.112234, 2021.
Smith, L. C., Pavelsky, T., Lettenmaier, D. P., Gleason, C. J., Pietroniro, A., Applejohn, A., Arvesen, J. C., Bjella, K., Carter, T., Chao, R., Cooley, S. W., Cooper, M. G., Cretaux, J. F., Douglass, T., Faria, D., Fayne, J., Fiset, J. M., Goodman, S., Hanna, B., Harlan, M., Langhorst, T., Marsh, P., Moreira, D. M., Minear, J. T., Onclin, C., Overstreet, B. T., Peters, D., Pettit, J., Pitcher, L. H., Russell, M., Spence, C., Topp, S., Turner, K. W., Vimal, S., Wilcox, E., Woodward, J., Yang, D., and Zaino, A.: AirSWOT flights and field campaigns for the 2017 Arctic-Boreal Vulnerability Experiment (ABoVE), in: AGU Fall Meeting Abstracts, C21F-1176, 2017a.
Smith, S. L., Roy, L.-P., Lewkowicz, A. G., and Chartrand, J.: Ground thermal data collection along the Alaska Highway corridor (KP1559-1895), Yukon, summer 2016, Geological Survey of Canada, 2017b.
Spence, C. and Hedstrom, N.: Hydrometeorological data from Baker Creek Research Watershed, Northwest Territories, Canada, Earth Syst. Sci. Data, 10, 1753–1767, https://doi.org/10.5194/essd-10-1753-2018, 2018.
Sun, G., K. J. Ranson, D. S. Kimes, J. B. Blair, and K. Kovacs (2008), Forest vertical structure from GLAS: An evaluation using LVIS and SRTM data, *Remote Sens. Environ.*, **112**, 107–117, doi:10.1016/j.rse.2006.09.036.

Tabatabaeenejad, A., and M. Moghaddam, 2011. Retrieval of surface and deep soil moisture and effect of moisture profile on inversion accuracy. IEEE Geosci. Remote Sensing Lett., vol. 8, no. 3, pp. 477- 481, May 2011.

Tabatabaeenejad, A., Burgin, M., Duan, X., and Moghaddam, M.: P-Band Radar Retrieval of Subsurface Soil Moisture Profile as a Second-Order Polynomial: First AirMOSS Results, IEEE Trans. Geosci. Remote Sens., 53, 645–658, https://doi.org/10.1109/TGRS.2014.2326839, 2015.

Tabatabaeenejad, A., Chen, R. H., Burgin, M. S., Duan, X., Cuenca, R. H., Cosh, M. H., Scott, R. L., and Moghaddam, M.: Assessment and Validation of AirMOSS P-Band Root-Zone Soil Moisture Products, IEEE Trans. Geosci. Remote Sens., 58, 6181–6196, https://doi.org/10.1109/TGRS.2020.2974976, 2020.

Tank, S., Olefeldt, D., Department of Renewable Resources, University of Alberta, Edmonton, Alberta, Canada, Quinton, W., Centre for Cold Regions and Water Science, Wilfred Laurier University, Waterloo, Ontario, Canada, Spence, C., Environment and Climate Change Canada, Saskatoon, Saskatchewan, Canada, Dion, N., Water Resources Department, Government of Northwest Territories, Yellowknife, Northwest Territories, Canada, Ackley, C., Centre for Cold Regions and Water Science, Wilfred Laurier University, Waterloo, Ontario, Canada, Burd, K., Department of Renewable Resources, University of Alberta, Edmonton, Alberta, Canada, Hutchins, R., Department of Biological Sciences, University of Alberta, Edmonton, Alberta, Canada, Mengistu, S., and Department of Biological Sciences, University of Alberta, Edmonton, Alberta, Canada: Fire in the Arctic: The effect of wildfire across diverse aquatic ecosystems of the Northwest Territories, Polar Knowl. Aqhaliat Rep., 1, 31–38, https://doi.org/10.35298/pkc.2018.04, 2019.

Touzi, R., Deschamps, A., and Rother, G.: Phase of Target Scattering for Wetland Characterization Using Polarimetric C-Band SAR, IEEE Trans. Geosci. Remote Sens., 47, 3241–3261, https://doi.org/10.1109/TGRS.2009.2018626, 2009.

Touzi, R., Omari, K., Sleep, B., and Jiao, X.: Scattered and Received Wave Polarization Optimization for Enhanced Peatland Classification and Fire Damage Assessment Using Polarimetric PALSAR, IEEE J. Sel. Top. Appl. Earth Obs. Remote Sens., PP, 1–26, https://doi.org/10.1109/JSTARS.2018.2873740, 2018.

Touzi, R., Hong, G., Motohka, T., Shinichi, S., and De Lisle, D.: Investigation of Compact SAR L and C band Complementarity for Permafrost Characterization In Arctic Regions, IGARSS 2019 - 2019 IEEE International Geoscience and Remote Sensing Symposium, 4665–4667, https://doi.org/10.1109/IGARSS.2019.8898510, 2019a.

Touzi, R., Pawley, S., Hosseini, M., and Jiao, X.: Polarimetric L-band PALSAR2 for Discontinuous Permafrost Mapping In Peatland Regions, in: IGARSS 2019 - 2019 IEEE International Geoscience and Remote Sensing Symposium, IGARSS 2019 - 2019 IEEE International Geoscience and Remote Sensing Symposium, Yokohama, Japan, xvii–ccxxii, https://doi.org/10.1109/IGARSS.2019.8900243, 2019b.

Tsuyuzaki, S., Iwahana, G., and Saito, K.: Tundra fire alters vegetation patterns more than the resultant thermokarst, Polar Biol., 41, 753–761, https://doi.org/10.1007/s00300-017-2236-7, 2018.

Ullmann, T., Banks, S. N., Schmitt, A., and Jagdhuber, T.: Scattering Characteristics of X-, C- and L-Band PolSAR Data Examined for the Tundra Environment of the Tuktoyaktuk Peninsula, Canada, Appl. Sci., 7, 595, https://doi.org/10.3390/app7060595, 2017.

Vincent, W. F., Callaghan, T. V., Dahl-Jensen, D., Johansson, M., Kovacs, K. M., Michel, C., Prowse, T., Reist, J. D., and Sharp, M.: Ecological Implications of Changes in the Arctic Cryosphere, AMBIO, 40, 87–99, https://doi.org/10.1007/s13280-011-0218-5, 2011.

Walker, B., Wilcox, E. J., and Marsh, P.: Accuracy assessment of late winter snow depth mapping for tundra environments using Structure-from-Motion photogrammetry1, Arct. Sci., https://doi.org/10.1139/as-2020-0006, 2020.

Walker, X. J., Rogers, B. M., Baltzer, J. L., Cummings, S. R., Day, N. J., Goetz, S. J., Johnstone, J. F., Turetsky, M. R., and Mack, M. C.: ABoVE: Wildfire Carbon Emissions and Burned Plot Characteristics, NWT, CA, 2014-2016, ORNL DAAC, https://doi.org/10.3334/ORNLDAAC/1561, 2018a.

Walker, X. J., Rogers, B. M., Baltzer, J. L., Cumming, S. G., Day, N. J., Goetz, S. J., Johnstone, J. F., Schuur, E. A. G., Turetsky, M. R., and Mack, M. C.: Cross-scale controls on carbon emissions from boreal forest megafires, Glob. Change Biol., 24, 4251–4265, https://doi.org/10.1111/gcb.14287, 2018b.

Walker, X. J., Baltzer, J. L., Laurier, W., Cumming, S. G., Day, N. J., Goetz, S. J., Johnstone, J. F., Potter, S., Rogers, B. M., Schuur, E. a. G., Turetsky, M. R., and Mack, M. C.: ABoVE: Characterization of Carbon Dynamics in Burned Forest Plots, NWT, Canada, 2014, ORNL DAAC, https://doi.org/10.3334/ORNLDAAC/1664, 2019a.

Walker, X. J., Baltzer, J. L., Cumming, S. G., Day, N. J., Ebert, C., Goetz, S., Johnstone, J. F., Potter, S., Rogers, B. M., Schuur, E. A. G., Turetsky, M. R., and Mack, M. C.: Increasing wildfires threaten historic carbon sink of boreal forest soils, Nature, 572, 520–523, https://doi.org/10.1038/s41586-019-1474-y, 2019b.

Whalen, D., Forbes, D. L., Hopkinson, C., Lavergne, J. C., Manson, G. K., Marsh, P., and Solomon, S. M.: Topographic LiDAR-Providing a new perspective in the Mackenzie Delta, 2009.

Whitley, M., Frost, G. V., Jorgenson, M. T., Macander, M., Maio, C. V., and Winder, S. G.: ABoVE: Permafrost Measurements and Distribution Across the Y-K Delta, Alaska, 2016, ORNL DAAC, https://doi.org/10.3334/ORNLDAAC/1598, 2018a.

Whitley, M. A., Frost, G. V., Jorgenson, M. T., Macander, M. J., Maio, C. V., and Winder, S. G.: Assessment of LiDAR and Spectral Techniques for High-Resolution Mapping of Sporadic Permafrost on the Yukon-Kuskokwim Delta, Alaska, Remote Sens., 10, 258, https://doi.org/10.3390/rs10020258, 2018b.

Wilcox, E. J., Keim, D., Jong, T. de, Walker, B., Sonnentag, O., Sniderhan, A. E., Mann, P., and Marsh, P.: Tundra shrub expansion may amplify permafrost thaw by advancing snowmelt timing, Arct. Sci., https://doi.org/10.1139/as-2018-0028, 2019.

Wilson, C., Dann, J., Bolton, R., Charsley-Groffman, L., Jafarov, E., Musa, D., and Wullschleger, S.: In Situ Soil Moisture and Thaw Depth Measurements Coincident with Airborne SAR Data Collections, Barrow and Seward Peninsulas, Alaska, 2017, https://doi.org/10.5440/1423892, 2021.

Woodward, A. and Beever, E. A.: Conceptual ecological models to support detection of ecological change on Alaska National Wildlife Refuges, 2011.

Yi, Y., Kimball, J. S., Chen, R. H., Moghaddam, M., Reichle, R. H., Mishra, U., Zona, D., and Oechel, W. C.: Characterizing permafrost active layer dynamics and sensitivity to landscape spatial heterogeneity in Alaska, The Cryosphere, 12, 145–161, https://doi.org/10.5194/tc-12-145-2018, 2018.

Zhang, Y., Touzi, R., Feng, W., Hong, G., Lantz, T. C., and Kokelj, S. V.: Landscape-scale variations in near-surface soil temperature and active-layer thickness: Implications for high-resolution permafrost mapping, Permafr. Periglac. Process. J., 2021.